UNIVERSITY OF OXFORD

DEPARTMENT OF CHEMISTRY

Carbon Nitride Based Materials For Heterogeneous Photocatalysis

BY

MUHAMMAD ABDULLAH KHAN

WOLFSON COLLEGE

A THESIS SUBMITTED FOR THE DEGREE

DOCTOR OF PHILOSOPHY

2016

Carbon Nitride Based Materials For Heterogeneous Photocatalysis

BY

Muhammad Abdullah Khan

446444

Wolfson College

Supervisor

Prof. S. C. Edman Tsang

Internal Assessor

Professor Kylie Vincent

A THESIS SUBMITTED FOR THE DEGREE

DOCTOR OF PHILOSOPHY

2016

Abstract

Photocatalysis on semiconductor surfaces has grown tremendously in the last four decades. One reason for this is its analogy with photosynthesis, the most important natural photochemical process. Semiconductors to some extent can mimic the key steps of this fascinating heterogeneous photocatalytic process, i.e., photochemical charge generation, charge trapping, interfacial electron exchange and subsequent reaction. Building on this premise this thesis constitutes an investigation into the photocatalytic properties and applications of semiconducting layered framework carbon nitride based materials. Similar to traditional photocatalysts, the photocatalytic activity and efficiency of carbon nitride systems developed thus far is limited mainly by the fast recombination and low mobility of photogenerated excitons. Here, by exploiting the band alignment strategy, carbon nitride isotype (type II) and carbon nitride-niobium oxide of type II semiconductor heterojunctions were successfully constructed with the aim of suppressing the exciton recombination and improving charge extraction for the successful initiation of desirable redox chemistry. These features were demonstrated by employing the materials in heterogeneous photocatalysis for water splitting, organic pollutant decomposition and photochemical organic synthesis.

Carbon nitride isotype heterojunctions constructed by controlled thermal condensation are shown to exhibit lower recombination of excitons relative to the pristine carbon nitride. As a consequence photocurrent generation and visible light driven H_2 production activity was enhanced. This increase is attributed to the surface passivation and improved electron mobility of built-in electric field which arises from the topology-induced band offset of favoured type II heterojunction configuration. Building on the insights into the

heterojunction-activity dependence, new type II graphitic carbon nitride (C_3N_4), Nb_2O_5 (C_3N_4-Nb_2O_5), heterojunctions synthesised *via* a hydrothermal method were exploited for their photodegradation ability of the organic pollutants. The synergic effect of carbon nitride and Nb_2O_5 coupling leads to the substantial photocatalytic activity improvement which can be attributed to the formation of an intimate interface and gradual attenuation of energy-wasteful charge recombination processes in C_3N_4-Nb_2O_5 heterojunctions materials.

While water splitting and pollutant decomposition using semiconductors has received the bulk of attention, the possibilities concerning chemical synthesis are only beginning to be meaningfully exploited. We, therefore, employed carbon nitride to catalyse photo organic synthesis. It was demonstrated for the first time that carbon nitride can efficiently catalyse the photoacetalization reactions of aldehydes/ketones with alcohols, forming acetals at high yields using visible light under ambient conditions. Mechanistic studies suggest that the transient charge separation at the surface of this material is sufficient to catalyse the reaction in the absence of Lewis or Brønsted acids or solvent systems. Since the photoacetalization of aldehydes occurs under conditions similar to those of alcohols oxidation, both using visible light and carbon nitride as a catalyst, the two reactions actually proceed via different mechanisms. This study also demonstrates, visible light induced heterogeneous auto-tandem catalysis, coupling the oxidation and subsequent acetalization of alcohols in a single chemical process. This green strategy can be applicable to a wide variety of organic photo-induced syntheses.

Declaration

I confirm that this in my own work and the use of all material from other sources has been properly and fully acknowledged.

M. A. Khan

Dedication

For my father, who wished to live for this day.

Acknowledgments

First and foremost, I would like to thank Professor Edman Tsang for providing me the opportunity to join his research group and pursue my research interests under his guidance and support. I would also like to thank the Higher Education Commission (HEC) Pakistan for 10% Overseas scholarship, as well as Wolfson College Oxford for partial financial assistance. The Department of Chemistry and the University of Oxford are thanked for the provision of research environment and facilities necessary for my research.

This thesis is the result of five years of research. The effort to translate and analyse the research data in a thesis form, however, started last year and was not possible without the valuable assistance and support from following individuals: Ivo F Teixeira for his assistance with the organic synthesis part (Chapter 6 and 7), exhausting discussions, my most exacting critic and my friend; Dr Simon Fairclough for TEM and help in organising the experimental work; Dr Clive Eley for discussion about the photocatalytic activities (Chapter 5); Dr Asif A. Tahir (University of Exeter) for discussions on carbon nitride heterojunctions (Chapter 4); Molly M. J for performing the PL measurements; Dr Ashley Shepherd for assistance in BET data collection and analysis; Dr. Alison Crossley (Materials, University of Oxford) for XPS data collection and Muhammad Arshad XPS data analysis (NCP Pakistan); Dr Simon Jones, Dr Cheng-Tar and Dr Amy Kolpin for support and general assistance in early years of my research. In addition to all these peoples who have contributed to the understanding of my research, I am also thankful to the staff of Inorganic Chemistry Laboratory (ICL), who have assisted me with solving administrative and instrumental problems faced along the way and, in particular, the staff of ICL stores who facilitated the procurement of the chemicals used throughout this work.

Many friends and colleagues read various chapters of the thesis and provided immense help in improving the text with their valuable comments and encouragement. I am thankful to Ieuan T. Ellis, Ian Mcpherson, Dr. Rafaqat Hussain and Dr. Yusuke Koito for being kind readers. My gratitude is also due to Tsang group members, past and present for their support and entertainment throughout my DPhil project.

I would like to thank my family for their unconditional love, support and encouragement. Their constant motivation enabled me to keep going and complete this work. Also heartfelt thanks to Sultan Al Shuhri for keeping my spirits up in times of extreme stress and the frustrations of experiment failures.

Finally, for loving support and patience, I wish to save my warmest thanks of all for my wife Dr. Tayyaba Khan and my son Ahmad, who I saw grow up on Skype.

Any errors of fact, interpretation, or judgment expressed in this thesis is of course entirely my own and should not be attributed to the institutions I remained associated with or the individuals mentioned above.

Thesis Contents

Chapter 1: Introduction

Chapter 3: Experimental Methods

Chapter 4: Construction of Carbon Nitride Isotype Heterojunctions

Overview

Chapter 5: Carbon Nitride- Niobium Oxide Heterojunctions

Overview

Chapter 6: Photoacetalization of Aldehyde/Ketones

Chapter 7: Concurrent Tandem Photo-oxidation / Acetalization of Alcohols

Chapter 8: Conclusions and Future Perpecetive

List of Figures

List of Tables

Schemes

List of Abbreviations

BJH - Barrett– Joyner–Halenda

BQ - benzoquinone

BET - Brunauer- Emmett-teller

CN - carbon nitride

CN-CN - carbon nitride-carbon nitride

CCDs - charged coupled devices

CHN – carbon, hydrogen, nitrogen

CB – conduction band

CTC - concurrent tandem catalytic

^{13}C CPMAS NMR- Carbon-13 Cross-Polarization Magic Angle Spinning nuclear magnetic resonance

DCP - dichlorophenol

CVD – Chemical vapour deposition

DFT – Density function theory

DCDA - Dicyandiamide

DMF – dimethylforamide

EDTA – ethylenediaminetetraacetate

ESCA - electron spectroscopy for chemical analysis

ET - electron transfer

FEG-SEM – field emission gun scanning electron microscope

FTO – fluoride-doped tin oxide

FTIR - Fourier transform infrared

FWHM – full width half maximum

HOMO - highest occupied molecular orbital

HER - hydrogen evolution reaction

ISD - inherent safer design

ISC - inter system crossing

IFET - interfacial electron transfer

IC - internal conversion

IPA – isopropanol

JCPDS – Join Committee on Powder Diffraction Standards

LOMO lowest occupied molecular orbital

MB - Methylene blue

NHE - normal hydrogen electrode

NMR- nuclear magnetic resonance

ORR - oxygen reduction reaction

PL – Photoluminescence

PS - polymeric semiconductor

SCs – semiconductors

SET - single electron transfer

TCD - thermal conductive detector

THF- tetrahydrofuran

TCSPC - time-correlated single photon counting

TEM - Transmission electron spectroscopy

TEOA – triethanolamine

TR-PL - time-resolved photo-luminescence

UHV - ultra-high vacuum

UV-vis - Ultraviolet-visible absorption

VB - valence band

VR - vibrational relaxation

XRD - X-ray diffraction

XPS - X-ray photoelectron spectroscopy

Chapter 1: Introduction

Overview

Overview

This chapter presents a review of the photocatalytic (selective) applications of carbon nitride (CN) based materials. Visible light driven heterogeneous catalysis is part of a new ‘green chemistry’ and three applications will be considered, namely hydrogen production from water, aerobic degradation of organic pollutants, and fine chemical (organic) synthesis. The concept of ‘green chemistry’ in the context of photocatalysis is introduced, starting with the details of the fundamental principles of photocatalysis, water splitting (hydrogen production), aerobic photooxidation and photochemical organic transformations. Further, a comprehensive research survey of carbon nitride materials, focusing on their synthesis, structure and relevant applications is carried out, and a brief introduction to the concept of photocatalysis is given. This background is then used to introduce the rationale and motivation behind this work.

1.1 Green Chemistry and Catalysis

Traditional chemical manufacturing is energy intensive, wasteful and often involves the use of hazardous substances. It is widely acknowledged that there is a growing need to focus on resource efficiency and on the design of chemical products and processes that are environmentally benign.[1–5] This trend towards what has become known as 'Green Chemistry' necessitates a paradigm shift from conventional concepts of process efficiency, that have overwhelming focus on chemical yield, to one that is simple, sustainable and assigns economic value to reduction or elimination of the use (or generation) of hazardous substances in the design, manufacture and application of chemical products.[6–9]

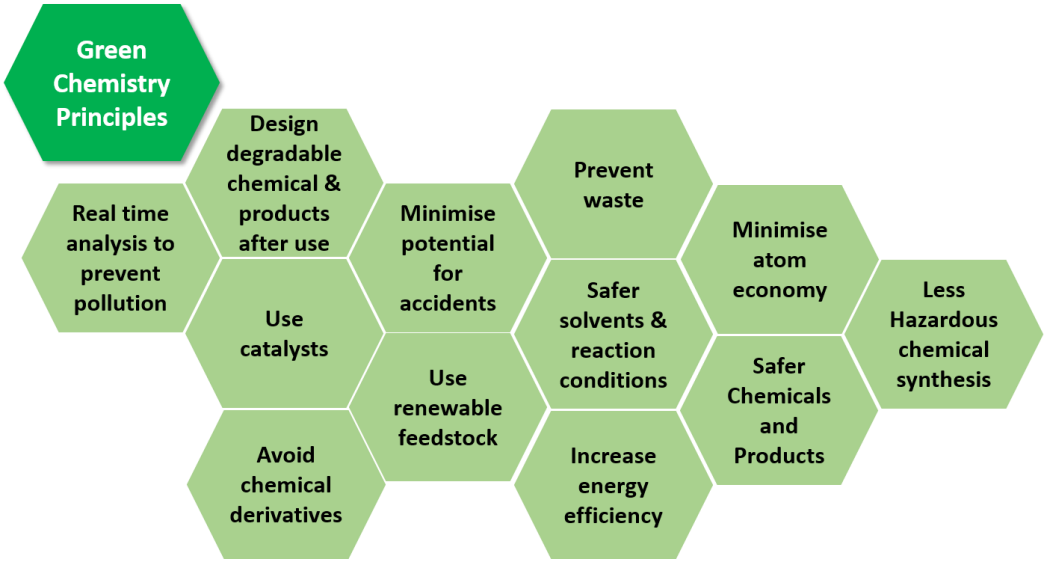

Figure 1.1 Principle of green chemistry developed by Paul Anastas and John Warner. The list outlines an early conception of what would make a greener chemical, process, or product.

Green chemistry is the design of chemical products and processes that reduce or eliminate the use and generation of hazardous substance.[4,10] It utilizes a set of ideals (Figure1.1) that go

beyond reducing cost, waste generation, energy usage and tedious work up during chemical synthesis/process and emphasise the use of renewable feedstocks, less hazardous auxiliary agents (solvents) and inherent safer design, (ISD) thus, taking out the risk altogether.[5] It has led to the invention of a number of clever processing technologies, to save time and energy or reduce waste production but most of these only exist in academia, with few exceptions, with industry hesitant to use them. Green chemical technology includes in particular the use of heterogeneous catalysis (well established in some sectors but relatively less explored for fine chemicals synthesis, Chapter 7 presents an example), photocatalysis and synthetic electrochemistry for green, renewable fuel and fine chemical synthesis and all these replacements for conventional methods can lead to the improved yields, reduced reaction times, and reduced by product formation.[11]

In the context of green chemistry, to achieve these goals predominately (i) heterogeneous and (ii) photo catalysis have been employed. Although homogeneous catalysis (detailed description of homogeneous catalysis is beyond the scope of this thesis) generally offers good activity and a homogeneous distribution of active sites, there are however inherent problems with regard to separation and their reuse.[3,4] On the contrary, heterogeneous catalysis is often environmentally benign and relatively safe to handle (e.g, silica supported sulfonic acid for acid catalysis compared to sulfuric acid) and affords easy separation (e.g., zeolites used in petroleum refining can be reactivated and reused).[11] In many cases heterogeneous catalysts outdo the homogeneous analogs, often because of cooperative effects of surface sites (e.g., clayznic for Friedal-Crafts catalysis compared to zinc chloride).[11] The disadvantage of heterogeneous catalysis is added synthesis costs, large amount of material required, and blockage of catalysts (sometimes restricted access) sites. Photocatalysis is relevant to heterogeneous catalysis because it brings the possibility of using the sunlight as clean energy

source with no waste. Hence *heterogeneous photocatalysis* as a green practice is the recurrent theme in subsequent chapters.

1.2 Fundamentals of Semiconductor Photocatalysis

1.2.1 Photocatalysis

Photocatalysis, which forms a significant part of global effort to develop green technologies, comprises class of reactions which use a catalyst activated by light.[12] Light is not the catalyst during the reactions, but is rather a reactant consumed in the chemical process. The actual photocatalysts themselves are usually solid semiconductors (SCs) which are (i) chemically inert and stable during photochemical transition and (ii) capable of accelerating or initiating chemical reaction in presence of light. In a typical photocatalytic reaction, a semiconductor is excited by light of energy higher than the band gap (E_g) results in the formation of energy rich charged electron-hole pair states (excitons). The catalytic reaction itself occurs when the energy is momentarily stored and transferred to reactant molecules. In some instances, the exciton energy remains within the heterogeneous catalyst forming the surface bound exciton and interacting (surface adsorbed) species interface, which causes direct photochemical transformations. Photocatalyst materials are generally left unchanged after numerous cycles and can be recovered at the end of the process.[13] Depending on the nature of the relative phases of photocatalyst and of the reactant involved in the photocatalysis, it can be either homogeneous or heterogeneous process.

Photocatalytic processes involve the initial absorption of photons by a molecule or substrate to produce highly reactive electronically excited states.[14] This initial excitation may participate in an electron transfer *to* and *from* an appropriate partner and subsequent de-excitation processes that leads to chemical reactions through changing the electron population

in molecular orbitals. Figure 1.2 schematically illustrates electron transfer between donor D and acceptor A where reactive centre can be a molecule or a surface reactive site in photoreaction. In photoexcited molecule an electron transfer process is a one-electron reaction in which electron is promoted from the HOMO to the LUMO in either the donor or ($D \rightarrow A^*$ or $D^* \rightarrow A^*$) acceptor molecule. Depending when the reduction potential is negative it donates an electron to acceptor and *vice versa*. The initial excitation requires the overlap between the occupied donor orbital and the acceptor orbital, which may be empty or half-filled. The electron transfer results in an ion pair forming of the donor cation and the acceptor anion. Whereas the energy transfer occurs when a photon from *D** is spontaneously absorbed by the acceptor resulting in overlapping spectrum.

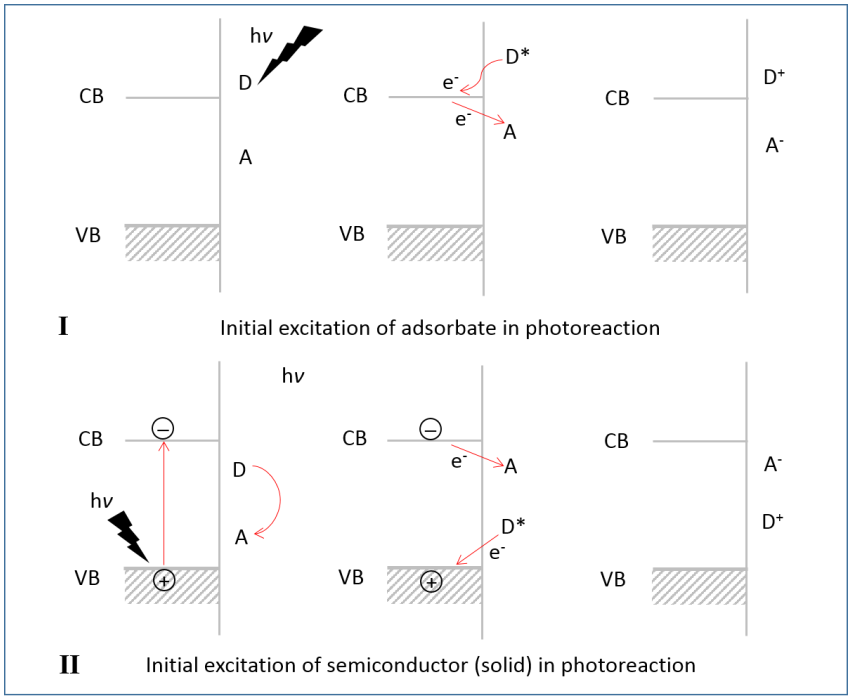

Figure 1.2 Catalysed photoreaction initial excitation of adsorbate (I), and Sensitized photoreaction, initial excitation of solid (II).

The term 'photoreaction' is sometimes indiscriminately used for a 'photoinduced' or 'photoactivated' reaction, all to the same effect. Depending on where photoexcitation primarily occurs, photocatalysis, in reference to substrate-catalyst interaction, is subdivided into two classes.[15] If the initial photoexcitation process occurs in the molecule, followed by interaction with a SC catalyst, the process is referred to as a *catalysed photoreaction* e.g., $TiCl_4$ catalysed photoreaction of 2-acetyl-1,3-dicarbonyl compounds in methanol.[14,16,17] Conversely, if the photoexcitation takes place in SC followed by interaction with a ground state of the interacting substrate, then the process is *sensitised photoreaction* e.g., heterogeneous electron transfer from dye sensitised nanocrystalline TiO_2 to $[Co(bpy)_3]^{3+}$.[14,18] Throughout this thesis the term *photocatalysis* is exclusively refers to the *heterogeneous semiconductor sensitised photoreactions.* In particular, its relevance here is to the light absorption by polymeric carbon nitride based materials, to generate energy rich charges-carriers (excitons), which subsequently carry out the redox reactions with surface bound/interacting substrate molecules in surrounding aqueous media.

1.2.2 Electronic processes and mechanism of photocatalysis

1.2.2.1 Molecular excitation and deexcitation events

When a molecule absorbs light, it is transformed to a species of higher energy, the *excited state*. Depending on the specific molecular structure, lifetime[a] of this new molecular state ranges from picoseconds to microseconds. The energetic relation between allowed excitation and deexcitation processes for a molecule are given in energy level diagram, as shown in Figure 1.3.[19] The lowest vibrational ground singlet energy state (defined by the vibrational

[a] The life time is defined as the time when the initial concentration has decreased by a factor 1/e, that is, by about 37%.[19]

quantum number $v = 0$) of the molecule is represented by S_0 and three vibrational states of three excited states are represented as S_1 and S_2 for the singlet states and T_1 for the triplet state. The energy levels of the molecules in excited state are important when dealing with photocatalysed reaction of organic molecules. After absorption of a photon of energy hv_1, the molecule moves to an electronically and vibrationally excited state S_2 which on vibrational relaxation (VR, 10^{-13} s) reaches to the vibrational ground energy state S_2. A nonradiative isoenergetic transition of same multiplicity (internal conversion IC) from S_2 to S_1 can also occur,[b] and generates the S_1 state, the lowest state within the singlet multiplicity, and then emits radiation to vibrational states of S_0.[c] [19]

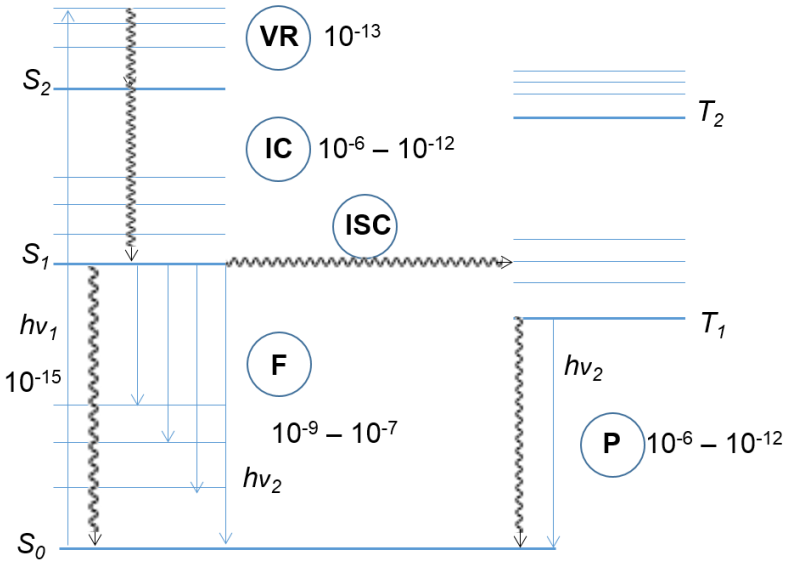

Figure 1.3 Visualization of photophysical excitation deexcitation processes in a molecule. Wavy arrows indicate nonradiative processes and average life times for vibrational relaxation (VR), internal conversion (IC), inter system conversion (ISC), fluorescence (F) and phosphorescence are given in seconds. Figure is modified from the reference [19].

[b] The corresponding higher lying vibrational states of S_1 are omitted in the Figure 1.3 but isoenergetic nature of radiationless transitions is depicted for ISC from S_1 to T_1.[19]

[c] Electronic transitions in which both the vibrational and electronic quantum number change (absorption of a photon, IC, ISC) are called *vibronic transitions.*

Usually de-excitation events are much slower so that they proceed *via* other emission pathways such as fluorescence or phosphorescence or *via* radiationless decay. However, the deexcitation of excited molecules favour the route which will minimise the lifetime of the excited state. In accordance with the selection rule (Kasha's rule)[d] fluorescence is observable from S_1 and not from S_2 because the rate constant of a radiationless transition (internal conversion IC, inter system crossing ISC) increases exponentially with decreasing band gap (ΔE) between two states. This means that ΔE between S_2 and S_1 is much smaller than that of between S_1 and S_0. Hence, the IC (10^{-6}-10^{-12}) from S_2 to S_1 is so fast that light emission is not possible whereas it is slow enough from the S_1 to S_0 transition and therefore a spin conserved emission called *fluorescence* (F, 10^{-9}-10^{-7}) becomes possible.[20]

In case of molecules containing heavy atoms a radiationless transition including a spin flip is sometimes favoured. This inter system crossing is an isoenergetic process and produces a triplet state T_1 in a vibrationally excited state. On thermal relaxation, spin-forbidden light emission called *phosphorescence* (P, 10^{-2}-10^{-6} s) reforms the singlet ground state. It is noted that transitions between states of different spin multiplicity are in general forbidden and considerably slower than the allowed transitions within one multiplicity.

1.2.2.2 Mechanism of semiconductor photocatalytic action

The initial process for heterogeneous photocatalysis of organic and inorganic compounds by SCs is the generation of electron-hole pairs in the semiconductor. An overview of the process of SC photocatalysis is illustrated in Figure 1.4. As indicated electron-hole pairs can be generated in a semiconductor by the absorption of photon of light, of energy greater than or

[d] In condensed phase, the emission in polyatomic molecules in general occurs from the lowest vibrational level of the lowest excited state within a given multiplicity.

equal to band gap ($h\nu \geq E$g). The success of photocatalytic action depends on the fate of these photogenerated excitons as they migrate to the surface of the semiconducting material, before they initiate the redox reaction in adsorbed substrate molecules. Amongst the possibilities, include i) electron-hole recombination at the surface ii) or electron-hole recombination in the bulk of the SC and subsequent charge neutralisation. In some instances, iii) the semiconducting material effectively reduces the external species at the surface by an electron coupled with iv) oxidation of an external species by a hole.[13] Efficient photocatalysis should reduce the exciton recombination (i and ii) which is the major form of energy loss in photocatalytic process.[21] A more detailed description of the particular photocatalysis and fine chemical synthesis by carbon nitride, and carbon nitride heterojunction materials in aerated, and aqueous conditions is included in Chapter 6 and 7.

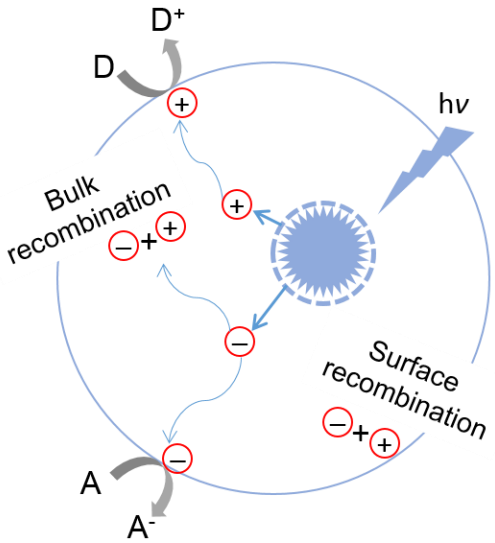

Figure 1.4 Schematic of photoexcitation and deexcitation events in SC surface and in the bulk.

1.3 Photocatalytic semiconductor materials

Transition metal oxides are a widely investigated class of photocatalytic materials.[14,22,23] For example: TiO_2,[14,24] ZnO,[25] Nb_2O_5[26] Fe_2O_3[27] and WO_3[28] have been shown to be photo active materials however detailed discussion on metal oxide photocatalysts is beyond the scope of this thesis. A very brief overview of widely used inorganic SCs with aim of providing some context, in particular, to the carbon nitride based semiconducting materials follows.

TiO_2, by far, received more attention than any other metal oxide material. This is due to its high photocatalytic activity and inherent stability in aqueous conditions. Many review papers have been dedicated to TiO_2.[14,29] Nonetheless, a major drawback to metal oxides SCs (TiO_2 Eg = 3.0 eV) is their wide band gap meaning they are only active in UV region. ZnO also suffers from having large band (Eg = 3.3 eV) and is prone to mild photo-corrosion in aqueous conditions. Nb_2O_5 is only beginning to draw attention due to its unique acidic and photocatalytic properties.[17] Some other oxides including WO_3, $BiVO_4$, and so forth are visible-light-responsive but cannot conduct water reduction to produce H_2 because their conduction bands are lower than the reduction potential of water.[23,30] Other than oxide SCs, sulfides (i.e. CdS and ZnS,) have been successfully demonstrated to be effective for photocatalytic applications yet they have a major disadvantage of leaching (Cd^{2+}) which is toxic and photo-corrosion (i.e. oxidation of S^{2-} to S^0) in oxygenated aqueous conditions.[23,31] Additionally, a wide band gap of metal oxide materials can generate the strong hydroxyl non-selective radical during photolysis that virtually limit their use for chemical synthesis because it initiates many unwanted side reactions. Due to these shortcomings, there is major shift towards the search for non-oxide metal free semiconducting materials. In this pursuit carbon nitride[30,32] (Eg = 2.7) has recently received substantial attention as a metal free photocatalytic material, which is covered in section 1.8.

1.4 Applications of semiconductor photocatalysis

There has been substantial research and investment in renewable technologies over the last few decades, motivated by an increasing awareness, concern and negative impact of burning fossil fuels. Specifically, photocatalysis has led to the development of green, sunlight assisted methods for environmental cleaning (aerobic degradation of organic pollutants) and fine chemical synthesis to minimise the deleterious effect of existing chemical processes on the environment. The applications of semiconductor photocatalysis are growing as continued research into this field provides novel semiconducting materials and deepens our understanding of its fundamental chemistry. As mentioned before applications of semiconductor photocatalysis can be divided into three main categories: (i) water splitting, oxidation or reduction, (ii) aerobic decomposition of organic and inorganic pollutants (iii) and chemical synthesis.

In this *thesis* three areas of application are covered. One research chapter is dedicated to photocatalytic hydrogen production from water and decomposition of organic pollutants each and two chapters to the relatively new area of organic synthesis using semiconductor material (carbon nitride) and visible light.

1.5 Photocatalytic water splitting/ hydrogen production

1.5.1 Principle, thermodynamics and electronic structure

Crystalline SCs are ordered materials defined by a forbidden energy gap (typically 0.5-2.5 eV), separating the valence band (VB) and conduction (CB). The translational periodicity of crystalline semiconductor structures in bulk form, generates a superset of wave functions (finely spaced molecular orbitals) to form a continuum of energy states, referred to as

bands.[33] At 0 K the lower energy levels (valence band) are filled with electrons while higher energy levels (conduction band) are unoccupied, separated by a characteristic energy band gap (*E*g).

As mentioned before when a semiconductor absorbs photons of energies $E \geq Eg$, electrons in the valence band are excited to the conduction band resulting in generation of exciton. These photogenerated carriers can drive reduction and oxidation reactions if the charge injections into the reactants are thermodynamically favourable.

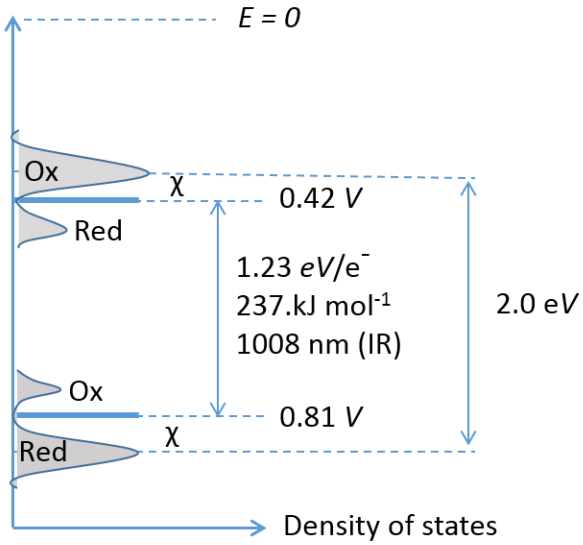

Figure 1.5 Schematics of energy requirements for the water splitting reaction into its component H_2 and O_2. Figure is not to the scale.

The water splitting reaction is non-spontaneous, uphill reaction in which require 237 kJ mol^{-1} (56.6 kcal.mol^{-1} or 1.23eV/e^-) of energy for combustion for mole of water to its component in H_2 and O_2.[34] In case of water dissociation into its elemental components, that is, the formation of molecular hydrogen and oxygen, the thermodynamic requirement (Figure 1.5) is that the standard reduction potentials match the electrochemical potentials of the reactive

electrons and holes, i.e. the potentials for water splitting have to be located within the band gap. For the latter, the band edges are generally taken as approximate values (χ).[e]

$$H_2O \rightarrow H_2 + \frac{1}{2}O_2 \qquad 2.46\ \text{eV} \qquad (1.1)$$

$$2H_2O \rightarrow O_2 + 4H^+ + 4\,e^- \qquad 0.81\ \text{V} \qquad (1.2)$$

$$2H_2O + +2\,e^- \rightarrow H_2 + 2OH^- \qquad -0.42\ \text{V} \qquad (1.3)$$

The minimum band gap is 1.23 eV and potentials of reactive electrons and holes have to be equal or above – 0.42 V and equal or below 0.81 V, respectively. This consideration applies at standard conditions, zero overpotential (η) and zero reorganization energies of the interfacial electron transfer (IFET) reaction a condition never met in practical water splitting.[f] [19] Assuming that the sum of later two energies is about 0.4 eV both for water oxidation and reduction, a semiconductor with a band gap of at least in the range of 2 eV would be more reliable for water splitting.[g] Several inorganic SCs fulfil that requirement.[34–36]

In addition, optical processes in semiconductor materials can be interpreted as creation and annihilation of the electron hole pairs as photons are absorbed and emitted respectively by semiconducting material. All the electronic transitions are subjected to selection rules: besides the requirement of that $h\nu \geq E$g the wave vector k (momentum) should be conserved.[19]

As the plot of energy (E) versus wave vector k (momentum) for the valence and conduction bands in a solid give rise to band structure, two characteristic relevant cases here are shown

[e] The overpotential in the case of photosynthesis in green plants (PS II) is 0.3 V.

[f] The overpotential refers to the potential difference between the standard redox potential and the potential at which the reaction is observed. $E_{op} = 1.23\,V + \eta_{anode} + \eta_{cathode} + \eta_{other}$

[g] Both reorganization energy and overpotential strongly depend on the nature of the semiconductor surface and redox catalyst coated thereon. A rather low overpotential for oxygen formation of 0.41 V was reported for a cobalt phosphate catalyst.[60]

in Figure 1.6. SCs for which the maximum of the valence band and minimum of conduction band are located at the same value of k ($k = 0$) and the absorption of photon is fully allowed are said to have *direct band gap*. The SCs where the minimum of the conduction band is displaced to a large k value, hence the lowest transition entails a change in wavenumber as the law of conservation of momentum requires. For these large k SCs, a phonon in addition to the photon has to absorb because the lowest energy transition between conduction and valence bands is formally forbidden. This type of SCs are said to have an *indirect band gap* and normally have a low probability for a two body process of direct transitions.[h]

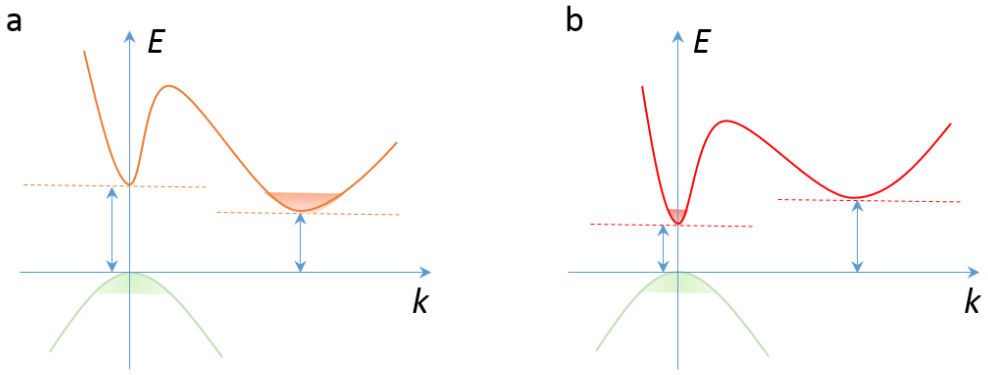

Figure 1.6 Simplified electronic band structure of semiconductor showing (**a**) an indirect-bandgap semiconductor and (**b**) direct-bandgap.

The same selection rules apply to the emission spectrum, when electron comes down from excited states to lower unfilled levels. The annihilation/recombination of exciton results in emission of photon with lifetimes and frequencies characteristics of the band gap across which they recombined.

To conclude the electronic structure *Fermi level* (E_F) is important to be included. From the statistical point of view, the energy at which probability of an energy level being occupied by

[h] In direct band gap materials, photon absorption and subsequent electronic transitions are more likely and have large absorption coefficients compared to three body (photon, electron and phonon) process.

an electron is 0.5 whereas in thermodynamic sense it corresponds to the electrochemical potential of an electron in solid which in pure intrinsic semiconductor lies in middle of the band gap. The fermi level can be positioned near to valence or conduction band by *p-type* (extra holes) and *n-type* (extra electrons) doping respectively. A classic example is doping of silicon with boron and phosphorus. The exact position of E_F depends primarily on the dopant concentration. Also possible is the combination of both *n*- and *p*- type doping in the same structure (*p-n* junctions) which adds to the versatility of the semiconductor structure

1.5.2 Water splitting

Honda and Fujishima reported the first overall photosplitting of water at a semiconductor (TiO_2) electrode under UV illumination.[37] They used a rutile single-crystal photoanode electronically connected to a Pt counter electrode, both immersed in water. The authors described the evolution of oxygen at the TiO_2 as 'photosensitized electrolytic oxidation' and demonstrated that photogenerated conduction band electrons from TiO_2 flowed to the Pt electrode where proton reduction to hydrogen occurred.

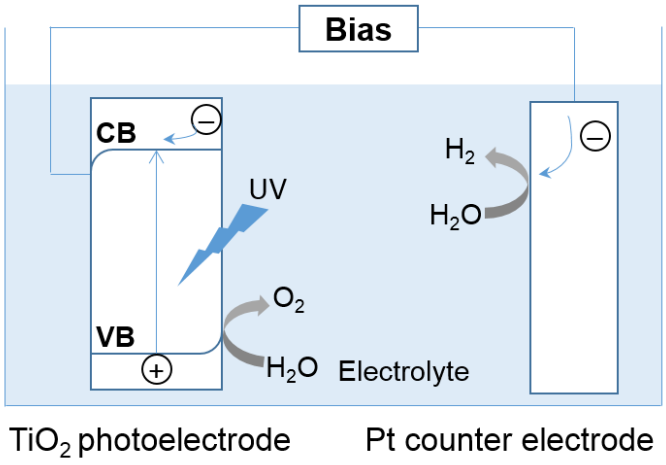

Figure 1.7 Photoelectrochemical cell design for water splitting.

Since this seminal demonstration of semiconductor photolysis, much attention is focused on development of a complementary semiconductor material that may replace the metal electrode. In the late 1970s, Bard *et al.* transformed the photoelectrochemical cell into a simpler powder system by attaching the counterelectrode in the form of a few weight percent Pt nanoparticles onto the titania surface.[38,39] They further draw an analogy between photocatalysis at semiconductor particles to photosynthesis, proposing, in addition to simple one-particle system, also a *Z*-scheme like two particles system which can channel electrons between the two components.[38] Similarly, many semiconductor powdered, colloidal and nanoarchitectures for efficient photolysis driven by solar radiation have been developed.[36,40] Furthermore, employing powder nanoarchitectures photocatalysis, as distinct from a photoelectrochemical cell consisting of two separates electrodes, both H^+/H_2 and O_2/H_2O redox couple occurring simultaneously (or in rapid succession) on the surface of single semiconductor particle have also been demonstrated. [17,41] Despite the significant research and development, commercially viable and efficient semiconductor materials that could alter our global energy economy remain elusive but not impossible.

1.5.3 Requirements for water splitting photocatalysts

Selecting specific semiconductor material for visible light respective photocatalysis is challenging and the difficulty lies in the lack of known materials that meet the requirements of suitable band gap, photostability and visible light absorption, etc. Taking into account for the basic principle, thermodynamics and processes of photocatalytic hydrogen evolution from water (reduction half reaction), several factors are important to develop an efficient photocatalyst, of which three are outlined here. One is that the valence (VB) and conduction

band (CB) potentials relative to H^+/H_2 (0 eV vs. NHE[i]) and O_2/H_2O (1.23 eV vs. NHE) should lie between the band gap of the semiconducting materials. Secondly, as the visible region accounts for 43 % of total solar energy, it is necessary to harvest visible light for effective solar-to-hydrogen conversion because UV light accounts only for a small portion (4 %) of solar energy. Therefore a photocatalyst that can utilize visible light having suitable band gap (1.23 eV < *E*g < 3.26 eV) is desired.[34,36] Even the semiconductors that can satisfy these minimum requirements, still have a low energy conversion from light to hydrogen. It is also of utmost importance that the charge separation in photocatalyst and the redox reactions on its surface must proceed within the lifetimes of photoexcited carriers. A general limitation is the recombination of the electrons and holes (efficiency of any photocatalytic process), which takes place both in the bulk and (where the charge carriers are formed) and at the surface that must be deterred to achieve viable water splitting.

1.5.4 Sacrificial reagents

Indeed, the kinds of photocatalysts that are capable of generating a steady overall water splitting performance under visible light are very limited.[42–44] A possibility to check the reactivity of a SC photocatalyst separately on its hydrogen and oxygen-producing properties is to carry out reactions in the presence of reducing and oxidizing reagents, respectively. The basic principle of photocatalytic reactions using sacrificial reagents is depicted schematically in Figure 1.8. This is achieved adding an electron donor such as methanol ($e_{vb}{}^+$ oxidize methanol instead of H_2O, thus facilitating water reduction) and an electron acceptor such as the silver cation ($e_{cb}{}^-$ reduce electron acceptors instead of H^+, thereby promoting water

[i] The normal hydrogen electrode (NHE) is defined as the potential of a platinum electrode immersed on a 1N solution under a hydrogen pressure of 1 atm.

oxidation) to the reaction solution to measure the photocatalytic activity for the hydrogen and oxygen reactions, respectively.[44] These reagents (more reactive than water) are consumed in the process and are called *sacrificial regents*.[j] Therefore, photocatalytic splitting with the aid of sacrificial agents is regarded as half reactions of water splitting.

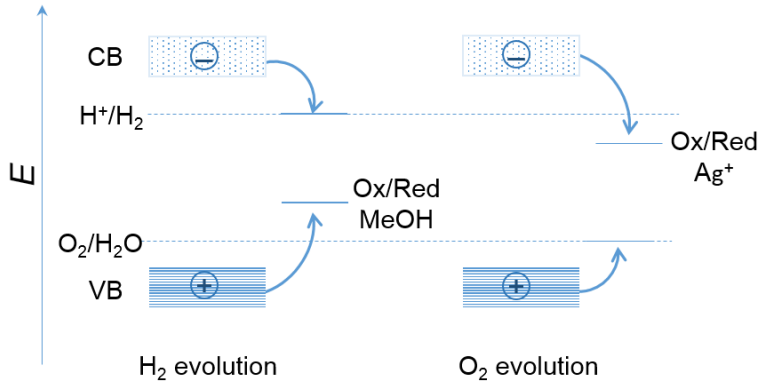

Figure 1.8 Photocatalytic reactions in the presence of sacrificial reagents.

The overall reactions in the presence of methanol (hole scavengers) or silver ions (electron scavengers) can be expressed as follows:

$$CH_3OH + H_2O \rightarrow CO_2 + 3H_2 \qquad (1.4)$$

$$Ag^+ + 2H_2O \rightarrow O_2 + 4Ag^0 + 4H^+ \qquad (1.5)$$

Sacrificial photocatalytic water splitting can proceed as long as the thermodynamic requirements for hydrogen or oxygen evolution are satisfied. Note that a photocatalyst is not

[j] The standard electrode potential for reduction of carbonic acid to methanol (E^0 H_2CO_3/CH_3OH, +0.04 V) is more negative than that for reduction of oxygen to water (E^0O_2/H_2O, +1.23 V). That is, methanol is thermodynamically more easily oxidized than water. Similarly, the standard electrode potential for reduction of proton to hydrogen (E^0H^+/H_2, 0 V) is more negative than that for reduction of silver cation to metallic silver (E^0Ag^+/Ag, +0.80 V). Therefore, silver cation is more easily reduced than proton from the thermodynamic perspective.[42]

necessarily active for overall water splitting even if it is active for both the sacrificial hydrogen and oxygen evolution reactions, because charge separation can be strongly influenced by sacrificial reagents.[36]

1.5.5 Hydrogen evolution reaction (HER)

A great number of SCs,[36,42] including metal free polymeric carbon nitride,[45] have conduction band edge positions negative enough for the reduction of water to hydrogen. To observe H_2 evolution, the valence band has to match the reduction potential of reducing agent. Typical electron donors such as alcohols, alkylamines, sulfides and sulphites, formic acid and EDTA, are used to increase H_2 production by irreversibly oxidizing the reducing agent instead of water, therefore improving the photocatalytic activity.

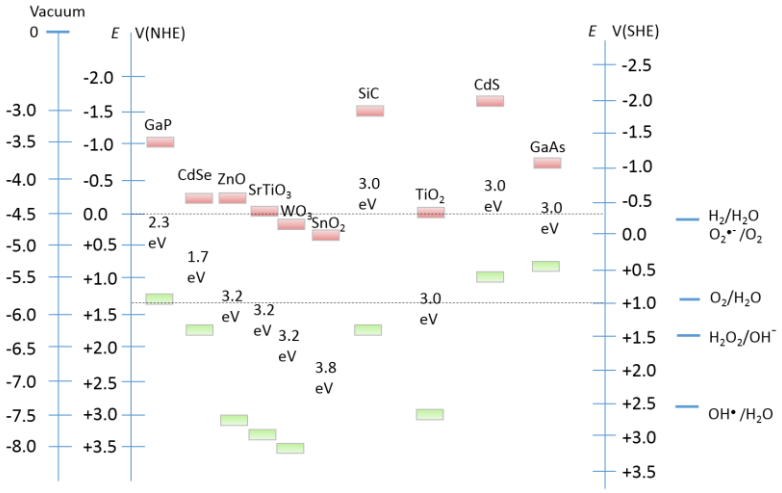

Figure 1.9 Valence and conduction band potentials of common solid semiconductors relative to normal hydrogen electrode (NHE), standard hydrogen electrode (SHE) or the vacuum level[k] as a reference. On the right side the standard potential of water redox couples and radicals is presented against the standard hydrogen electrode potential at pH = 7. Figure modified from reference [46].

[k] The vacuum is the energy level of an electron positioned at rest (within a distance sufficient for the electron to experience the full impact of the surface dipole) outside the solid, *i.e.* with zero kinetic energy with respect to the sample surface. All the potential are noted for pH 7 unless stated otherwise.

The majority of SCs oxides with conduction band potential negative enough for proton reduction and positive enough for water oxidation, such as TiO_2[14,24] and ZnO[25] have a large band gap nonetheless they absorb only a small portion of solar spectrum towards UV region. Although CdS[31] has an ideally suited band gap for visible light capture, it undergo oxidation (S^{-2} to S) by photogenerated holes a process called *photo-corrosion.*

Zuo and Zhang wrote an excellent review on hydrogen evolution reaction (HER), here the only representative elements are briefly stated for contextual purpose.[47] Kubacka *et al.*[36] listed the metal oxide based nanocatalysts for solar photocatalytic applications. A body of work on layered materials in particular metal sulfides; such as crystalline MoS_2, MoS_2, nanoparticles, and MoS_2 nanosheets prepared using different approaches (ball milling, chemical exfoliation, hydro(solvo)thermal and CVD methods) demonstrated good HER activity.[47] Sulfides and selenides of other metals (W, Fe, Co, Ni) have also been found to be active for HER. Among others metal carbide, phosphides and nitrides are also recently been confirmed to show great catalytic activities towards HER.[47] Further detail about the activity of metal free photocatalysts towards HER is given in section 1.11.1.

1.5.6 Evaluation of photocatalytic hydrogen production

In the presence of sacrificial agents,[l] it is difficult to prove experimentally that H_2 originates from water. The actual test is to carry out the reaction in D_2O and analyse the isotopic composition of hydrogen evolved.[48] Formation of D_2 is then usually taken as proof that water is consumed. The activity of photocatalytic hydrogen evolution from water splitting can be evaluated by calculating the amount of hydrogen directly or measuring the amount of

[l] For H_2 evolution reaction using alcohols as sacrificial agents, it is possible that H_2 may come from decomposition of alcohols molecules instead of water splitting.

electrons transferred from SCs indirectly. Nevertheless, a reasonable approximate correlation can be established across the results by normalizing the hydrogen evolution rate within the unit of time or reactant. In this work all the hydrogen evolution rate results are listed in units of $\mu L.\ h^{-1}$ or $\mu L.\ h^{-1}\ g^{-1}$catalyst. The apparent quantum yield can be measured to evaluate the photocatalytic activity of water splitting by the ratio of number of electrons (value calculated back from products i.e., H_2) to the number of incident photons.

1.6 Aerobic Oxidation (photodegradation of organic pollutants)

In addition to solar driven photocatalysis to produce H_2, a major area of application of heterogeneous semiconductor photocatalysis is the aerobic photodecomposition of organic and inorganic pollutants.[21,49] This can be achieved by employing photocatalysts either in solution/suspension (water purification) or embedded within surfaces (self-cleaning windows.).[21,50] Ever since, Frank and Brad demonstrated the decomposition of cyanide in presence of TiO_2, interest in oxidation of harmful compounds using light has grown steadily.[51] The first clear recognition and implementation of semiconductor sensitizers for organic pollutant oxidative mineralization came in 1983 with the work of Ollis and co-workers on the photomineralization of halogenated hydrocarbons, including trichloroethylene, dichloromethane, chloroform and carbon tetrachloride, sensitized by TiO_2.[52]

1.6.1 Redox chemistry in aerobic aqueous systems

As the oxidation of water to oxygen is 4 electron process, thermodynamically allowed at many semiconductor surfaces, it has however a high kinetic barrier. Therefore when other substrates are present in water they preferentially oxidized via one- or two electron transfer

steps.[19] This is the basis of the use of aerobic photocatalysis for environmentally friendly cleaning of air and water.

In presence of air (O_2), in many cases, when exhaustive oxidation of organic and inorganic substrates happens, process is often referred to as *photomineralization* (i.e. oxidation of organic compounds to CO_2, H_2O, and associated inorganic components such as HCl, HBr, SO_4^{2-}).[50] This arises from the formation of photogenerated excitons which in turn generate the radical species ($OH^{\bullet}$, $O_2^{\bullet-}$ or $HOO^{\bullet}$) in water that subsequently initiate reactions and indiscriminately attack the molecules in the surrounding solution (e.g. hydroxyl radical attack of organic dye molecules).[50]

A summary of the most relevant reactions occurring after generation of reactive excitons in such aerated system is described by equations (1.6-1.9) and events happening in surface of the photocatalyst along with the redox potentials (V vs NHE) of species involve in the reaction.

$$O_2 + e^- \rightarrow O_2^{\bullet-} \qquad (1.6)$$

$$O_2^{\bullet-} + 2H^+ + e^- \rightarrow H_2O_2 \qquad (1.7)$$

$$H_2O_2 + H^+ + e^- \rightarrow HO^{\bullet} + H_2O \qquad (1.8)$$

The band–band excitation, produces the reductive conduction band electrons (e_{cb}^-) and oxidative valence band holes (e_{vb}^+). Oxygen on interaction with conduction band electron by taking one electron become superoxide radical ($O_2^{\bullet-}$)(equation 1.6) that is further reduced by another electron (equation 1.7) or reacts with hydroperoxyl radical $HOO^{\bullet}$ i.e., protonated $O_2^{\bullet-}$ to form H_2O_2 (equation1.8).[12,49]

There is broad consensus in the literature on chemical process involved in photodegradation of organics (R) after initial exciton formation.[m] In direct single electron transfer (SET) oxidation organic compounds require to be surface bound or adsorbed in order to interact with holes (h^+) that oxidize the organic substrates into their radicals that undergo a cascade of cleavages leading to simple non-toxic degradation products (equation 1.9).[19]

$$R\text{–}H + h_{vb}{}^{+} \rightarrow RH^{+\bullet} \leftrightharpoons R^{\bullet} + H \rightarrow \rightarrow \quad (1.9)$$

In aerated systems, photogenerated electrons are usually scavenged by O_2 to yield superoxide radical ($O_2^{\bullet-}$) anions (1.6). Indirect oxidation occurs when holes react with surface adsorbed H_2O to produce $^{\cdot}OH$ radicals. This way both the O_2 and organic substrates (R–H) are activated.

$$O_2 + e_{cb}{}^{-} \rightarrow O_2^{\bullet-} \quad (1.6)$$

$$H_2O + h_{vb}{}^{+} \rightarrow OH^{\bullet} + H^{+} \quad (1.10)$$

The oxygen and hydroxyl radicals formed in Equation 1.6 1.8 and Equation1.10 subsequently create a cascade of radical reactions, that usually have low or non-barriers, resulting in the facile oxidative degradation of organic substrates (Equations 1.11-1.13).[19,49]

$$R\text{–}H + OH^{\bullet} \rightarrow R^{\bullet} + H_2O \quad (1.11)$$

$$R^{\bullet} + O_2 \rightarrow ROO^{\bullet} \rightarrow \rightarrow O_2/H_2O \text{ Degradation} \quad (1.12)$$

$$R\text{–}H + OH^{\bullet} \rightarrow HROH^{\bullet} \rightarrow \rightarrow O_2/H_2O \text{ Degradation} \quad (1.13)$$

In the photocatalytic degradation, the net result is the transformation of organic pollutants into their degraded final products by absorption of light, while the photocatalyst is not

[m] Therein, R symbolises almost any functional group such as OH, CHO, CO_2H, NH_2, and SH.

consumed. [49] Given that O_2 is the only species capable of interacting with photoexcited electrons in the valence band (other than adsorbed organics), oxygen concentration is the critical factor determining the photocatalytic efficiency. Molecular oxygen is sometimes referred to as an *electron trap* that suppresses direct exciton recombination.[17]

The general classes of compounds that have been degraded, although not necessarily completely mineralized by semiconductor photocatalysis, include: alkanes, halo alkanes, alcohols, carboxylic acids, polymers, surfactants, herbicides, and dyes.[49,50] The materials for the decomposition of organic dyes in aqueous solution, based on carbon nitride are discussed in particular, in Chapter 5. In addition to organic compounds, a wide variety of inorganic compounds are sensitive to photochemical transformation on a SC surface. Examples include: dechlorination of CCl_4, ammonia, chromium species, copper cyanide, gold halide ions, iron and manganese species, mercury, nitrates, nitrites and nitric acid, ozone, sulfur species, etc.[50]

1.7 Chemical synthesis and transformations

SC photocatalysis can be used to drive various useful chemical photooxidation and photoreduction processes in chemical synthesis.[6,53] After the inspiring observation of photo-Kolbe reaction (equation 1.14), (irradiation of TiO_2 suspension in acetonitrile in presence of deuterated acetic acid with UV light afforded CH_3D and CO_2 as major products and 5 % ethane), many papers appeared dealing with photocatalytic organic reactions in presence of colloidal or suspended SC particles.[54] In general reactions, photogenerated electrons and holes are usually used in non-aqueous media to avoid oxygen and hydroxyl free radical formation, necessary for selective product formation. A comprehensive review of selective organic transformations and heterogeneous photocatalysts can be found in reference [55] and [5], respectively. Only representative examples of some typical conversions in an attempt to

represent the versatility of these methods are briefly cited below, however, a detailed discussion on specific reactions relevant to the work presented in this thesis using carbon nitride photocatalyst is given in section 1.11.3 an in Chapter 6 and 7.

1.7.1 Oxidation and Oxidative cleavage

Photooxidation is, by far, the most important class of known photocatalytic reactions of organic substrates. Virtually every organic functional group bearing either a nonbonded lone pair or any π conjugation can be activated toward TiO_2-photocatalyzed oxidative reactivity, either by dehydrogenation, oxygenation, or oxidative cleavage.[22] Examples in this class include: anaerobic photodehydrogenation of ethanol to acetaldehyde over irradiated TiO_2, oxidation of alcohols in acetonitrile,[56] and in water[57].

1.7.2 Reductions

Photocatalytic reductions are less common than oxidations. This is because the photogenerated electron in the CB of photoactive SCs has less reducing power than the oxidizing power of a photogenerated valence band holes. Besides, most of the reducible substrates do not compete kinetically with oxygen in trapping photogenerated conduction band electrons.[22] Hence in most cases, for photocatalytic reduction reactions to occur a co-catalyst (e.g. Pt, Pd, ZnS) is also required. Usually the co-catalysts are also active as hydrogenation catalysts.[58] In fact, the formation of photoreduction products is often accompanied by hydrogen (H_2) evolution, implicating a competition for surface-bound hydrogen. Examples include: CdS-mediated photoreduction of aqueous solutions of CO_2, reduction of acetylene to ethylene or ethane on colloidal aqueous dispersions of TiO_2 suspensions loaded with MoS_4^{2-}.[59]

1.7.3 Isomerisations

Geometric and valence isomerisations of unsaturated organic molecules occur on illuminated semiconductor catalysts.[22] Examples include: *cis-trans* isomerization of several simple alkenes on suspended particles of ZnS, and CdS, and vanadium oxides, usually in polar inert solvents.[60]

1.7.4 Substitutions, Condensation and polymerizations reactions

The selective photofluorination of olefins, phosphines, and phosphites on illuminated TiO_2 in the presence of AgF in acetonitrile produces,[61] in most cases, a single fluorinated product. Biologically important molecules, such as amino acids and nucleic acids have been assembled in very low yield by semiconductor-mediated photolysis of simpler organic and inorganic components.[22] Polymerization is usually observed only when oxygen and water are absent from a heterogeneous photocatalysis mixture.[62]

1.8 Carbon nitride based materials

1.8.1 Introduction

The search for suitable SCs for heterogeneous photocatalysis to optimise existing or design novel chemical processes with aim to minimise the environmental impact is one of the persistent goals of sustainable chemistry. An optimal material would combine an ability to absorb light in the visible range and high structural stability in extreme chemical and thermal conditions. Besides, it should be non-toxic, abundant and easily processable. Traditional inorganic SC materials are limited in the nature of their active sites and thus the scope of

applications that they can accomplish.[63,64] Mostly explored SCs materials so far are constructed from transition metal ions with d^0 or d^{10} electronic configuration, along with group VA or VIA ions as counter-anion components.[22,65–67] However, the main difficulty in the systematic optimisation of metal or metal oxide catalysts is the substantial chemical complexity of empirically optimised heterogeneous catalysts; rarely have these structures been targets of systematic optimisation.[32,45,64] On the other hand organic polymeric catalysts have the advantage of flexibility for optimization yet suffer from serious swelling and stability problems.[64] It is extremely desirable to have photoactive, stable, system that could allow large variation in the structure without having to change the overall composition.

Graphitic carbon nitride (C_3N_4) is one such highly active heterogeneous catalyst − at least as a starting point − that meets above mentioned requirements. Diamond like (β)C_3N_4 is predicted to be of similar hardness and low compressibility as of diamond whilst graphitic C_3N_4 is recognized as the most stable allotrope under ambient conditions.[63,68] The history of C_3N_4 can be traced back to the embryonic form, "melon"[n], made by Berzelius and named by Liebig in 1834 is regarded as one of the oldest synthetic polymer.[32,63,68] The framework topology of linear polymer "melon" is presumably consisting of interconnected tri-s-triazines via secondary nitrogens, while defect-rich C_3N_4 is in the form of p-conjugated planar 2D sheets of poly(tri-s-triazines) interconnected via tertiary amines.[68,69] The perfect g-C_3N_4 comprises solely of C and N bonds without electron localization in the π state has not been synthesised yet.[70] This difficulty of synthesising perfect carbon nitride is widely acknowledged as being a predominantly kinetic problem, and medium to poor crystallinity and a high degree of disorder of the as synthesized material are typical for all active products.[32,45,63] Real materials, like those prepared by polycondensation of dicyandiamide,

[n] A linear polymer of tri-s-triazine units

contain traces of hydrogen, in the form of primary and/or secondary amine groups on the terminating edges, thus promoting electron delocalisation on the surface, inducing Lewis-base character toward metal-free coordination chemistry and catalysis.[45,71] Besides, the polymeric character warrants the easy control of surface chemistry via molecular-level modification and designing.

From the viewpoint of applied photocatalysis, until now, all the active C_3N_4 materials are defective in terms of stacking pattern, grain boundaries and surface termination. Nevertheless, the crystalline perfection "only" adds to the bulk properties, such as the graphitic organisation, high thermal and chemical stability, and semiconductor electronic structure.[45,72] Likewise, the polymeric nature of C_3N_4 also assures adequate flexibility of the structure, which assists as a host matrix of exceptional compatibility to numerous inorganic nanoparticles; this later feature is very valuable for the design of C_3N_4 based composite materials.[32,68]

1.8.2 A brief development history of carbon nitride

As already mentioned, the history of carbon nitride and its precursors can be traced back to very early days of Berzelius and Liebig in1834 (as described in references [32,45,68]). In 1922 Franklin in structural pursuits of these compounds suggested that C_3N_4 might be the final deamination product of the series of ammono carbonic acids.[73] However, the tri-s-triazine unit as the basic structural motif of these polymeric derivatives was first pointed out by Pauling and Sturdivant in 1937.[74] Later, Redemann and Lucas recognised a close semblance between melon and graphite, describing Franklin's carbon nitride as a probable oligomeric condensation product of 2,5,8-triamino-tris-s-triazine; that is, $C_{126}H_{21}N_{175}$.[75]

Acknowledging these findings it is consensus now that one single structure should perhaps not be assigned to melon as it possibly is a mix of polymers of different size and architecture.

The synthesis and characterization of C_3N_4 is a challenging task by itself, and until today, a large number of different experimental attempts have been made.[63,76–82] A slight change in synthetic conditions yields an altered product and the reason why some structures remained unclear in detail until today is their chemical inertness and their insolubility in virtually all solvents. Despite the fact that carbon nitride was known for a more than a century, in 1990 theoretical prediction of new low compressibility sp^3-bonded phase rekindle the interest to synthesise the material. However, the synthesis of single-phase sp^3-hybridized carbon nitride material[83,84] turned out to be a challenge because of its low thermodynamic stability. [85]

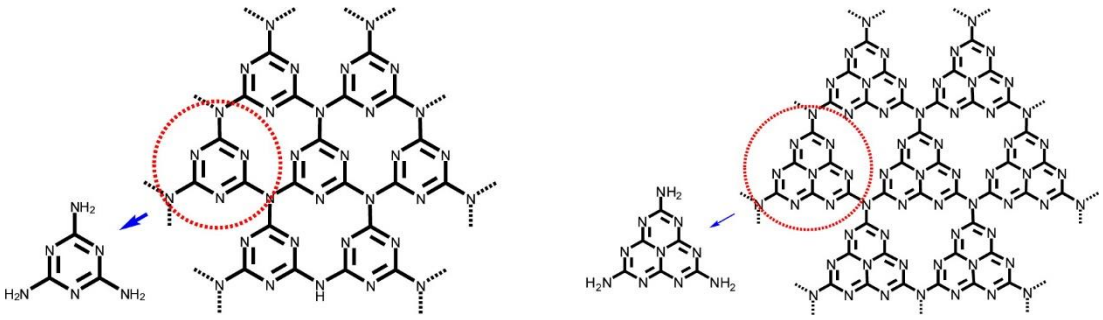

Figure 1.10 *s*-Triazine (left) and tri-*s*-triazine as building blocks of g-C_3N_4, reproduce from reference [45] with permission.

The synthetic elusiveness, inertness and high degree of disorder in as synthesised material constitutes the difficulty of acquiring experimental data, there are speculations about the actual existence of a graphitic material with idealized composition C_3N_4. Inspired by the structure of graphite, triazine (C_3N_3) had been put forward as fundamental building blocks (Figure 1.10

);[86–91] however, another possible block, tri-s-triazine (heptazine) rings, which are structurally related to the hypothetical polymer melon,[32,45,63,73] were found to be energetically favoured with respect to the triazine-based modification.[91,92]

The fact that melem (triamino-tri-s-triazine) readily formed during heating of dicyandiamide might be indicative of a generally higher thermodynamic stability of tri-s-triazine derivatives and maybe even their oligomers and polymers as compared to those derived from s-triazine.[79,80] Recent experimental work indicated that polymer is a built up from melem units, confirming that this tecton is the most stable local connection pattern.[32,63] Whereas the theoretical work also indicated C_3N_4 to be the most stable allotrope at ambient conditions.[84,87]

1.8.3 Design of C_3N_4 based photocatalysts

Carbon nitride materials are extremely sensitive to the selection of precursors, atmosphere, and doping which sets the basis for structural diversity and modification. Building on this fact, relevant synthetic procedures for carbon nitride materials, some of these applied in this thesis are summarised below.

1.8.3.1. Synthesis of pristine C_3N_4

Synthesis of carbon nitride can be conducted either in inert atmosphere (e.g., N_2, Ar) or in an air atmosphere, with no significant changes in the bulk structure but may lead to differences in the product yield, degree of condensation and especially, surface properties (Table 1.1). The most common precursors used for chemical synthesis of C_3N_4 are reactive nitrogen-rich and oxygen-free low cost compounds such as cyanamide, [93] dicyandiamide, [65] melamine,[94] thiourea, [95] or mixtures thereof.[96,97]

Table 1.1 Bandgaps and specific surface areas for the typical C_3N_4 synthesis from different precursors. (Table is reproduce/modified from reference [68] with permission).

Precursor	Reaction temperature, time and atmosphere	Band gap [eV]	Surface area [m^2 g^{-1}]
Cyanamide	550 °C, 4 h	2.70	ca. 10
Melamine	500 °C, 2 h, air	2.80	ca. 8
	580 °C, 2 h, air	2.75	ca. 10
Dicyandiamide	550 °C, 2 h, air	2.75	ca. 10
Thiourea	450 °C, 2 h, air	2.71	ca. 11
	550 °C	2.58	ca. 18
	650 °C	2.76	ca. 52
Urea	550 °C, 0 h, air	2.72	ca. 31
	550 °C	2.68	ca. 62
	550 °C	2.72	ca. 75
	550 °C	2.78	ca. 288
Sulfuric acid treated-melamine	600 °C, 4 h, Ar gas	2.69	ca. 16
Sulfur-mixed melamine	650 °C, 2 h, N_2 gas	2.65	ca. 26
Guanidine	550 °C, 2 h, N_2 gas	2.74	ca. 8
Thiocyanate	700 °C, 2 h, N_2 gas	2.89	ca. 42

The condensation pathways from cyanamide to dicyandiamide to melamine (350-390 °C) (by release of ammonia) and all other C/N materials are good synthetic routes to generate slightly defected polymeric species.[63,71] Condensation of these units to polymer, networks and to potentially the final polymeric C_3N_4 occurs at around 520 °C and formation of low thermodynamic stability prebonded C−N core structures such as triazine and heptazine, is the reason behind the generation of defect materials. Material is unstable slightly above 600 °C which on heating to 700 °C results in the residue-free disappearance of the material *via* generation of nitrogen and cyano fragments. Comprehensive reviews on use of different

precursors for synthesis and structural part of carbon nitride are given by Antonietti,[32,45,63] Blinov,[72] Carabineiro,[71] and Matsumoto.[98]

The *ab initio*, DFT studies on reaction steps reveal that the cohesive energy[o] of the molecules increase along the polyaddition path as summarised in Figure 1.11.

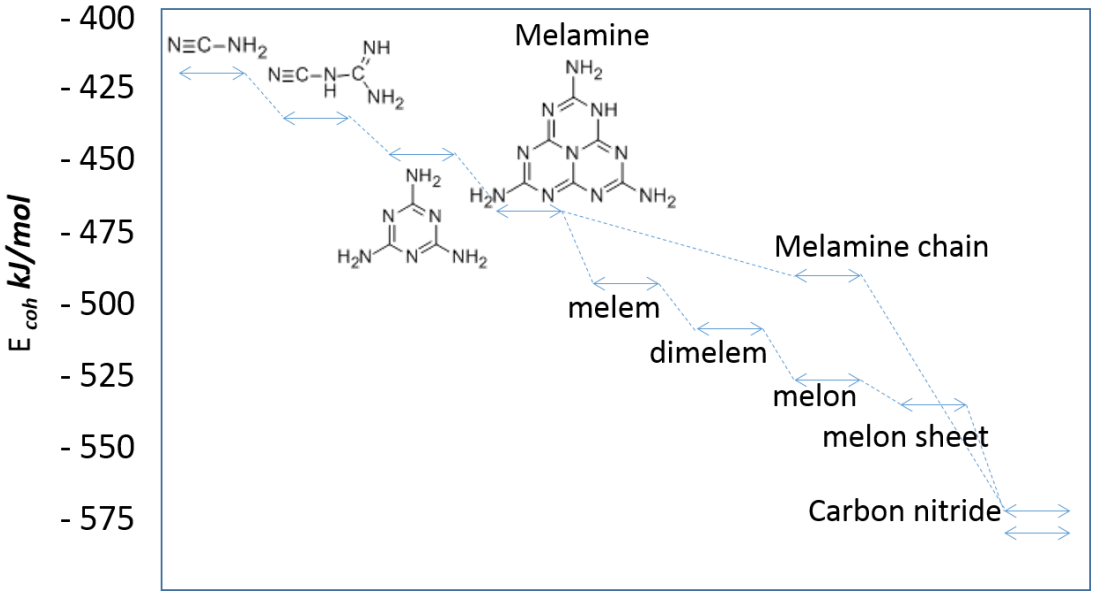

Figure 1.11 Calculated energy diagram for the synthesis of carbon nitride. The condensation of cyanamide proceed via the triazine route (dash-dot line) to C_3N_4, or melamine can form melem and then follow the tri-s-triazine route (dashed line) to form C_6N_8 modified from reference [63] by permission of The Royal Society of Chemistry.

As the intramolecular bonds give the dominant contribution to the cohesive energy, therefore total energy calculations for the molecules confirmed that melamine is formed from the stepwise heating cyanamide precursor. In addition, melam (melamine dimers) are probably

[o] The strong covalent bonds inside the molecular building blocks and forces that hold crystal together by weak interactions, such as hydrogen bonding and van der Waals interactions and the intramolecular bonds energies give the dominant contribution to the cohesive energy. Here it is taken as total energy calculations for the molecules.

formed as metastable intermediates and that melem is the likely product after polymerization as the cohesive energy increases from melamine via melam to melem.[92,99,100] This suggests that the polymerization via the tri-s-triazine path is preferred. The melem units thus formed undergo further condensation into a melon chain, by further release of NH_3 molecules where the competition between energy gain of extending p-electron system into linear chain and the repulsion N atoms on the edge of the tri-s-triazine units determine the shape. It is proposed that the strongly buckled melon chain constructed from dimers, where the top corner is connected to a side corner, form a staircase shape which is 20 kJ mol^{-1} more stable than a linear chain.[79,92,100] Whilst the final polymerization structure is held together by hydrogen bonds between the NH_2 groups and the N edge atoms which is more stable than the isolated melon chains by 63 kJ mol^{-1}. [63]

The heptazine ring structure and high degree of condensation allow metal free carbon nitride to possess many advantages such as good physicochemical stability (discussed in section 1.9), as well as unique electronic structure with medium band gap 2.7 eV. These distinctive features make carbon nitride a favourable candidate for visible light induced photocatalysis. However, photocatalytic ability of pristine carbon nitride is hampered by fast recombination rate and low visible light utilization efficiency. In subsequent sections strategies have been discussed in an attempt to address these problems.

1.9 Properties of carbon nitride

1.9.1 Thermal and chemical stability of carbon nitride

It is important for a photocatalyst to be thermally stable and chemically inert when it is employed in catalytic reaction under extreme conditions. Unlike other organic materials that usually suffer from low thermal stability, carbon nitride is robust and nonvolatile.

Thermogravimetric analysis (TGA) of the material reveals that it is stable up to 600 °C in air, a value which is one of the highest among organic materials. For instance, higher stability than those of all high-temperature polymers, such as aromatic polyamides and –imides is encountered. Further heating of carbon nitride leads to an endothermal peak at 630 °C, paralleled by consecutive weight loss, showing total thermal decomposition and complete vaporization of the fragments. However, variations in thermal stability were noted for carbon nitride prepared from different precursors, probably due to the variations in degree of condensation and change in packing motifs. [65,93–97]

Chemical stability of photocatalysts is an essential feature for photocatalytic reaction applications. As mentioned in section 1.3 most of the metal oxides having wide band gap are only active in UV region and often generate metal waste during photochemical reactions. Likewise, visible light active, metal sulfides are susceptible to leaching and photocorrosion. Conversely, metal free carbon nitride is active in visible region, has graphite like stacking with optimised van der Waals bonding between the layers, and is chemically inert in extreme pH conditions, features deemed crucial for photocatalytic reactions. Furthermore, carbon nitride is virtually insoluble in most of the conventional solvents, including water, alcohols, DMF, THF, diethyl ether and toluene with no detectable reactivity.[101] However Zhou *et al*. recently demonstrated the dissolution in concentrated sulfuric acid. These author argued that acid protonated the carbon nitride to induce electrostatic repulsion and the intercalation that results eventually in interlayer separation.[102] As an another exception, treating C_3N_4 in molten alkalihydroxides resulted in a hydroxolysis of the structure.

1.9.2 Optical and electrochemical properties

Polymeric carbon nitride shows the typical absorption pattern of an organic semiconductor with a very strong, stepwise gap and UV/Vis adsorption at about 420 nm. It generally exhibits strong blue photoluminescence at room temperature over a wide range (430–550 nm) and has a maximum at about 470 nm. These values vary with the slight difference in preparation methods and conditions thus affecting the absorption edge of carbon nitride, which arises from differences in local structure, and packing defects specific to the preparation or modification processes. Further these properties can be easily tuned with elemental and molecular doping. For example doping of S, (blue shift) B, F and P and barbituric acid, (red shift) can modify the texture, bandgap and the redox ability.[103–111]

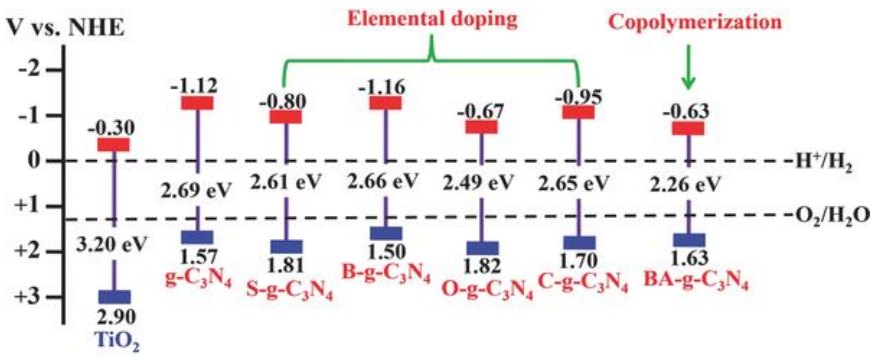

Figure 1.12 Schematic illustration of the band structures of Carbon nitride with elemental and molecular doping. Band positions of TiO_2 are also given. (Figure taken from reference [68] with permission)

In photoelectrochemical applications, the generation of photocurrent was observed on C_3N_4 under the illumination of visible light ($\lambda > 420$ nm).[111–113] At present the value for photocurrent generation is rather low. However, it is envisaged that structural and textural modifications can partly improve the photocurrent generation of carbon nitride

photoelectrode.[111–113] The limitations of grain boundary defects and the inability to synthesize larger domain sizes carbon nitride having high crystallinity with current synthetic methods, the photocurrent is still remained very low.

1.10 Strategies to improve the photocatalytic performance

The bottleneck affecting the photocatalytic efficiency is the recombination of photogenerated excitons with successful initiation of intended redox chemistry. This results in energy loss either in the form of light energy or heat[p] inhibiting the photocatalytic material for real world applications. This inefficiency is generally referred to an internal recombination in literature, but it is noted that exciton recombination can also occur on the surface of the photocatalyst.[17]

Several strategies are in vogue to inhibit this inefficiency and improve the photocatalytic performance. Two strategies with reference to the carbon nitride employed in this thesis namely, i) construction of heterojunction and ii) doping are discussed in detail.

1.10.1 Heterostructured carbon nitride type II heterojunctions

It is already mentioned that carbon nitride structures are extremely sensitive to the synthesis conditions such as temperature, choice of precursors and doping, which set the base for band structure modification. The electronic interface between distinct layers of semiconductor is responsible for the unique properties of heterostructures. Thus the semiconductor heterojunction has been an effective architecture to enhance photocatalytic activity by promoting photogenerated charge separation Depending on the combination of SCs

[p] Fluorescence emission or non-radiative lattice relaxation process discussed in section 1.2.2.1

comprising the different carbon nitride materials can create spatial charge separation that is favourable for photocatalysis. Heterojunctions are classified in terms of type depending relative band offsets between the valence and conduction bands: in type I larger band gap entirely straddles the smaller one, in type II band gaps are in staggered arrangement and in type III band gap do not share any overlap (Figure 1.13)

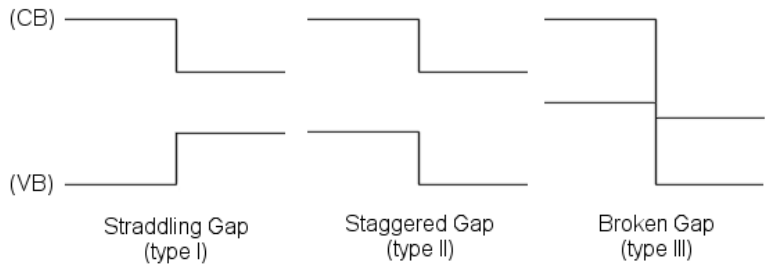

Figure 1.13 Three types of semiconductor heterojunctions organised by band alignment. CB: conduction band; VB: valence band.

Of particular interest are type II heterojunctions which result in the movements of electron and holes across the semiconductor junction. This band alignment design of SCs is generally adopted to promote the dissociation of excitons and facilitate the subsequent collection and separation of charge at the interfaces of two SCs, minimizing charge recombination.

1.10.2 Carbon nitride/layered material type II (metal free) heterojunctions

Many combinations of modified carbon nitride materials are capable of forming type II heterojunctions, in which both the CB and VB positions of the C_3N_4 are either higher or lower than those of semiconductor. The difference of chemical potential between the two semiconductor units results in band bending at the contact interface of the heterojunction. This band bending induces a built-in electric field, which can drive the opposite migration of

photogenerated electrons and holes.[114] Moreover, the creation of tight junctions between two SCs not only depends on the electronic structure of the SCs but also on other material properties, such as electron affinity and work function.[115]

Earliest report of heterostructured carbon nitride layered material (graphene) heterojunctions appears to be by Sun *at al.* in 2010 which described seemingly improved electrocatalytic performance on oxygen reduction reaction (ORR).[116] This was quickly followed by Xiang *et al*.'s utilization of C_3N_4/graphene heterojunction for visible light photocatalytic H_2 production.[117] They obtained the heterostructured material by combining a impregnation-chemical reduction strategy where graphene assisted the electron transfer during photoreaction.

Since the reports of aforementioned work, a large number of novel semiconductor heterostructures carbon nitride materials have been developed for broadening the applications of C_3N_4-based coupled heterojunctions. For instance, these excellent C_3N_4 based non-metal heterojunctions includes MWNTs (multi-walled carbon nanotubes)/C_3N_4,[118,119] polypyrrole/C_3N_4,[120] C_3N_4/sulfur-doped C_3N_4 (CN/CNS) [105] and C_{60}/C_3N_4,[121] etc. An exhaustive list is given in reference [122]. The photocatalytic performance of these non-metal heterostructures was superior to that of pristine carbon nitride in all cases and attributed to exciton separation across contact junctions between the coupled materials.

In an approach based on the band alignment by coupling one layer over the other non-metal layer, this strategy for carbon nitride was further advanced by Wang *et al.* by constructing CN/CNS isotype[q] heterojunctions by depositing the layer of sulfur doped carbon nitride over C_3N_4.[105] The design exploit docking sites containing -NH_2 groups on the surface for chemical

[q] The combination between two *n*-type or *p*-type semiconductors that have appropriate band offset are called isotype heterojunctions.

modification and the slight difference in their electronic band structures. The resulting CN-grafted CNS hybrids, close-contact polymeric isotype heterojunction demonstrated effective charge separation and enhancement in the photocatalytic activity for hydrogen evolution. Time resolved photoluminescence studies (Figure 1.14b) reveal that exciton recombination was greatly suppressed with the localization of electrons in one side (CNS) and holes in the other side (CN) by the band offsets. In addition, the lifetime (τ_2) of charge carriers in CN/CNS (12.94 ns) was 2.15 ns longer than that of parent CN (10.79 ns).[105]

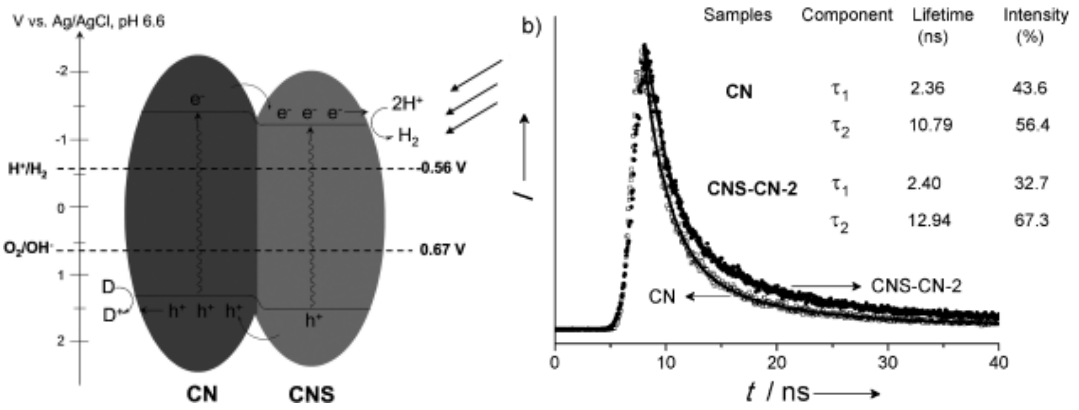

Figure 1.14 Schematic illustration of the heterojunction formed between CN and CNS b) time-resolved photoluminescence spectra monitored at 480 nm under 420 nm excitation for CN and CNS–CN reproduced from reference [105] with permission.

In a similar report CN-thiourea/CN-urea (CN-T/CN-U) metal-free isotype heterojunctions were constructed *in situ*, using the band alignment approach using composite molecular precursors consisting of urea and thiourea and treated simultaneously under the same thermal conditions Figure 1.15.[96] Upon visible light irradiation, the photogenerated electrons transfer from the CB of CN-T to CN-U, driven by the conduction band offset of 0.10 eV, whereas the photogenerated holes transfer from the VB of CN-U to CN-T driven by the valence band

offset of 0.40 eV. This novel metal-free isotype heterojunction was demonstrated to promote charge separation and prolong the lifetime of charge carriers. This results in a significant enhancement in the photocatalytic activity for NO removal under visible light irradiation.[96] In very recent article CN and boron modified CN organic isotype semiconductor heterojunction was also shown to have enhanced visible light photocatalytic activity.[123]

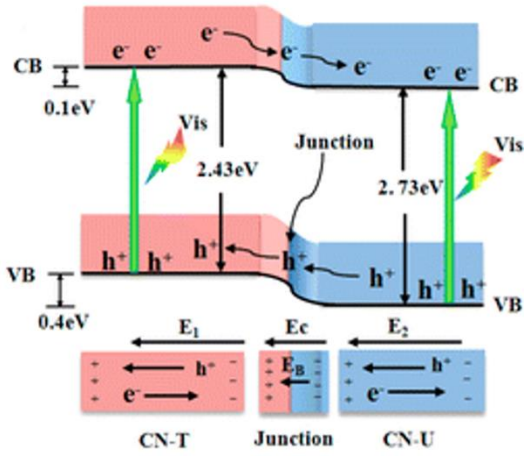

Figure 1.15 Schematic illustration of charge separation and transport at the g-C_3N_4/g-C_3N_4 heterojunction interface and in both semiconductors synthesise using urea/thiourea composite molecular precursor.Reproduce from reference [96] with permission.

Inspired by these studies a new CN/CN heterojunction system from same precursor (dicyandiamide) was successfully constructed in this work (presented in chapter 4) and resulting heterostructure materials showed enhanced photocatalytic hydrogen production.[124] These successful attempts show that the application specific design and construction of isotype heterojunctions could open up a new avenue for the development of new efficient visible-light photocatalysts.

1.10.3 Carbon nitride /metal oxide/sulfide heterojunctions

Another strategy to enhance visible light photocatalytic performance of carbon nitride (CN) is to couple it with metal oxide SCs. The band structure of appropriately matched materials assists the separation and transfer of photogenerated charges across the interface that effectively impedes the recombination rate. Moreover, in heterojunctions suitable band positions and creation of interfaces also enables and extend the optical absorption range of the coupled materials.

Applying this approach several researchers independently reported the fabrication of carbon nitride-TiO_2 heterostructures. The resulting C_3N_4-TiO_2 heterojunctions showed enhanced visible light photocatalytic activity towards methylene blue (MB) degradation, reduction of hazardous Cr (VI) ions and for formaldehyde decomposition in air.[125,126] Similar to this in C_3N_4-WO_3 heterojunction have been prepared. For instance, Zang *et al.* obtained environmentally benign C_3N_4-WO_3 composites via a facile mixing–heating procedure, which showed superb performance in photodegradation of methyl orange (MO).[127] In other applications C_3N_4/WO_3 heterojunction were employed for degradation of MB, 4-chlorophenol, [128] and to decontaminate the organic gas pollutant acetaldehyde (CH_3CHO).[129] The remarkably high performance of WO_3-C_3N_4 was mainly ascribed to the synergistic effects of the enhanced optical absorption in the visible region, enlarged specific surface areas and suitable band positions.

Similarly, utilising the same principle, a number of photocatalytic heterojunctions have been developed by combining different types of photocatalysts. For example, C_3N_4-TiO_2,[130] C_3N_4-ZnO,[131] C_3N_4-CdS,[132] C_3N_4-TaON,[133] C_3N_4-$SrTiO_3$,[134] C_3N_4-Bi_2WO_6[135], and C_3N_4-$BiVO_4$[136] and a comprehensive updated list of carbon nitride/metal oxide heterojunctions can be found in reference [122]. In all examples reported increase in catalytic efficiency was

attributed, similar to the reasons mentioned for metal free carbon nitride heterojunctions, to the dissociation of excitons and subsequent collection and separation of charge at the interfaces of two SCs, which deter the exciton recombination significantly. [115] Hence, this strategy is very useful for the design of material for specific applications.

1.11 Application of Carbon nitride

Carbon nitride is a medium-bandgap SC and in that role an effective photocatalyst and chemical catalyst for a broad variety of reactions. Its interesting properties such as high thermal and photochemical stability, ease of chemical modification, medium band gap and low cost makes it suitable for range of applications.

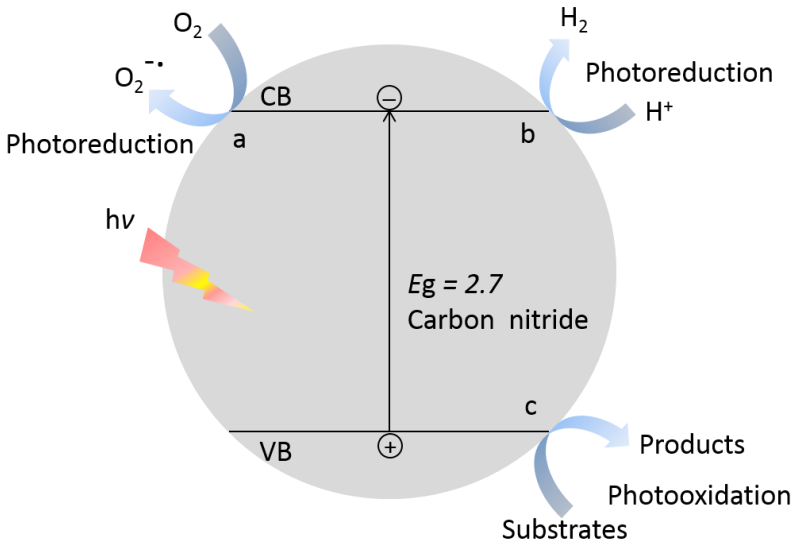

Figure 1.16 Strategies to realize visible light induced heterogeneous photocatalysis: (a) hydrogen evolution from water, (b) photochemical activation of O_2, and (c) photocatalytic oxidation or degradation of organic substrates.

In particular carbon nitride is attractive for its promise to resolve the growing environmental pollution problem and energy crisis in feasible way utilizing inexhaustible sunlight and avoiding secondary contamination. In following section some of the recent, most remarkable examples relevant here are summarised.

1.11.1 Carbon nitride as photocatalyst for water splitting

A fundamental discussion about the principle of water splitting, requirement and introductory summary of most common reaction and materials is covered in section 1.5, here the predominant focus is on carbon nitride. Ideally, the required energy to produce hydrogen from water as given in equations (1.1-3) is 1.23 V. However, the overall four-electron water oxidation encounters a large overpotential which makes photon of energy of 1.8 V or above, practically suitable for this reaction (section 1.5.1). This corresponds to a wavelength of light of 690 nm or less. Most importantly, both the HOMO and the LUMO of the semiconductor photocatalyst should encompass the oxidation and reduction potential of water.

C_3N_4 holds all these prerequisites for a water splitting; catalyst has the correct electronic structure with an appropriate band gap of 2.7 eV, corresponding to an optical wavelength of 460 nm and band position straddling the redox potential of water as shown in Figure 1.12. This band gap is sufficiently large to overcome the endothermic character of the water-splitting reaction for both photocatalytic water reduction and oxidation reactions due to its appropriate CB and VB positions. Moreover, C_3N_4 exhibits an appropriate microstructure, with surface termination with defects and nitrogen atoms for electron localization or for anchoring the active sites.[105,112]

Although only a few reports on photocatalytic oxygen evolution and overall water splitting exist [65,93,97,137–139], the utilization of C_3N_4 as a photocatalyst for hydrogen evolution has been

intensively studied in recent years. The detailed discussion on hydrogen production using carbon nitride can be found in excellent reviews.[32,45,68,116] Here it would be appropriate to selectively mention the reports and modification that are strictly related to the strategies explored in this work.

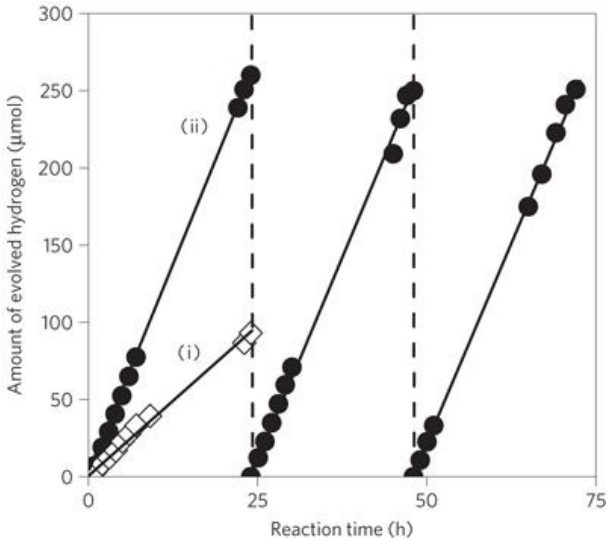

Figure 1. 17 Stable hydrogen evolution from water by C_3N_4. A typical time course of H_2 production from water containing 10 vol% triethanolamine as an electron donor under visible light ($\lambda > 420$ nm). Squares represent rate of H_2 production on unmodified C_3N_4 (i) while circles represent the rate of H_2 production on 3.0 wt% Pt-deposited C_3N_4 photocatalyst. The reaction was continued for 72 h, with evacuation every 24 h (dashed line). Reprinted with permission from Macmillan Publishers Ltd: *Nature materials*, reference [65], copyright (2009).

Carbon nitride catalysts exhibit activities for hydrogen production in the presence of proper sacrificial agents even in the absence of noble metal cocatalysts[r] (Figure 1.17). A range of methods and modifications have been used to explore and optimise the H_2 evolution activity. In an initial development Wang *et al.* reported hydrogen production from water under

[r] Cocatalyst is thought to be essential for viable hydrogen production from CN. In most commonly employed cocatalysts are Pt, Ru, and Au and quantities used are as low as 0.1-3%.

visible light using carbon nitride which was synthesised by heating cyanamide at 550 °C.[65] To achieve the stable H_2 production a small amount of Pt (3%) was photodeposited which facilitated the electron transfer in conduction band to speed up the HER. This was presumably due to kinetic effect as the splitting of a Pt-H bond have lower kinetic hindrance than splitting of N-H bond. Since then several reports emerged with the emphasis on the optimisation of the surface area by formation of a porous structure to provide mass-diffusion channels for enhance photocatalytic H_2 production[140] and references cited in [68]. It is also shown that elemental doping (B, S, F and P) and molecular doping (barbituric acid) can modify the texture, bandgap for desired redox activity.[103–110] As mentioned in section 1.10, CN-CNS,[105] CNT-CNU[96] and CN-Boron doped CN (CN-CNB) [123] have improved visible light photocatalytic activities due to heterojunction formation likewise several studies showed that the construction of semiconductor–semiconductor heterojunctions could promote charge separation. [45,68,122]

Interestingly, photocatalytic H_2 evolution activity of from C_3N_4 prepared from various precursors differs due to the variation in structures.[32,45,63,68]s For example, recently it was reported that urea-derived structure controlled C_3N_4 exhibits an internal quantum yield of 26.5% surprisingly higher than that for any other existing pure C_3N_4 photocatalyst.[141] In contrast to the report on polymeric C_3N_4 structure Vincent *et al.* demonstrated that low molecular weight carbon nitride with a predominantly melem (tri-s-triazines) active phase has three times the activity of the polymer under visible light conditions, despite absorbing less in the visible region. Alternatively, Katharina *et al.* reported structurally unambiguous crystalline 2D carbon nitride prepared by ionothermal synthesis of the layered bulk material poly-triazine imide (PTI), followed by one-step liquid exfoliation in water, that showed

[s] References therein

significantly enhanced visible-light driven photocatalytic activity toward hydrogen evolution.[142]

In summary, polymeric CN-based photocatalysts are considered as a viable alternative for hydrogen production under visible-light irradiation with the assistance of appropriate co-catalysts. Carbon nitride's textural richness, and polymeric nature allow large scale variation in structure without having to change the overall composition of the material have serious potential for catalysis *via* modifications. However, the limitation of use of noble-metal co-catalysts is unsuited for realization of fully economical system for clean energy production. Thus, the search for CN based materials that are independent of the requirement of noble-metal co-catalysts for visible-light-induced photocatalytic hydrogen are still needed.

1.11.2 Photodegradation of pollutants

The oxidation of the organic pollutants into CO_2, water, and other nonhazardous compounds using O_2 as a clean oxidant is one of the few effective approaches to remove the organic pollutants rapidly and in an environmentally friendly manner.[45,49,143] Water soluble organic dyes are widely used as substrates for testing the photocatalytic efficiency of semiconductor materials. Dyes have several advantages such as: they exhibit good stability in aqueous solution under ambient condition, consist of organic moieties and /or charged centres that can interact with different crystal surfaces of the SCs and their photocatalytic decomposition can be monitored spectroscopically. In addition to these practical testing benefits, the efficient and cheap removal of organic dyes from waste water is significant and real challenge faced by textile industries and environmental agencies worldwide.[17]

MB (structure shown in Figure 1.18) was used as model reagent to estimate the photocatalytic activity of the C_3N_4-Nb_2O_5 heterojunctions (Chapter 5). MB shows main visible absorption peak at 660-664 nm which is ascribed to the monomer, while the peak at 605-614 nm is that of the dimer. The decomposition of MB over the heterogeneous semiconductor surface involved an initial cleavage of the central aromatic ring, due to adsorption to the surface through the N or S heteroatoms, and subsequent decomposition of aromatic intermediates.[17,144]

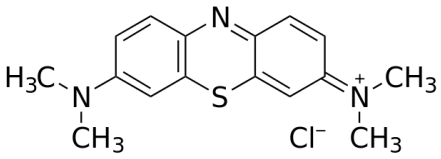

Figure 1.18 Molecular structure of Methylene Blue.

It is well known that $O_2^{-\cdot}$, H_2O_2, e^-, h^+ and $OH^\cdot$ are probable reactive species involved in photocatalytic degradation reactions of organic pollutants.[49,123,135,145] During photodegradation of a contaminant, the involvement of particular species can be investigated by introduction of the relevant radical scavengers such as; ammonium oxalate, catalase, isopropanol, benzoquinone (BQ), and NO_3^-. A mmonium oxalate is a scavenger of h^+, catalase acts as an H_2O_2 scavenger, isopropanol is a scavenger of $OH^\cdot$ radicals, BQ acts as an $O_2^{-\cdot}$ radical scavenger, and NO_3^- ions mainly acts as an e^- scavenger. [68,143]

Owing to the unique electronic structure and physicochemical properties, C_3N_4 has been widely employed for the photocatalytic degradation of various dyes, including methyl orange, rhodamine B, MB, aromatic compounds, aldehydes, and so on. The removal of the inorganic toxic gas NO in air and the reduction of heavy metal ion Cr(VI) have also been

investigated.[68,133] Recently, Zou and co-workers demonstrated successful degradation of MO and RhB using pristine C_3N_4.[145] Their comparison studies showed that the photodegradation activity of MO over C_3N_4 is predominantly due to the photoreduction initiated by electrons, whereas the degradation of RhB over C_3N_4 is mainly due to the photooxidation by the holes. In CN-CNB heterojunction materials the photodegradation of MO was governed by $O_2^{\bullet-}$, $OH^{\bullet}$ and h^+ rather than by single species.[123]

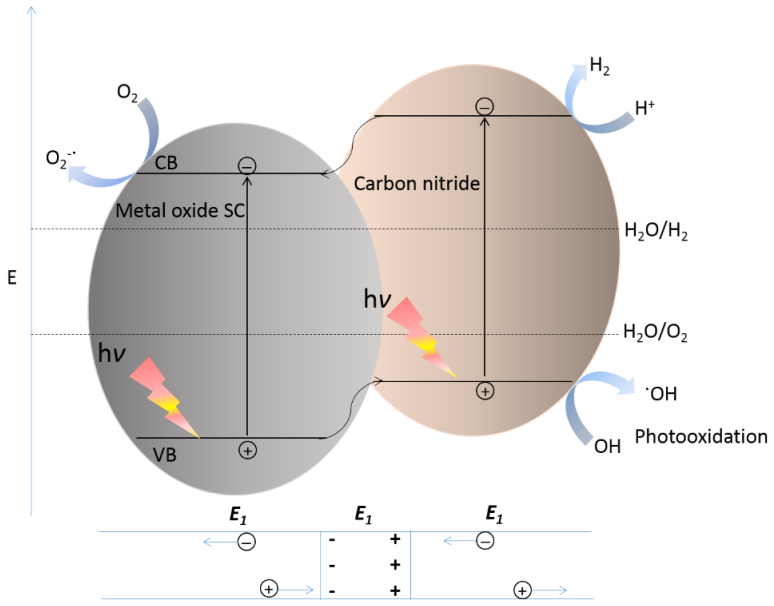

Figure 1.19 Scheme for electron–hole separation and transport at the visible-light-driven organic–inorganic composite photocatalyst interface and in both semiconductors.

Several strategies have been devised to modify the C_3N_4 for improved photodegradation of the contaminants. Particularly, Au[146] or Ag[147] nanoparticle deposition on C_3N_4 exhibited excellent photocatalytic activity for the decomposition of MO due to the synergistic action of surface plasmon resonance and the electron-sink effect of Au or Ag nanoparticles. These semiconductor–metal junctions create a space–charge separation region (called the Schottky barrier) at the interface of the two components. This aligns the Fermi energy levels for

effective charge transfer. On the other hand, the surface plasmon resonance (SPR) of noble metals could increase the visible light utilization and probably show special synergistic effects with g-C_3N_4.[122] In bid to replace the use of noble metals, Han *et al*. introduced Co_3O_4 into C_3N_4 to trap the photogenerated holes of C_3N_4, which resulted in efficient MO degradation.[148]

Also C_3N_4-carbon composites are advantageous for the degradation of various pollutants. The conductive nature of carbon materials facilitate the electron-transfer and charge separation of photogenerated excitons. Further, carbon materials may act as co-catalysts providing sufficient catalytic sites in additions to absorbing the longer wavelengths. Examples include: C_3N_4/mesoporous carbon[149] C_3N_4/graphene [117], and C_3N_4/C_{60}[121] for RhB degradation etc. Another widely investigated class is C_3N_4/metal oxide heterojunction photocatalysts. A typical schematic diagram is shown in Figure 1.19. As previously mentioned, the polymeric structure of C_3N_4 is flexible to modifications, therefore favours the facile construction of heterostructure with close interconnection between C_3N_4 and other SCs. A large number of materials have been synthesised by coupling the SCs with C_3N_4 to form semiconductor–semiconductor heterojunctions that greatly improve the efficiencies of the photocatalysts and promote their applications in the energy production and environmental remediation. For example, the decomposition of methanal and ethanal was hardly noticed with pure C_3N_4, whereas it was efficient with the Z-scheme heterojunctions of C_3N_4-TiO_2,[130], C_3N_4- sulfur-doped TiO_2 , [150] and C_3N_4-WO_3 .[151,152] In another case, the C_3N_4-MoO_3 Z-scheme heterojunction[153] showed its universality for the degradation of different dyes including MO, RhB and MB. Other such examples include; C_3N_4-TiO_2,[130] C_3N_4-ZnO,[131] C_3N_4-CdS,[132] C_3N_4-TaON,[154] C_3N_4-$SrTiO_3$,[134] C_3N_4-Bi_2WO_6[135], C_3N_4-$BiVO_4$[136] etc. Based on this approach C_3N_4-modified Nb_2O_5 heterojunctions were constructed and further discussed in Chapter 5.

1.11.3 Photocatalytic organic synthesis

The use of SCs as sensitizers for various organic photosynthetic processes stems from the early work of Kraeutler and Bard[155] on the use of platinized TiO_2 as a sensitizer for the conversion of acetic acid to methane and carbon dioxide: (an alternative photoinduced Kolbe reaction).[51] It is acknowledge that photoexcited states formed during photochemical reaction are rich in energy and reactions may occur that are highly endothermic in the ground state.[t] Typically, photoexcitation leads to the formation of both singlet and triplet states, unlike the thermal excitation that usually form singlet state, and the intermediates which are not accessible under thermal conditions.

In particular, C_3N_4-based photocatalysts have been employed recently in various selective organic transformations under mild conditions. One of the early examples of photocatalytic of an organic reaction using C_3N_4 for the activation of benzene to perform more sustainable Friedel–Crafts reactions by allowing to directly use carboxylic acids, alcohols and even quaternary ammoniums or urea as electrophiles.[156] After this research many papers appeared on the use of C_3N_4 for photocatalytic reactions. Recently, *Wang et al.* reported carbon nitride catalysed oxidation of aromatic alcohols using O_2 and visible light with high selectivity.[56,57] The authors argued that the whole reaction is surface-mediated; that is, the $\cdot O_2^-$ stays excitonically coupled to its countercation radical. Further the study on effect of substitution indicated the involvement of the electron deficient species which, presumably, are stabilized by the basic character of the carbon nitride. Akin to this many effective photocatalytic organic transformations have been reported using C_3N_4-based photocatalysts, including the

[t] The equation $E = h \times \nu$ can correlate light of a wavelength of 350 nm to an energy of 343 kJ/mol.

selective oxidation of benzene to phenol,[157,158] aromatic alcohols to aldehydes, [56,57] oxidation of alkanes, [157–159] olefins, [110] CO_2 reduction[160–162] and so on.

In very recent report, boron- and fluorine-doped carbon nitride was found to promote the oxygenation of cyclohexane with high selectivity (90%) at conversions of about 1–8%.[110] Apart from C-H and O-H oxidation, under the illumination of visible light, mpg-C_3N_4 also promoted the oxidation of amines into imines, which then undergo consecutive reactions.[163] One optimization reaction is complete conversion of benzylamine into N-(benzylidene)benzylamine in 3.5 h.

The potential of carbon nitride for photocatalytic organic synthesis can be seen clearly from these highlights. Note that the use of carbon nitride can be extended to other substrates. On this premise, carbon nitride was employed for photoacetalization of aldehyde/ketones and sequential oxidation/acetalization of alcohols in this thesis work and results are presented in chapter 6 and 7.

1.12 Summary and Objectives

This chapter briefly summarises semiconductor based photocatalysis, asserting that polymeric carbon nitride can be used for multiple heterogeneous photocatalytic applications. In particular, this chapter described the conditions and requirements to develop an effective photocatalyst for hydrogen generation from water splitting, and the necessary photocatalytic conditions it needs to meet. In addition it is shown that the species involved in the redox chemistry of photocatalytic aerobic pollutant oxidation, vary with the particular photocatalyst involved.

In context of carbon nitride, it is summarised that C_3N_4 is promising visible-light photocatalyst due to its unique electronic structure with both a narrow bandgap and appropriate CB and VB positions, as well as high stability against high temperature, acids, bases, and organic solvents. Admittedly, to make the material a more effective photocatalyst, it is necessary to enhance the photogenerated charge separation. Co-catalyst loading, semiconductor combinations and substrates also need to be investigated systematically, as these factors can influence the separation, mobility and lifetime of the charge carriers. Furthermore, low cost material can be prepared simply by thermal condensation of vastly available nitrogen rich precursors whose chemical structure, though not completely understood, can be readily tuned by careful choice of synthesis conditions.

Additionally, construction of heterojunctions with SCs of appropriate match or C_3N_4-based semiconductor composites resulted in improved photocatalytic performances. Mostly these semiconductors were formed of the traditional type-II and all-solid-state Z-scheme heterojunctions. The aforementioned modification strategies gave rise to a series of C_3N_4-based photocatalysts that can be used for various photocatalytic applications, such as water splitting, CO_2 reduction, pollutant degradation and organic syntheses. Therefore, using this strategy C_3N_4- C_3N_4, C_3N_4-metal oxide heterojunctions will be fabricated which are expected to show the high activity in photocatalytic applications.

The selected examples of heterogeneous photocatalysis as a synthetic route for organic reaction employing SCs, shows that photocatalysis can be applied as a green synthetic route in organic synthesis and this potential with carbon nitride in organic transformations is already realised.

The objectives of this thesis are threefold: firstly, the properties and structural changes with the variation of temperature and construction of new non-metal heterojunctions will be

explored in detail in order to extend their application in hydrogen evolution reaction from water. Secondly, the construction C_3N_4-metal oxide (in this case Nb_2O_5) heterojunctions for photodegradation of organic pollutants, and the mechanistic investigations of the species involved in the reaction, will be presented. Thirdly this study will include the visible light driven organic transformations and their underlying mechanistic details employing carbon nitride as metal free photocatalyst.

1.13 References

[1] J. F. Hartwig, *Science* **2002**, *297*, 1653–4.

[2] B. Trost, *Science* **1991**, *254*, 1471–1477.

[3] E. S. Beach, Z. Cui, P. T. Anastas, *Energy Environ. Sci.* **2009**, *2*, 1038.

[4] P. Anastas, N. Eghbali, *Chem. Soc. Rev.* **2010**, *39*, 301–12.

[5] Y. Qu, X. Duan, *Chem. Soc. Rev.* **2013**, *42*, 2568–80.

[6] C.-J. Li, B. M. Trost, *Proc. Natl. Acad. Sci. U. S. A.* **2008**, *105*, 13197–202.

[7] I. T. Horváth, P. T. Anastas, *Chem. Rev.* **2007**, *107*, 2169–73.

[8] M. Nosonovsky, B. Bhushan, *Philos. Trans. A. Math. Phys. Eng. Sci.* **2010**, *368*, 4677–94.

[9] T. P. Anastas, C. T. Williamson, *Green Chemistry: Frontiers in Benign Chemical Syntheses and Processes*, Oxford University Press, **1998**.

[10] P. T. Anastas, M. M. Kirchhoff, *Acc. Chem. Res.* **2002**, *35*, 686–694.

[11] K. Wilson, A. F. Lee, Eds. , *Heterogeneous Catalysts for Clean Technology: Spectroscopy, Design, and Monitoring*, Wiley-VCH Verlag GmbH & Co. KGaA, **2013**.

[12] P. Pichat, Ed. , *Photocatalysis and Water Purification: From Fundamentals to Recent Applications*, Wiley-VCH, **2013**.

[13] A. Mills, S. Le Hunte, *J. Photochem. Photobiol. A Chem.* **1997**, *108*, 1–35.

[14] A. L. Linsebigler, J. T. Yates Jr, G. Lu, G. Lu, J. T. Yates, *Chem. Rev.* **1995**, *95*, 735–758.

[15] T. Jia, Photocatalytic Hydrogen Production over Layered Materials, University of Oxford, **2014**.

[16] K. Saito, H. Yuki, T. Shimada, T. Sato, *Can. J. Chem.* **1981**, *59*, 1722–1723.

[17] C. Eley, The Rational Design of Photocatalytic Semiconductor Nanocrystals, University of Oxford, **2014**.

[18] Y. Liu, J. R. Jennings, S. M. Zakeeruddin, M. Grätzel, Q. Wang, *J. Am. Chem. Soc.* **2013**, *135*, 3939–52.

[19] H. Kisch, *Semiconductor Photocatlysis Principles and Applications*, Wiley-VCH Verlag GmbH & Co. KGaA, **2015**.

[20] M. Kasha, *Discuss. Faraday Soc.* **1950**, *9*, 14.

[21] A. Fujishima, Z. Xintong, A. T. Donald, *Int. J. Hydrogen Energy* **2007**, *32*, 2664–2672.

[22] M. A. Fox, M. T. Dulay, *Chem. Rev.* **1993**, *93*, 341–357.

[23] R. M. Navarro Yerga, M. C. Alvarez Galván, F. del Valle, J. A. Villoria de la Mano, J. L. G. Fierro, *ChemSusChem* **2009**, *2*, 471–85.

[24] J. Pan, G. Liu, G. Q. M. Lu, H.-M. Cheng, *Angew. Chem. Int. Ed.* **2011**, *50*, 2133–7.

[25] L. Jing, F. Yuan, H. Hou, B. Xin, W. Cai, H. Fu, *Sci. China Ser. B Chem.* **2005**, *48*, 25–30.

[26] Y. Zhao, C. Eley, J. Hu, J. S. Foord, L. Ye, H. He, S. C. E. Tsang, *Angew. Chem. Int. Ed.* **2012**, *51*, 3846–9.

[27] T. K. Townsend, E. M. Sabio, N. D. Browning, F. E. Osterloh, *Energy Environ. Sci.* **2011**, *4*, 4270.

[28] I. M. Szilágyi, B. Fórizs, O. Rosseler, Á. Szegedi, P. Németh, P. Király, G. Tárkányi, B. Vajna, K. Varga-Josepovits, K. László, et al., *J. Catal.* **2012**, *294*, 119–127.

[29] A. Fujishima, T. N. Rao, D. A. Tryk, *J. Photochem. Photobiol. C Photochem. Rev.* **2000**, *1*, 1–21.

[30] S. Cao, J. Yu, *J. Phys. Chem. Lett.* **2014**, *5*, 2101–7.

[31] J. H. Bang, P. V Kamat, *ACS Nano* **2009**, *3*, 1467–76.

[32] Y. Wang, X. Wang, M. Antonietti, *Angew. Chem. Int. Ed.* **2012**, *51*, 68–89.

[33] T. Trindade, P. O'Brien, N. L. Pickett, *Chem. Mater.* **2001**, *13*, 3843–3858.

[34] T. Hisatomi, J. Kubota, K. Domen, *Chem. Soc. Rev.* **2014**, *43*, 7520–7535.

[35] Y. Wu, P. Lazic, G. Hautier, K. Persson, G. Ceder, *Energy Environ. Sci.* **2012**, 157–168.

[36] A. Kubacka, M. Fernández-García, G. Colón, *Chem. Rev.* **2012**, *112*, 1555–1614.

[37] A. Fujishima, K. Honda, *Nature* **1972**, *238*, 37–38.

[38] A. J. Bard, *J. Photochem.* **1979**, *10*, 59–75.

[39] A. J. Bard, *J. Phys. Chem. C* **1982**, *86*, 172.

[40] J. Zhu, M. Zäch, *Curr. Opin. Colloid Interface Sci.* **2009**, *14*, 260–269.

[41] J. S. Jang, H. G. Kim, J. S. Lee, *Catal. Today* **2012**, *185*, 270–277.

[42] T. Hisatomi, J. Kubota, K. Domen, *Chem. Soc. Rev.* **2014**, *43*, DOI: 10.1039/C3CS60378D.

[43] A. Kudo, Y. Miseki, *Chem. Soc. Rev.* **2009**, *38*, 253–278.

[44] K. Maeda, K. Domen, *J. Phys. Chem. C* **2007**, *111*, 7851–7861.

[45] X. Wang, S. Blechert, M. Antonietti, *ACS Catal.* **2012**, *2*, 1596–1606.

[46] M. Grätzel, *Nature* **2001**, *414*, 338–344.

[47] X. Zou, Y. Zhang, *Chem. Soc. Rev.* **2015**, *44*, 5148–5180.

[48] Y. Okamoto, S. Ida, J. Hyodo, H. Hagiwara, T. Ishihara, *J. Am. Chem. Soc.* **2011**, *133*, 18034–18037.

[49] C. Chen, W. Ma, J. Zhao, *Chem. Soc. Rev.* **2010**, *39*, 4206–19.

[50] M. R. Hoffmann, S. T. Martin, W. Choi, D. W. Bahnemann, *Chem. Rev.* **1995**, *95*, 69–96.

[51] S. N. Frank, A. J. Bard, *J. Am. Chem. Soc.* **1977**, *99*, 303–304.

[52] A. Mills, S. Le Hunte, *J. Photochem. Photobiol. A Chem.* **1997**, *108*, 1–35.

[53] C. K. Prier, D. A. Rankic, D. W. C. Macmillan, *Chem. Rev.* **2013**, *113*, 5322–5363.

[54] B. Kraeutler, A. J. Bard, *J. Am. Chem. Soc.* **1978**, *100*, 5985–5992.

[55] X. Lang, X. Chen, J. Zhao, *Chem. Soc. Rev.* **2014**, *43*, 473–86.

[56] F. Su, S. C. Mathew, G. Lipner, X. Fu, M. Antonietti, S. Blechert, X. Wang, *J. Am. Chem. Soc.* **2010**, *132*, 16299–16301.

[57] B. Long, Z. Ding, X. Wang, *ChemSusChem* **2013**, *6*, 2074–2078.

[58] M. Halmann, J. Tobin, K. Zuckerman, *J. Electroanal. Chem. Interfacial Electrochem.* **1986**, *209*, 405–411.

[59] L. Lin, R. R. Kuntz, *Langmuir* **1992**, *8*, 870–875.

[60] S. Yanagida, K. Mizumoto, C. Pac, *J. Am. Chem. Soc.* **1986**, *108*, 647–654.

[61] C. M. Wang, T. E. Mallouk, *J. Am. Chem. Soc.* **1990**, *112*, 2016–2018.

[62] W. G. Becker, M. M. Truong, C. C. Ai, N. N. Hamel, *J. Phys. Chem.* **1989**, *93*, 4882–4886.

[63] A. Thomas, A. Fischer, F. Goettmann, M. Antonietti, J.-O. Müller, R. Schlögl, J. M. Carlsson, *J. Mater. Chem.* **2008**, *18*, 4893.

[64] D. S. Su, J. Zhang, B. Frank, A. Thomas, X. Wang, J. Paraknowitsch, R. Schlögl, *ChemSusChem* **2010**, *3*, 169–80.

[65] X. Wang, K. Maeda, A. Thomas, K. Takanabe, G. Xin, J. M. Carlsson, K. Domen, M. Antonietti, *Nat. Mater.* **2009**, *8*, 76–80.

[66] A. Harriman, I. J. Pickering, J. M. Thomas, P. A. Christensen, *J. Chem. Soc. Faraday Trans. 1 Phys. Chem. Condens. Phases* **1988**, *84*, 2795.

[67] M. Litter, *Appl. Catal. B Environ.* **1999**, *23*, 89–114.

[68] S. Cao, J. Low, J. Yu, M. Jaroniec, *Adv. Mater.* **2015**, *27*, 2150–76.

[69] Y. Zheng, J. Liu, J. Liang, M. Jaroniec, S. Z. Qiao, *Energy Environ. Sci.* **2012**, *5*, 6717.

[70] F. Su, M. Antonietti, X. Wang, *Catal. Sci. Technol.* **2012**, *2*, 1005.

[71] J. Zhu, P. Xiao, H. Li, A. C. Carabineiro, *ACS Appl. Mater. Interfaces* **2014**, *6*, 16449–16465.

[72] A. V. Semencha, L. N. Blinov, *Glas. Phys. Chem.* **2010**, *36*, 199–208.

[73] E. C. Franklin, *J. Am. Chem. Soc.* **1922**, *44*, 486–509.

[74] L. Pauling, J. H. Sturdivant, *Proc. Natl. Acad. Sci. U. S. A.* **1937**, *23*, 615–20.

[75] C. E. Redemann, H. J. Lucas, *J. Am. Chem. Soc.* **1940**, *62*, 842–846.

[76] X. Bai, C. Cao, X. Xu, *Mater. Sci. Eng. B* **2010**, *175*, 95–99.

[77] M. J. Bojdys, J.-O. Müller, M. Antonietti, A. Thomas, *Chemistry* **2008**, *14*, 8177–82.

[78] B. Jürgens, E. Irran, J. Senker, P. Kroll, H. Müller, W. Schnick, *J. Am. Chem. Soc.* **2003**, *125*, 10288–300.

[79] L. Seyfarth, J. Seyfarth, B. V Lotsch, W. Schnick, J. Senker, *Phys. Chem. Chem. Phys.* **2010**, *12*, 2227–37.

[80] A. Sattler, S. Pagano, M. Zeuner, A. Zurawski, D. Gunzelmann, J. Senker, K. Müller-Buschbaum, W. Schnick, *Chemistry* **2009**, *15*, 13161–70.

[81] M. Döblinger, B. V Lotsch, J. Wack, J. Thun, J. Senker, W. Schnick, *Chem. Commun.* **2009**, 1541–3.

[82] D. R. Miller, J. Wang, E. G. Gillan, *J. Mater. Chem.* **2002**, *12*, 2463–2469.

[83] A. Y. Liu, M. L. Cohen, *Science* **1989**, *245*, 841–842.

[84] D. M. Teter, R. J. Hemley, *Science* **1996**, *271*, 53–55.

[85] D. C. Nesting, J. V. Badding, *Chem. Mater.* **1996**, *8*, 1535–1539.

[86] Y. Miyamoto, M. L. Cohen, S. G. Louie, *Solid State Commun.* **1997**, *102*, 605–608.

[87] A. Y. Liu, R. M. Wentzcovitch, *Phys. Rev. B* **1994**, *50*, 10362–10365.

[88] J. E. Lowther, *Phys. Rev. B* **1999**, *59*, 11683–11686.

[89] Z. Zhang, K. Leinenweber, M. Bauer, L. A. J. Garvie, P. F. McMillan, G. H. Wolf, *J. Am. Chem. Soc.* **2001**, *123*, 7788–7796.

[90] J. L. Zimmerman, R. Williams, V. N. Khabashesku, J. L. Margrave, *Nano Lett.* **2001**, *1*, 731–734.

[91] E. Kroke, M. Schwarz, E. Horath-Bordon, P. Kroll, B. Noll, A. D. Norman, *New J. Chem.*

2002, *26*, 508–512.

[92] J. Sehnert, K. Baerwinkel, J. Senker, *J. Phys. Chem. B* **2007**, *111*, 10671–80.

[93] K. Maeda, X. Wang, Y. Nishihara, D. Lu, M. Antonietti, K. Domen, *J. Phys. Chem. C* **2009**, *113*, 4940–4947.

[94] S. C. Yan, Z. S. Li, Z. G. Zou, *Langmuir* **2009**, *25*, 10397–401.

[95] G. Zhang, J. Zhang, M. Zhang, X. Wang, *J. Mater. Chem.* **2012**, *22*, 8083.

[96] F. Dong, Z. Zhao, T. Xiong, Z. Ni, W. Zhang, Y. Sun, W.-K. Ho, *ACS Appl. Mater. Interfaces* **2013**, *5*, 11392–401.

[97] A. B. Jorge, D. J. Martin, M. T. S. Dhanoa, A. S. Rahman, N. Makwana, J. Tang, A. Sella, F. Corà, S. Firth, J. A. Darr, et al., *J. Phys. Chem. C* **2013**, *117*, 7178–7185.

[98] S. Matsumoto, E.-Q. Xie, F. Izumi, *Diam. Relat. Mater.* **1999**, *8*, 1175–1182.

[99] B. V Lotsch, W. Schnick, *Chemistry* **2007**, *13*, 4956–68.

[100] B. V Lotsch, M. Döblinger, J. Sehnert, L. Seyfarth, J. Senker, O. Oeckler, W. Schnick, *Chemistry* **2007**, *13*, 4969–80.

[101] E. G. Gillan, *Chem. Mater.* **2000**, *12*, 3906–3912.

[102] Z. Zhou, J. Wang, J. Yu, Y. Shen, Y. Li, A. Liu, S. Liu, Y. Zhang, *J. Am. Chem. Soc.* **2015**, 150204134018003.

[103] Z. Zhang, J. Long, L. Yang, W. Chen, W. Dai, X. Fu, X. Wang, *Chem. Sci.* **2011**, *2*, 1826–1830.

[104] Z. Lin, X. Wang, *Angew. Chem. Int. Ed.* **2013**, *52*, 1735–1738.

[105] J. Zhang, M. Zhang, R.-Q. Sun, X. Wang, *Angew. Chem. Int. Ed.* **2012**, *51*, 10145–9.

[106] Y. Chen, J. Zhang, M. Zhang, X. Wang, *Chem. Sci.* **2013**, *4*, 3244.

[107] Y. Zhang, T. Mori, J. Ye, M. Antonietti, *J. Am. Chem. Soc.* **2010**, *132*, 6294–6295.

[108] J. Hong, X. Xia, Y. Wang, R. Xu, *J. Mater. Chem.* **2012**, *22*, 15006.

[109] Y. Wang, Y. Di, M. Antonietti, H. Li, X. Chen, X. Wang, *Chem. Mater.* **2010**, *22*, 5119–5121.

[110] Y. Wang, J. Zhang, X. Wang, M. Antonietti, H. Li, *Angew. Chem. Int. Ed.* **2010**, *49*, 3356–9.

[111] Y. Zhang, T. Mori, J. Ye, M. Antonietti, *J. Am. Chem. Soc.* **2010**, *132*, 6294–5.

[112] Y. Zhang, M. Antonietti, *Chem. Asian J.* **2010**, *5*, 1307–11.

[113] J. C. Byers, F. Billon, C. Debiemme-Chouvy, C. Deslouis, A. Pailleret, O. A. Semenikhin, *ACS Appl. Mater. Interfaces* **2012**, *4*, 4579–87.

[114] Y. Wang, Q. Wang, X. Zhan, F. Wang, M. Safdar, J. He, *Nanoscale* **2013**, *5*, 8326–39.

[115] J. Tersoff, *Phys. Rev. B* **1984**, *30*, 4874–4877.

[116] Y. Sun, C. Li, Y. Xu, H. Bai, Z. Yao, G. Shi, *Chem. Commun.* **2010**, *46*, 4740–2.

[117] Q. Xiang, J. Yu, M. Jaroniec, *J. Phys. Chem. C* **2011**, *115*, 7355–7363.

[118] Y. Xu, H. Xu, L. Wang, J. Yan, H. Li, Y. Song, L. Huang, G. Cai, *Dalton Trans.* **2013**, *42*, 7604–13.

[119] L. Ge, C. Han, *Appl. Catal. B Environ.* **2012**, *117-118*, 268–274.

[120] Y. Sui, J. Liu, Y. Zhang, X. Tian, W. Chen, *Nanoscale* **2013**, *5*, 9150–5.

[121] B. Chai, X. Liao, F. Song, H. Zhou, *Dalton Trans.* **2014**, *43*, 982–9.

[122] Z. Zhao, Y. Sun, F. Dong, *Nanoscale* **2015**, *7*, 15–37.

[123] H. Li, Y. Liu, X. Gao, C. Fu, X. Wang, *ChemSusChem* **2015**, *8*, 1189–96.

[124] M. A. Khan, I. F. Teixeira, M. J. L. Molly, S. C. E. Tsang, *Chem. Mater.* **2015**, *submitted*.

[125] K. Sridharan, E. Jang, T. J. Park, *Appl. Catal. B Environ.* **2013**, *142-143*, 718–728.

[126] J. Yu, S. Wang, J. Low, W. Xiao, *Phys. Chem. Chem. Phys.* **2013**, *15*, 16883–90.

[127] Y. Zang, L. Li, Y. Zuo, H. Lin, G. Li, X. Guan, *RSC Adv.* **2013**, *3*, 13646.

[128] L. Huang, H. Xu, Y. Li, H. Li, X. Cheng, J. Xia, Y. Xu, G. Cai, *Dalton Trans.* **2013**, *42*, 8606–16.

[129] K. Katsumata, R. Motoyoshi, N. Matsushita, K. Okada, *J. Hazard. Mater.* **2013**, *260*, 475–82.

[130] H. Yan, H. Yang, *J. Alloys Compd.* **2011**, *509*, 26–29.

[131] J.-X. Sun, Y.-P. Yuan, L.-G. Qiu, X. Jiang, A.-J. Xie, Y.-H. Shen, J.-F. Zhu, *Dalt. Trans.* **2012**, *41*, 6756.

[132] J. Fu, B. Chang, Y. Tian, F. Xi, X. Dong, *J. Mater. Chem. A* **2013**, *1*, 3083.

[133] S. C. Yan, S. B. Lv, Z. S. Li, Z. G. Zou, *Dalt. Trans.* **2010**, *39*, 1488–1491.

[134] X. Xu, G. Liu, C. Randorn, J. T. S. Irvine, *Int. J. Hydrogen Energy* **2011**, *36*, 13501–13507.

[135] Y. Tian, B. Chang, J. Lu, J. Fu, F. Xi, X. Dong, *ACS Appl. Mater. Interfaces* **2013**.

[136] Y. Tian, B. Chang, Z. Yang, B. Zhou, F. Xi, X. Dong, *RSC Adv.* **2014**, *4*, 4187–4193.

[137] X.-H. Li, J. Zhang, X. Chen, A. Fischer, A. Thomas, M. Antonietti, X. Wang, *Chem. Mater.* **2011**, *23*, 4344–4348.

[138] J. Zhang, J. Sun, K. Maeda, K. Domen, P. Liu, M. Antonietti, X. Fu, X. Wang, *Energy*

Environ. Sci. **2011**, *4*, 675–678.

[139] S. Chu, Y. Wang, Y. Guo, J. Feng, C. Wang, W. Luo, X. Fan, Z. Zou, *ACS Catal.* **2013**, *3*, 912–919.

[140] X. Wang, K. Maeda, X. Chen, K. Takanabe, K. Domen, Y. Hou, X. Fu, M. Antonietti, *J. Am. Chem. Soc.* **2009**, *131*, 1680–1.

[141] D. J. Martin, K. Qiu, S. A. Shevlin, A. D. Handoko, X. Chen, Z. Guo, J. Tang, *Angew. Chem. Int. Ed.* **2014**, *53*, 9240–5.

[142] K. Schwinghammer, M. B. Mesch, V. Duppel, C. Ziegler, J. Senker, B. V Lotsch, *J. Am. Chem. Soc.* **2014**, *136*, 1730–3.

[143] Y. Wang, X. Wang, M. Antonietti, *Angew. Chem. Int. Ed.* **2012**, *51*, 68–89.

[144] A. Houas, *Appl. Catal. B Environ.* **2001**, *31*, 145–157.

[145] S. C. Yan, Z. S. Li, Z. G. Zou, *Langmuir* **2010**, *26*, 3894–901.

[146] N. Cheng, J. Tian, Q. Liu, C. Ge, A. H. Qusti, A. M. Asiri, A. O. Al-Youbi, X. Sun, *ACS Appl. Mater. Interfaces* **2013**, *5*, 6815–9.

[147] Y. Yang, Y. Guo, F. Liu, X. Yuan, Y. Guo, S. Zhang, W. Guo, M. Huo, *Appl. Catal. B Environ.* **2013**, *142-143*, 828–837.

[148] C. Han, L. Ge, C. Chen, Y. Li, X. Xiao, Y. Zhang, L. Guo, *Appl. Catal. B Environ.* **2014**, *147*, 546–553.

[149] L. Shi, L. Liang, J. Ma, F. Wang, J. Sun, *Dalton Trans.* **2014**, *43*, 7236–44.

[150] K. Kondo, N. Murakami, C. Ye, T. Tsubota, T. Ohno, *Appl. Catal. B Environ.* **2013**, *142-143*, 362–367.

[151] S. Chen, Y. Hu, S. Meng, X. Fu, *Appl. Catal. B Environ.* **2014**, *150-151*, 564–573.

[152] H. Katsumata, Y. Tachi, T. Suzuki, S. Kaneco, *RSC Adv.* **2014**, *4*, 21405.

[153] Y. He, L. Zhang, X. Wang, Y. Wu, H. Lin, L. Zhao, W. Weng, H. Wan, M. Fan, *RSC Adv.* **2014**, *4*, 13610.

[154] S. C. Yan, S. B. Lv, Z. S. Li, Z. G. Zou, *Dalton Trans.* **2010**, *39*, 1488–1491.

[155] B. Kraeutler, A. J. Bard, *J. Am. Chem. Soc.* **1978**, *100*, 2239–2240.

[156] F. Goettmann, A. Fischer, M. Antonietti, A. Thomas, *Chem. Commun.* **2006**, 4530.

[157] X. Chen, J. Zhang, X. Fu, M. Antonietti, X. Wang, *J. Am. Chem. Soc.* **2009**, *131*, 11658–9.

[158] X. Ye, Y. Cui, X. Wang, *ChemSusChem* **2014**, *7*, 738–42.

[159] U. Schuchardt, D. Cardoso, R. Sercheli, R. Pereira, R. S. da Cruz, M. C. Guerreiro, D. Mandelli, E. V. Spinacé, E. L. Pires, *Appl. Catal. A Gen.* **2001**, *211*, 1–17.

[160] G. Dong, L. Zhang, *J. Mater. Chem.* **2012**, *22*, 1160–1166.

[161] J. Mao, T. Peng, X. Zhang, K. Li, L. Ye, L. Zan, *Catal. Sci. Technol.* **2013**, *3*, 1253.

[162] P. Niu, Y. Yang, J. C. Yu, G. Liu, H.-M. Cheng, *Chem. Commun.* **2014**, *50*, 10837.

[163] F. Su, S. C. Mathew, L. Möhlmann, M. Antonietti, X. Wang, S. Blechert, *Angew. Chem. Int. Ed.* **2011**, *50*, 657–660.

Chapter 2: Analytical Techniques

2.1 Introduction

The chemical nature and structure of a photocatalyst are crucial for design that governs the catalytic behaviour for specific photocatalytic reactions. To have a clear perspective on underlying principles of observed catalysis and effect of altering the properties of catalyst materials needs solid grasp on its structural, physical and chemical properties. Generally, the aspects probed by an individual technique are limited therefore a variety of complementary characterization methods based on spectroscopy, microscopy and diffraction are necessary to help explain such unifying relationship between structure and property during catalysis.

In chapter one, the structural complexity of polymeric semiconducting (PS) carbon nitride, basis of formation of carbon nitride composite heterojunction along with mechanistic aspects of photocatalytic hydrogen production from water, dye photo-degradation and carbon nitride as organo-photocatalyst have been discussed. Additionally, changing the electronic structure, states and morphology of the carbon nitride materials resulted in significant changes in catalytic reactivity. Thus it is vital to understand the catalytic activity and selectivity of a material and the influence of modifications (here construction of heterojunctions) so to better predict and design the material for improved specific applications.

The aim of this chapter is to briefly explain and introduce major analytical techniques and experimental procedures for material characterization presented and discussed in subsequent chapters. In particular details concerning specific instrument types, operational parameters, theoretical principles and examples of information obtained from such techniques are briefly covered.

2.2 X-Ray diffraction (XRD)

X-ray diffraction (XRD) is one of the most widely used diffractions technique for structure determination in solid state chemistry and material science. The technique is used to determine the positions of atoms ions that make up a solid compound and hence provides a description of structures in terms of features such as bond lengths, bond angles and relative positions of ions and molecules in unit cell.[1,2] It also provides information on the composition, phase composition and size of crystallite materials.[3,4] In this work it is used to identify the structure of the carbon nitride materials.

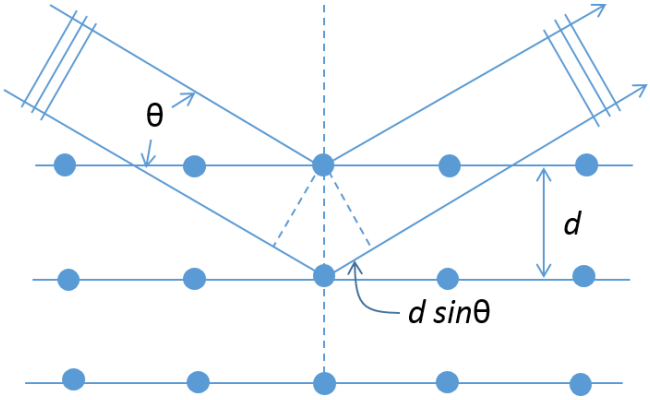

Figure 2.1 Illustration of Bragg's Law derived by treating layers of atom as reflecting planes. X-rays interfere constructively when the additional path length 2 *d* sin *θ* is equal to integral multiple of the wavelength λ.

XRD patterns are collected by directing the X-ray beam towards crystalline sample at different angles. XRD is based on constructive interference of X-rays and scattering occurs by the electron cloud of the atoms and diffraction occurs for periodic array of parallel atom planes separated by a distance similar to the wavelength of radiation (100 pm), such as exist in crystal.[1] The pattern that result from this X-ray diffraction are separated by the lattice

spacing d (Figure 2.1), when scattering angle θ at which constructive interference occurs between wavelength λ of source is given by Bragg's equation:

$$n\lambda = 2d\ sin\ \theta \qquad (2.1)$$

where n is an integer depending on the layer of scattering.

Powdered crystalline solids contain enormous number of crystallites oriented at random relative to incident beam. Then intensity of diffracted X-ray is measured as a function of angle with detector to obtain the diffraction pattern. Using peak positions and full width half maximum (FWHM) of each peak, the lattice spacing and crystallite size can be calculated. Furthermore, the perpendicular distance d_{hkl} between parallel planes (h, k, l) of a unit cell with lengths a, b, and c is often described as inter-planar spacing.[5] Bragg equation can be used to obtain the lattice spacing of a particular system. For example, a cubic structured crystal, such as ZnS, the plane spacing is described by:

$$d_{hkl} = \frac{a}{\sqrt{h^2 + k^2 + l^2}} \qquad (2.2)$$

and for orthogonal system:

$$\frac{1}{d^2_{hkl}} = \frac{h^2}{a^2} + \frac{k^2}{b^2} + \frac{l^2}{c^2} \qquad (2.3)$$

Combining equation 2.2 with Bragg's law:

$$\left(\frac{\lambda}{2a}\right)^2 = \frac{\sin^2\theta}{h^2 + k^2 + l^2} \qquad (2.4)$$

where a is the lattice spacing and h, k, l are miller indices of Bragg plane.

In XRD patterns of sufficiently small crystallite size peak broadening occurs, in particular at nanoscale where it have small lattice dimensions. Using Scherrer equation (equation 2.5) this broadening can be related to estimate the average size of the crystallite.[6]

$$D = \frac{K\lambda}{\Delta\theta} \qquad (2.5)$$

Equation 2.5 relates the crystallite size D to wavelength λ, angle θ and the breadth Δ of a peak at FWHM by constant K (Scherrer constant). As the constant K depends on measurement of peak breadth, it is necessary to subtract the intrinsic instrument peak broadening in determining the particle size of the powder crystals.

2.3 X-ray photoelectron spectroscopy

XPS is one of the most versatile techniques used to study surfaces chemically, in particular oxidation state and band structure of solids. As the mean free path of electron in solids is about 1 nm, so XPS is suitable for elemental analysis and in this application it is commonly known as electron spectroscopy for chemical analysis (ESCA). In XPS, incident monochromatic beam of X-ray on interaction with atoms of a solid surface, whereby provided photon energy ($h\nu$) is greater than the work function (ϕ) of the sample, induces the photoemission from both core (inner quantum shells) and valance (outer quantum shells) levels of outer surface atoms into the vacuum, (energy zero) Figure 2.2.

The key to chemical identification is that core electrons deep inside atoms are largely insensitive to their surrounding in condensed solid phase and retain characteristic binding energies E_B of an atom (i.e. the number of protons in the nucleus). The outermost electrons that are chemically active, are broadened into a valance band.

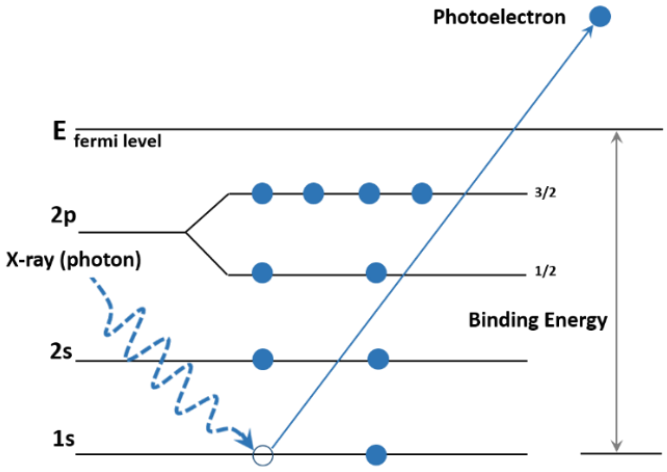

Figure 2.2 Schematic representation of the X-ray photoelectron emission of an electron from the 1s shell of an atom.

Applying the principle of conservation of energy the kinetic energy gained by photoelectrons during X-ray induced emission that is related to the energy of the incoming photon according to the photoelectric effect:

$$E_{KIN} = h\nu - E_B + \phi \qquad (2.6)$$

Although the binding energy E_B of core level is measured relative to the Fermi level E_f of the solid and energy required to excite the core electron for photoemission must overcome the potential barrier associated with attraction of electron from the nucleus. The energy thus remained is transformed into characteristic E_{KIN} of emitted photoelectrons varying systematically from element to element and XPS spectra generally plot number of photoelectron (e.g counts) against their binding energy.[7]

The XPS measurements are carried out in UHV chamber where quartz crystal monochromatizes the X-ray due to Bragg's angle and focuses it into a spot which is then incident onto the sample. This controlled X-ray is typically in the form of Mg K_α with hν = 1253.6 eV or Al K_α with hν = 1486.3 eV. The sample absorbs this radiation and emit

characteristic photoelectron having a pass energy which electrostatic energy analyzer (consisting of two concentric hemisphere with a potential difference between them) separates and sent through to the detector as shown in figure 2.3. The relative intensity of the different XPS peaks depends on concentration of atoms of an element at the selvedge, probable occurrence of photoemission and the instrumental response whereas a typical spatial sensitivity can vary from 100 µm to 1 mm. Normal surface penetration is about 5-10 nm, however, penetration depth can be increased using Ti K_α of 2040 eV or synchrotron radiation if desired. As a rule atom in high formal oxidation state will yield XPS peak at high binding energy relative to same atom in a low oxidation state, thus, peaks can analysed and fitted to reveal relative proportions of different chemical states in an element.[3,7]

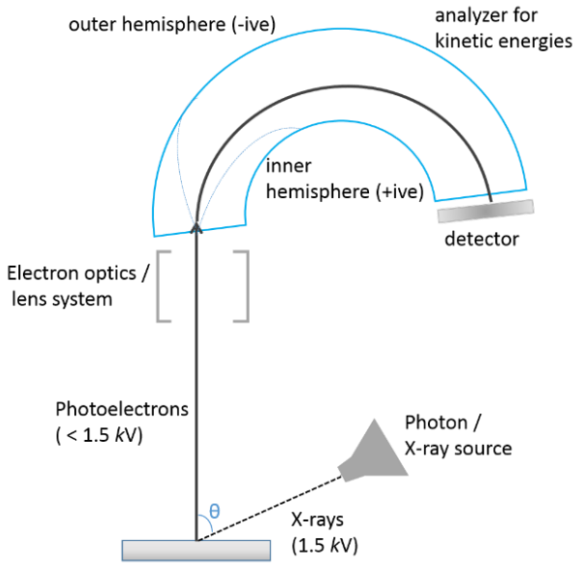

Figure 2.3 schematic illustration of XPS modified from reference [3]. X-rays are directed towards a sample in a UHV chamber (not shown). Photoelectron generated in the sample are then directed towards a spectrometer and detector.

Photoelectron peaks from XPS are labelled in accordance to the quantum number of the emitted electron. The basis of it lies in spin orbit coupling as electrons can either have $s = \pm$

$^{1}/_{2}$ when orbital momentum is $l \geq 1$ with total momentum $j = l + s$. For instance, Nb 3d give rise to two peaks, the $3d_{5/2}$ ($l = 2$ and $j = 2 + {}^{1}/_{2}$) and $3d_{3/2}$ ($l = 2$ and $j = 2 - {}^{1}/_{2}$) whereby their intensity ratio is governed according to the multiplicity $2j + 1$, that in this case is 3:2.

In XPS profiling one recurrent experimental problem is charge build up for non-conducting samples during photoemission process which led to shifts in binding energies to higher values for a specific element. Correcting for this charge build up is done by referencing known element and shifting observed E_b values accordingly.

2.4 Transmission electron spectroscopy (TEM)

TEM is a valuable analytical technique for the characterization of materials at nanoscale. It has extended the resolution for morphological studies from that dictated by the wavelength of visible light to dimensions which are well into the range required to image the lattice planes in any crystal structure, that is from the order of 0.3 μm to of the order of 0.15 nm.[8] It reveals information about the internal structure, composition as well as size and morphology of nanomaterials.

The TEM uses the electron beam as upside down, unlike the optical microscopy, and the recording system lies usually at the bottom. In order to achieve the sufficiently high resolution the electron gun replaces the light source and is maintained at voltage (typically 100-400 kV) while lanthanum hexaboride (LaB_6) crystals capable of generating the electron beam with current density of the order of 1×10^6 A m^{-2} or field emission source generates *ca* 1×10^{10} A m^{-2}. A thin layer of nanomaterials on the sample grid is exposed to this high energy electron beam that interacts with sample specimen to form high resolution image on the fluorescent screen or diffraction pattern.

To obtain TEM image, it is essential for electron to pass through the specimen. This is generally achieved to by mechanical thinning, electrochemical thinning, ion milling or by drop-dry methods using dispersion of the nanomaterials, to ensure the thickness of specimen is less than 100 nm. The high energy electrons from gun are focused by an electromagnetic condenser lens system, whose focus in turn is controlled by varying the lens current. In order to focus first image when beam strikes the sample, elastically scattered electrons transmitted through the specimen are refocused by projection lens by controlling their current and final image also employs the electromagnetic lenses to observe the image on a phosphor screen. Typical screen current densities are of the order of 10^{-10} to 10^{-12} Am^{-10} for high magnifications. Furthermore, as the high energy electron beam has a very limited path length in air, hence microscope column is kept under vacuum of 10^{-7} torr during operation and images are captured using a charges coupled camera or film.

Given that the maximum beam divergence in electron microscope is less than 1°, the Rayleigh criterion for the image of a point source can be reduced to following equation:

$$\delta_d = \frac{0.61\,\lambda o}{n \sin \alpha} \qquad (2.7)$$

Where α is semi-angle subtended at the subject by the lens, λ_0 is the wavelength of radiation in the object space and n is the refractive index. Thus, for a given *n* and α, the minimum resolvable distance in microscope is order of the wavelength. From the equation, a wavelengths of $\lambda_0 < 0.1$ nm are needed to resolve the crystal lattices on atomic scale and thus electrons ideal choice to achieve such resolution (at 200 kV has $\lambda_0 = 2.5$ pm).

In practice is possible to improve the microscope resolution by increasing the accelerating voltage, however most samples liable to radiation damage after prolong exposure. In operation of TEM, the resolution is much poorer than the theoretical Rayleigh limit due to

non-spherical nature of the lenses. This can be improved by reducing aberration coefficients for the electromagnetic lenses.

In TEM diffraction mode, similar to XRD, selected area electron diffraction (SAED) can be used to reveal elemental identification and specific structure of the surface and adsorbate layers, depending upon the long range order (diffraction pattern comprises of an array of spots) or superimposed crystallographic orientations (concentric rings pattern). Crystal lattices can be determined by measuring the spacing ratios as well as lattice parameter, although a standard measurements of known spacing are required under same operating conditions for calibration.

2.5 Fourier Transform infrared (FTIR) spectroscopy

The vibrational spectroscopy is used to characterize compounds in terms of strength, stiffness, and number of bonds that are present.[2] Since different molecules have different bond energies, infrared absorption is a useful tool for both quantitative and qualitative analysis of sample. It is also used to monitor the changes in concentration of species during the reaction, to determine the components of unknown compound. Besides it is employed to investigate the interaction between molecules and solid surface−for example IR absorption spectra of pre-adsorbed CO and NO can reveal information about the adsorption sites on heterogeneous catalyst.[3,9]

Regardless of molecular size and complexity all molecules possess resonant vibrational frequencies that changes on absorption of well-matched infrared light ($\Delta E = h\nu$) thereby changing the vibration energy state. The absorbed energy is eventually released as heat and the molecules revert from the excited state to the original state.

A bond in a molecule behave like two balls connected to a spring, acting as simple harmonic oscillator for which solution of Schrödinger equation gives the energies:[2]

$$Ev = \left(v + \frac{1}{2}\right) h\omega \qquad (2.8)$$

where $\omega = (k / \mu)^{1/2}$, v = 0, 1, 2,.., and μ is effective mass of oscillator. For diatomic molecules composed of atom m_A and m_B, $\mu = (m_A m_B / m_A + m_B)$. This effective mass is different for isotopologues which in turn lead to changes in E_v. A nonlinear molecule consisting of *N* atoms has 3*N*−6 independent vibrational modes while a linear molecule has 3*N*−5. Only those modes that cause dipole moment to fluctuate in congruence with changing electric field of the electromagnetic radiation are IR active. The lowest level of these mode have zero-point energy, lowest vibrational energy that a bond can possess. Whereas transitions from zeroth to second and third vibrational level also may occur leading to overtones.

An FTIR produces a source of incoherent infrared light using a heated filament. The radiation is funnelled through interferometer where beam first splits and recombine by set of mirrors. After it is directed to the sample and subsequently focused at the detector. IR spectrum of a compound is obtained by exposing the sample to infrared region and generating a plot of absorbance against frequency or wavelength. The spectrum is extracted from an interferogram by Fourier transformation, which converts information in time domain to the frequency domain (all the frequencies are measured simultaneously). For solid samples an attenuated total reflectance (ATR) geometry shown Figure 2.4 is used, where infrared light is introduced into a prism at an angle exceeding the critical angle for internal reflection. This produces an evanescent wave at the reflecting surface on which the sample is supported. Energy loss from the evanescent wave into the sample is measured producing a spectrum.

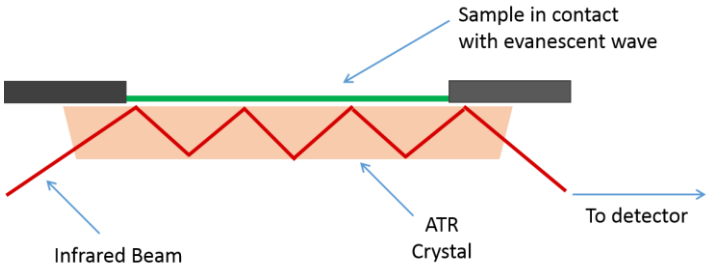

Figure 2.4 Typical set up of ATR-FTIR mode for solid samples.

2.6 Ultraviolet-visible (UV-vis) absorption spectroscopy

Ultraviolet-visible spectroscopy is the observation of the absorption of the electromagnetic radiation in the ultraviolet (UV) and visible regions of the spectrum (200-780 nm).[2] Since the absorption of UV-vis radiation results in the transitions among the electronic energy levels of the molecules is also termed as electronic spectroscopy. Molecules containing π-electron or *n*-electrons can absorb the energy in the form of UV or visible light to excite the electrons to higher energy levels (anti-bonding molecular orbitals).

The sample for a UV-visible measurements is usually a solution but is may also be a solid or gas. For solid samples, measurement of reflected intensity of UV-visible radiation from the sample is easy than measuring transmitted intensity of the solid and an absorption spectrum is obtained by subtraction of the reflected intensity from the intensity of the incident radiation. In liquid phase it is widely applied for characterization of solvated ions, molecules as well as colloidal dispersions containing semiconductors or semiconducting nanostructures. Usually the light emerging from solutions is less intense than the incident light due to reflections at the surface and scattering by suspended particles. However, it is primarily accounted for the absorption of photons by the dissolved or solvated species. The

empirical Beer-Lambert law is used to relate the absorbance *A* to the molar concentration [J] of absorbing species J to path length *L*, which can be expressed as follows [2]:

$$A = \log_{10} \frac{I_0}{I} = \varepsilon[J]L \qquad (2.9)$$

where the absorbance of light from the substance has a logarithmic dependence on the product of absorptivity (molar absorption coefficient or extinction coefficient) ε. Whereas I_0 is the intensity of incident light at a given wavelength and *I* is the transmitted intensity.

In an UV/Vis spectrophotometer, the source of visible radiation is usually a tungsten filament which provides the radiation of wavelength in the visible region. For radiation of ultraviolet region (160 nm to 360 nm), a hydrogen or deuterium discharge lamp is used. A gas or liquid is contained in a cuvette constructed of Pyrex glass for visible region and pure silica for wavelength of below 320 nm. Usually, the beam of incident radiation is split into two, may either by prisms or more often, diffraction gratings. The part of the beam passes through the sample and other through the cell in absence of sample and emerging beams are compared at the detector which often are photomultipliers or photodiodes. As an advancement, recently, charged coupled devices (CCDs) consisting of an array of silicon photosensors are mostly being used as multiplex detectors, typically in the range of 400-1050 nm.[3,10]

2.6.1 Band gap analysis

An important application of UV-Vis diffuse reflectance spectroscopy is the measurement of electronic band gap values of the semiconductor. The band gap values of all the materials presented in this thesis were calculated from the UV-vis absorption spectra using following equation[11]:

$$\alpha h\nu = A(h\nu - E_g)^n \qquad (2.10)$$

where $h\nu$ is energy of light (in eV) α, ν , E_g *and A* are the absorption coefficient (Kubelka-Munk function), light frequency, band gap, and a constant respectively.[12,13] The value of *n* is determined by the characteristics transition of the semiconductor depends whether the material have direct or indirect band gap. From the plot of $(\alpha h\nu)^{1/2}$ vs. $h\nu$ band-gap energy of the materials was thus obtained extrapolating the linear portion to the $h\nu$ axis to give the value of band gap.

2.6.2 Kinetic measurements

UV-Vis spectroscopy provides a powerful tool for the determination of photocatalytic activity and rate of many reactions which involve a change in absorbing group. The rate of reaction can be measured by following either decrease in absorbance or increase in absorbance as a function of time. The absorbance can be plotted against time either directly or after converting them into concentration units. For determination of unknown concentration a linearity curve of absorbance vs. concentration with a slop εL can be made by recording the absorbance of a series of different concentrations of standard solutions. The unknown concentration of samples can then be read from graph or calculated using linear formula.

2.7 Photoluminescence (PL) emission spectroscopy

Photoluminescence is spontaneous emission of light from a material under optical excitation.[14] It is offers electrical characterization of the samples and it is selective and powerful to probe discrete electronic states. In particular features of emission spectrum can be used to identify the surface, interface, and interface roughness. In this thesis the intensity of *PL* signal is measured to extract the information about quality and behaviour of surface and interface. In addition time-resolved *PL* studies which are useful for characterization of

most rapid processes in material have also been reported for carbon nitride based heterojunctions.

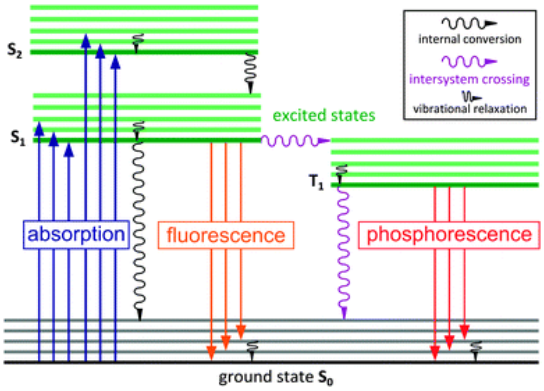

Figure 2.5 Energy level diagram showing photophysical processes in photoluminescent molecule; S denotes singlet, T triplet states; internal conversion and intersystem crossing are non-radiative processes; intersystem crossings are accompanied by a forbidden change in the spin state. Reproduce from the reference [15] by permission of The Royal Society of Chemistry.

Photoluminescence, encompasses both fluorescence (fast emission, ~ 10^{-8}) and phosphorescence emission (slow emission) is often used as fluorescence in literature.[3] The incident optical energy exceeding the band gap energy of semiconductor solids induces the promotion of valence band electrons to conduction band in order to establish an excited state. This state is characterized by existence of exciton and *PL* spectroscopy can be employed to probe the exciton behaviour and time scale of their recombination. An energy level diagram illustrating radiative and non-radiative transitions that are the basis of observation of photoluminescence are shown in Figure 2.5.

PL measurements depending on the nature of optical excitation can either be steady state or time resolved. In steady state *PL* a continuous excitation of sample at single wave length

(λ_{ex}) induces the stationary non-equilibrium state and the rate of carrier generation is in par with the rate of recombination, as shown in equation below:

$$\frac{P_{abs}}{E_{ex}} = V\left(\frac{2S}{d}n + \frac{B}{N}n^2 + Cn^3\right) \quad (2.11)$$

Here, P_{abs} is the absorbed laser power, E_{ex} is the laser energy, V is the volume, interface recombination velocity S, N is the photon recycling factor (average number of radiative recombination events required for a photon to escape the semiconductor) and B and C are parameters that describe the rates of radiative and Auger recombination respectively. The photo-generated intensity is constant in time while measurement of emission intensity across a range of frequencies yield a fluorescence spectrum.

In contrast, short laser pulses produces virtually instantaneous excited populations of carriers depending on time scale. Equation 3.11 can be rewritten in terms of nonequilibrium carrier life time τ as follows:

$$\frac{1}{\tau} = \left(\frac{2S}{d} + \frac{B}{N}n + Cn^2\right) \quad (2.12)$$

The photo-excited carriers then recombine in a manner that is characteristic of recombination path they follow. Hence, time resolved *PL* counts the number of emitted photon in a time domain to determine the carrier life time and characterize various recombination mechanisms.

In transient *PL* an incident photon on photodetector generates an electrical pulse that in conjunction with excitation reference pulse is fed into a constant fraction discriminator to obtain an output pulse. This output pulse is time corrected and independent of input pulse size and its height is proportional to the delay between input pulses. The output pulses are sorted out according to amplitude and counted by a multichannel analyser, yielding the transient *PL* decay.

2.8 BET

The determination of surface area of powders and porous materials depend on the measurement of adsorption. After Langmuir's comprehensive review on nature of adsorption (1916-1918) the first significant contribution was made by Brunauer and Emmett (1935, 1937) and later developed Brunauer- Emmett-teller (BET) theory in 1938. Since then the BET method has become a popular method for determining the surface area of adsorbents, catalysts, nanoparticles and various other finely divided porous materials.[16] In BET method, two stages are involved in the evaluation of the surface area from physisorption isotherm data. In the first stage a BET plot is constructed to derive the value of monolayer capacity, $\boldsymbol{n}_m$ and next stage is the calculation of specific surface area, a(BET), from $\boldsymbol{n}_m$ by careful consideration of average area, σ, occupied by each molecule in monolayer (i.e. the molecular cross sectional area).

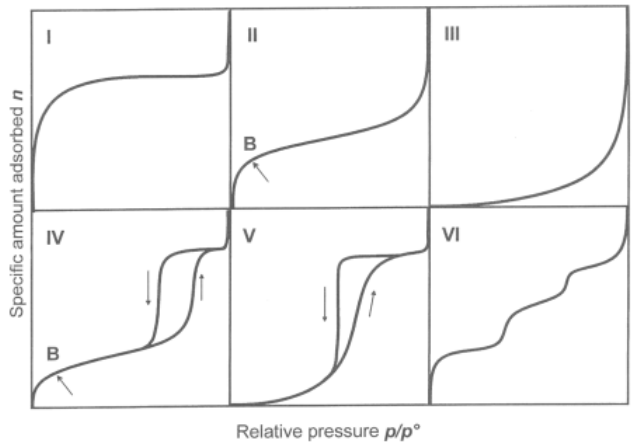

Figure 2.6 The six main types of gas physisorption isotherms, according to the IUPAC classification . Figure is modified from reference [17] with permission.

An absorption isotherm is a plot of the volume of gas adsorbed vs. the relative pressure, p/p^0. The six types of isotherm exhibited by a real surface are shown in Figure 2.6. Type I, is characteristic of only monolayer adsorption and requires a narrow relative pressure range to

attain the plateau which is indicative of a limited range of pore size while its horizontal shape is representative of the low surface area. The type II isotherm is typical unrestricted monolayer-multilayer adsorption on a heterogeneous substrate. The type III behaviour is relatively rare, corresponds to the situation where adsorbate-adsorbent interactions are weak and Type IV isotherm with hysteresis loop indicates the presence of mesopores. A type V isotherm exhibit a hysteresis loop is associated with the mechanism of pore filling also indicates the weak adsorbate-adsorbent interaction similar to the type III. Type VI stepped isotherm, is associated with layer-by-layer adsorption on a highly uniform surface. Conventionally, the surface area analysis is performed by N_2 adsorption. From these data, it is not only possible to calculate the (BET) surface areas but also the pore sizes of the materials. In addition, the shapes of the adsorption/ desorption isotherms can provide information on the nature of the material studied.

2.9 CHN analysis

CHN analysis is a useful technique to obtain the elemental percentage of carbon, hydrogen and nitrogen by high temperature decomposition. It can also determine the oxygen and sulfur content of the sample.

In this method the sample is heated at 900 °C in oxygen and mixture produced is then swept with the stream of helium into the tube furnace at 750 °C. In furnace tube, copper reduces the nitrogen oxide to nitrogen while carbon mono oxide is converted to carbon dioxide. The resulting mixture is analysed by passing through a series of thermal conductivity detectors and data obtained is reported as mass percentage C, H and N. For oxygen analysis, a special quartz tube filled with carbon containing catalytic amounts of platinum is used.

2.11 References

[1] D. Simon, G. Bruce, C. Martin, *Foundations of Molecular Structure Determination*, Oxford University Press, **2015**.

[2] A. Peter, O. Tina, R. Jonathan, W. Mark, A. Fraser, *Inorganic Chemistry*, Oxford University Press, **2010**.

[3] C. Eley, The Rational Design of Photocatalytic Semiconductor Nanocrystals, University of Oxford, **2014**.

[4] T. Jia, Photocatalytic Hydrogen Production over Layered Materials, University of Oxford, **2014**.

[5] M. G. Suryanarayana, C., Norton, *X-Ray Diffraction - A Practical Approach*, **1998**.

[6] B. D. Cullity, *Elements Of X Ray Diffraction*, Addison-Wesley Publishing Company, Inc, **1967**.

[7] B. : Gary, Attard: Colin, *Surfaces*, Oxford University Press, **2004**.

[8] B. David, K. Wayne, D, *Microstructural Characterization of Materials*, John Wiley & Sons, **1999**.

[9] J. Ryczkowski, *Catal. Today* **2001**, *68*, 263–381.

[10] J. M. Hollas, *Modern Spectroscopy*, Wiley, **2004**.

[11] J. Tauc, R. Grigorovici, A. Vancu, *Phys. status solidi* **1966**, *15*, 627–637.

[12] M. A. Butler, *J. Appl. Phys.* **1977**, *48*, 1914–1920.

[13] R. F. Brandão, R. L. Quirino, V. M. Mello, A. P. Tavares, A. C. Peres, F. Guinhos, J. C. Rubim, P. A. Z. Suarez, *J. Braz. Chem. Soc.* **2009**, *20*, 954–966.

[14] T. H. Gfroerer, *Encycl. Anal. Chem.* **2000**, 9209–9231.

[15] J. Heine, K. Müller-Buschbaum, *Chem. Soc. Rev.* **2013**, *42*, 9232–42.

[16] F. Rouquerol, J. Rouquerol, S. Kenneth, *Adsorption by Powders and Porous Solids Princiles, Methodology and Applications*, Academic Press, **1999**.

[17] K. S. W. Sing, D. H. Everett, R. A. W. Haul, L. Moscou, R. A. Pierotti, J. Rouquérol, T. Siemieniewska, *Pure Appl. Chem.* **1985**, *57*, 603–619.

Chapter 3: Experimental Methods

3.1 Synthetic procedures

3.1.1 Synthesis of carbon nitride at different temperatures

Polymeric semiconducting (PS) carbon nitride (C_3N_4) was synthesized according to the procedure reported by Wang *et al*.[1] A 3.0 g quantity of dicyandiamide (DCDA) was heated in a customised semi closed system in tube furnace (Figure 3.1) at 550 °C (ramp: 2.3 °C min^{-1}) under inert conditions (N_2 atmosphere) for 4 hours. Synthesised material was ground for testing without any other modification. Similarly, a series of samples were synthesised using the same precursor (DCDA) and treating it at different temperatures 400 °C, 450 °C, 500 °C, 550 °C and 600 °C (ramp rate: 2.3 °C min^{-1}) under inert conditions (N_2 atmosphere) for 4 hours. The resulting samples were denoted as CN400,[a] CN450, CN500, CN550 and CN600 respectively.

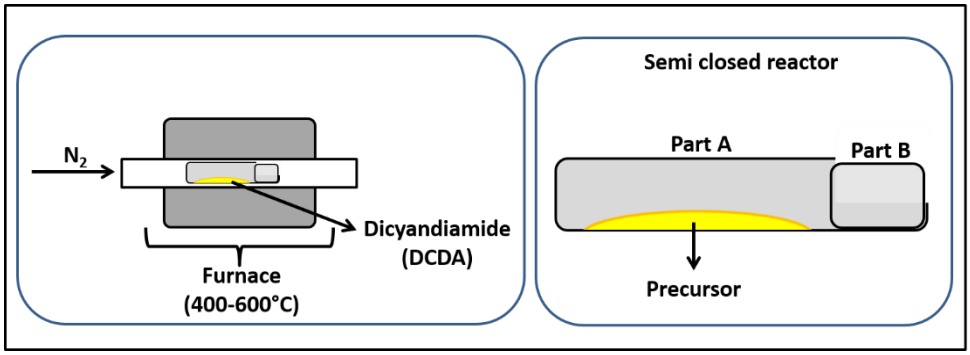

Figure 3.1 Schematic diagram for the synthesis of Carbon nitride

3.1.2 Carbon nitride-carbon nitride (CN-CN) heterojunctions composites

To prepare carbon nitride-carbon nitride (CN-CN) heterojunctions DCDA was heated at 600 °C to produce CN600 (CN represent carbon nitride and 600 is temperature it was treat)

[a] Carbon nitride is abbreviated as CN and the number at the end represent the synthesis temperature

semiconductor. Then 0.5 g of this as prepared CN600 was well dispersed in 10 mL water. To this mixture certain amount (0.2g, 0.4g, 0.6g) of DCDA was added followed by heating at 80 °C for 6 hours to form a composite. This resulting composite (dried in an oven at 80 °C for 24 hours) was further subjected to heat treatment at 500 °C and tempered for 3 hours to form the homogenized CN500 layer over CN600. The three resultant samples were denoted as CN-CN1, CN-CN2 and CN-CN3 respectively.

Workup: The yellow powder of CN600 was thoroughly ground to a fine powder prior to mixing with DCDA in water. Finally, synthesized CN-CN heterojunction composite materials were ground again for testing without any other modification.

3.1.3 Niobium pentoxide Nb_2O_5 nanospheres

Niobium oxide (Nb_2O_5) used in study was synthesised according to already reported method with some modifications.[2] In typical procedure Nb_2O_5 nanospheres were prepared by solubilizing ammonium niobate (V) oxalate hydrate $NH_4[NbO(C_2O_4)_2(H_2O)]\cdot(H_2O)n$ (14 g) in 100 mL of water at 90 °C, followed by precipitation with NH_4OH (5 mol L^{-1}) in dropwise manner until the pH of the mixture reached 7.5 and stirred further for 2 hours. Resulting mixture for hydrothermal treatment was then transferred to Teflon-lined steel autoclave and heated to 140 °C for 24 h. Subsequently the resultant product was collected filtered and washed several times with distilled water and dried at 80 °C for 24 hours and finally ground to powder.

3.1.4 Carbon nitride- Niobium oxide composite heterojunctions

C_3N_4-Nb_2O_5 heterojunctions were obtained by hydrothermal method with C_3N_4 and precursor of Nb_2O_5. In a typical procedure mixture of C_3N_4 and $NH_4[NbO(C_2O_4)_2(H_2O)](H_2O)n$ was dissolved in 30 mL of water at 90°C followed by vigorous stirring to obtained the uniform suspension. Then NH_4OH (5 M) was added dropwise until the pH of the mixture reached 7.5 and stirred for 2 h. Resulting mixture was then transferred to Teflon-lined steel autoclave which was heated to 140℃ for 24 h similar to the method 3.1.3 and resultant product was collected filtered and washed several times with distilled water and dried at 80℃ for 12 h and finally ground to powder. According to this method, different mass ratios of C_3N_4-Nb_2O_5 heterojunction 9:1, 7:3, 6:4, 5:5, and 3:7 were prepared and denoted as $0.9C_3N_4$-$0.1Nb_2O_5$, $0.7C_3N_4$-$0.3Nb_2O_5$, $0.6C_3N_4$-$0.4Nb_2O_5$, $0.5C_3N_4$-$0.5Nb_2O_5$ and $0.3C_3N_4$-$0.7Nb_2O_5$ respectively.

Table 2.1 Carbon nitride- niobium oxide composite heterojunctions

Sample	Mass ratio C_3N_4 : Nb_2O_5	Composite heterojunctions
1	9 : 1	$0.9C_3N_4$-$0.1Nb_2O_5$
2	7 : 3	$0.7C_3N_4$-$0.3Nb_2O_5$
3	6 : 4	$0.6C_3N_4$-$0.4Nb_2O_5$
4	5 : 5	$0.5C_3N_4$-$0.5Nb_2O_5$
5	3 : 7	$0.3C_3N_4$-$0.7Nb_2O_5$

3.1.5 Mechanically ground mixture of Carbon nitride-Niobium oxide

To compare the photocatalytic activity of C_3N_4-Nb_2O_5 physical mixture with the hydrothermally synthesized C_3N_4-Nb_2O_5 heterojunction, as a reference, a mechanically ground mixture of 6:4 C_3N_4-Nb_2O_5 sample was prepared.

3.2 Photocatalytic Testing

3.2.1 Preparation of Photoelectrode

The working electrode was prepared using fluoride-doped tin oxide (FTO) conducting glass substrate, which was cleaned sequentially in water, isopropanol, acetone and ethanol under 15 min of sonication respectively. The clean FTO glass was then kept in isopropanol for 24 hour prior to film deposition. For the film, 25 mg of photocatalyst sample was mixed with 1 mL of dimethylformamide containing 50 μL of 5 wt% Nafion (to aid the adhesion) under efficient sonication to make a slurry. The slurry was then dip-coated onto FTO substrate and tape casting technique was employed to ensure the same thickness for each electrode similar to reported methods.[3,4] After air drying, the electrode was annealed at 350 °C for 1 hour in tube furnace with ramp 2 °C/ min in N_2 to improve the adhesion. A gold plated crocodile clip was used to make the electrical contact on the bare area of the film.

3.2.2 Photoelectrochemical measurements

Photoelectrochemical measurements were carried out using Autolab, (PGSTAT302N) system in a standard three-electrode configuration CN film as working electrode, a Pt wire as counter electrode and an Ag/AgCl electrode as the reference electrode. The electrodes were immersed in 0.2 M Na_2SO_4 solution without any additive which was well purged with nitrogen to remove the air completely prior to the measurements.[5] The distance between irradiation source and film was kept where the light intensity 100 mW/cm^2 using 1.5 air mass filter while the wavelength of the incident light was controlled employing 420 nm cut off filter.[b] Moreover, in the photocurrent measurements, working electrode was irradiated from the back side in order to minimize the influence of thickness of film. During the operation

[b] Incident visible light solar spectrum: high noon, sea level solar flux conditions

the voltage scan speed was 0.01 V/s and light was chopped manually. Mott-Schottky experiments were performed in dark using a computer controlled potentiostat (Autolab, PGSTAT302N) three electrode system.[3] The perturbation signal was maintained at 10 mV while frequency was scanned between 1 KHz to 3 KHz at a potential range from -0.2 to 0.8 V vs $V_{Ag/AgCl}$.

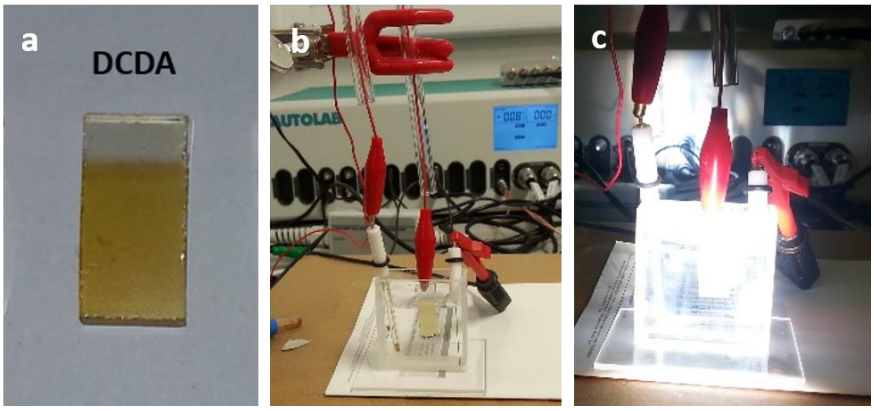

Figure 3.2 (a) Film of carbon nitride on fluorine tin oxide glass (FTO) prepared using tape casting technique, (b) carbon nitride film immersed in electrochemical cell and (c) visible light illuminated set up during photocurrent measurement.

3.2.3 Photocatalytic hydrogen evolution rate (HER) determination

The photoactivity of CN and CN-CN heterojunctions was tested in a custom Pyrex glass flask system, which was purged thoroughly with nitrogen prior to irradiation. For a typical reaction 100 mg of photocatalyst was suspended in aqueous solution (100 mL) containing triethanolamine (10 mL, TEOA) as a sacrificial electron donor. Further, Pt was photodeposited as co-catalyst using H_2PtCl_6 dissolved in reactant solution.[1,6,7] Prior to each hydrogen production experiment reactor was sealed, purged with N_2 and evacuated several times to remove air completely. The illumination source was 300 W Xe lamp with cut off filter ($\lambda > 420$ nm) to simulate the visible light conditions. This modification of using Pt as co-catalyst defies the 'metal free' principle but assists the hydrogen production with steady

rate. The concentration of evolved gases was analysed using gas chromatography equipped with thermal conductivity detector (TCD), and argon as carrier gas.

3.2.4 Photocatalytic activity (methylene blue degradation) study

Comparative catalytic testing was conducted at ambient laboratory temperature with aqueous methylene blue (MB) stock solution (11.2 mg L^{-1}) and 2,4 dichlorophenol (2, 4-DCP, 15 mg L^{-1}), as the degrading pollutant, to test the photocatalytic activities of as prepared C_3N_4-Nb_2O_5 heterojunctions. MB degradation is widely used as representative reaction for examining the performance of many visible light active photocatalysts[8,9] while 2, 4-DCP was used owing to no absorption in visible region. In each experiment 100 mg of catalyst was dispersed in 100 mL aqueous solution of MB or 2, 4-DCP and stirred for 30 minutes in the dark to allow dye adsorption/desorption on the surface of the photocatalyst to equilibrate.

The reaction mixture was then exposed to the visible light irradiations with constant stirring using a 70W EYE Colour Arc MTD70/D Metal Halide Lamp. The distance between the light source and reactor was kept at 15 cm for 2, 4-DCP and 35 cm for the degradation of MB, respectively. 3mL samples of catalyst/dye solution were extracted at 15 minute intervals. Dye concentration was determined tracking dye absorption at 664 nm using Perkin Elmer LAMBDA 750S UV/Vis/NIR spectrophotometer, after centrifuging at 5000 rmp for 10 min to the remove the suspended catalyst particles.

The decomposition of MB with time was fitted to the following pseudo first order rate equation:

$$C\,(t) \;=\; C_0\, e^{-kt} \qquad (3.1)$$

Where $C\,(t)$ is concentration at time t, C_0 is concentration at time $t = 0$, k is apparent rate constant and t is irradiation time. The linear form of equation 3.1 is as follows:

$$ln\left(\frac{C}{C_0}\right) = -kt \qquad (3.2)$$

Plotting $-ln(C/C_0)$ versus irradiation time t (according to equation 3.2) results in a straight line with a slope equal to k, which is quantitative measure of comparative kinetic efficiency of photoreaction.

The degradation efficiency (%) can be calculated as

$$E\ (\%) = c_0 - \frac{C}{C_0} \times 100 \qquad (3.3)$$

where c_0 is the initial concentration of dye and c is the final concentration after photoirradiation.

3.2.5 Photochemical reaction study (Photoacetalization reactions)

The photoacetalization reactions were carried out in an outer irradiation-type photoreactor (Pyrex glass). In all reactions approximately 0.025 g of the photocatalysts were dispersed with magnetic stirring in 5 mL of methanol and 1mM of substrate was added. The suspension was purged with O_2 for 5 min and irradiated with visible light. Constant magnetic stirring (400 rpm) was used during the experiment to ensure homogeneity of the suspension and to avoid sedimentation. After completion the reaction products were identified and quantified by GC-MS (Agilent 6890 and Agilent MSD 5973 (N)).

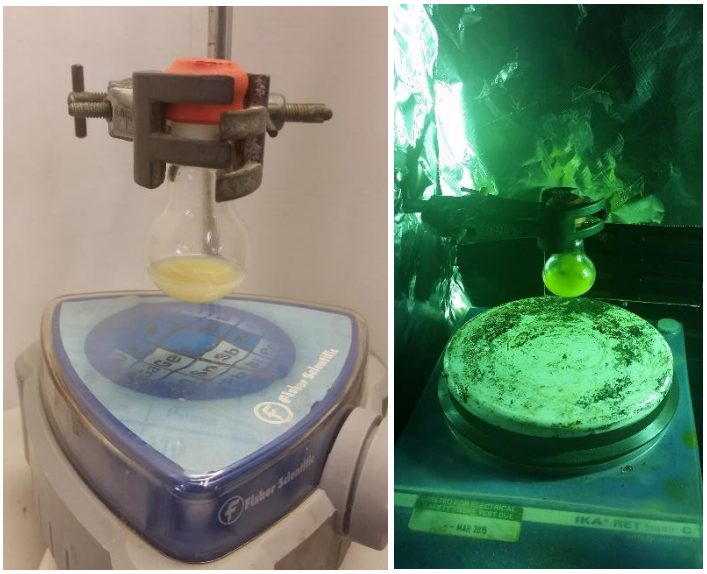

Figure 3.3 Set up of outer irradiation-type photoreactor for photochemical organic synthesis using carbon nitride and visible light.

3.2.6 Auto tandem photooxidation/acetalization of alcohols

The photo-oxidation/acetalization reactions were carried out in an outer irradiation-type photoreactor (Pyrex glass) as mentioned above. In all reactions concentration are comparable as described in section 3.2.5 and product were identified and quantified by GC-MS (Agilent 6890 and Agilent MSD 5973 (N)).

3.3 Characterisation procedures

3.3.1 XRD

X-ray diffractions (XRD) patterns were measured on PANanlytical X'Pert Pro PW 1710 diffractometer operating in Bragg–Brentano focusing geometry and using Cu Kα radiation (k = 1.5418 Å) from a generator operating at 40 kV and 40 mA. To achieve optimum results colloidal samples were prepared by drop-dry method and powder samples were prepared by

placing a layer of dry powdered sample onto fixed depth quartz glass slide and surface was pressed level. The patterns were collected between 5° and 80°.

3.3.2 XPS

XPS measurements were done using a Thermo Scientific K-Alpha XPS instrument equipped with a microfocussed monochromated Al X-ray source. The source was operated at 12 keV and a 400 micron spot size was used. The analyser operates at a constant analyser energy (CAE) 200 eV for survey scans and 50eV for detailed scans. An average of 5 scans between 0 and 1200 eV with a 1 eV step size, 0.1 seconds dwell time for survey spectra whereas for detailed high resolution specific regions an average of 10 scans each with step size of 0.1 eV and 0.2 second dwell time were collected. Charge neutralization was applied using a combined low energy / ion flood source.

The data acquisition and analysis was performed with Thermo Scientifics Avantage software. Peak fitting (Lorentzian / Gaussian (L/G) 30%) was applied following removal of a Smart background. Normalised atomic percentages were determined from peak areas of the elemental main peaks detected on the survey scan following background subtraction and application of Thermo sensitivity factors.

3.3.3 FTIR

The Fourier transform infrared (FTIR) was performed on a Nicolet 6700 FT-IR spectrometer with a MCT detector cooled. Liquid nitrogen was added to cool the detector compartment for 30 min before the IR beam was aligned for the best signal. All the powdered samples were pressed onto a smart ZeSe/ diamond crystal to form a film. The obtained spectra are

averaging the 128 scans with 2 cm^{-1} resolution over the wavenumbers ranging from 650 to 4000 cm^{-1}.

3.3.4 Solid state ^{13}C CPMAS NMR

Solid-state Cross-Polarization Magic Angle Spinning Carbon-13 (^{13}C CPMAS) NMR spectra was collected on Bruker Avance III HD 400MHz Solid state NMR.

3.3.5 BET

N_2 sorption was carried out using a Micromeritics TriStar II using BET method. All the samples were outgassed at 150 °C for 6 h prior to measurements. N_2 gas adsorbate was used with 2 min equilibration time at each point. The diameter volumetric distribution and mean pore diameter was determined by the Barrett– Joyner–Halenda (BJH) method, from the adsorption branch of isotherm, and the total pore volumes were estimated from the adsorbed amount at the constant C, where a relative pressure of P/P_0 = 0.90 was set. According to the accuracy of the instrument, the error is within 1%.

3.3.6 UV-vis absorption

Both liquid and solid state UV/Vis absorbance spectra were recorded at room temperature using Perkin Elmer LAMBDA 750S, UV/Vis/NIR spectrometer.

For liquid state analysis: Absorption spectra for aqueous methylene blue samples were collected in absorption mode after 100 % transmission baseline collected with sample cuvettes removed while matched quartz cuvettes were used for all liquid based measurements.

For solid state analysis: Samples were prepared by grinding the 5 mg of sample and 500 mg of dry KBr together to achieve uniform mixture. Sample pellets were made by compressing the solid into a sample disk (diameter = 13 mm, thickness = ~ 5 mm) using an applied force of 10 tons for 1 minute. The spectra were recorded in absorption mode after collecting 100 % transmission base line of solid disk pressed from pure KBr.

3.3.7 TEM

Transmission electron microscopy (TEM) images were recorded on JEOL 2010 equipped with a high-resolution pole piece running at 200 kV accelerating voltage. Samples were prepared by dispersing the powder products as slurry in 1:1 water ethanol solution which was then sonicated for 10 min before being deposited and dried on Agar Scientific 400 mesh Cu holey carbon support.

3.3.8 SEM

SEM, images were taken on JEOL 6500F FEG SEM with voltage of 5KV and working distance of 10mm.

3.3.9 Photoluminescence (PL)

3.3.9.1 Steady State and transient absorption measurements

The steady state absorption spectra were recorded with a Varian Cary 300 UV/Vis spectrometer using an integrating sphere to account for the optical losses outside of the active layer. Nanosecond transient absorption measurements were carried out with a LP920 laser flash spectrometer (Edinburgh Instruments) where samples were angled 45° to the excitation

beam and excited by a nanosecond pulse laser (pump pulse OPOLett-355II laser; 10 Hz repetition rate) and changes in time evolution of differential absorption were monitored by a continue wave (cw) light source probe (Xenon arc lamp). Two different detection system were employed; a liquid nitrogen cooled intensified CCD (ICCD) camera to detect the 350-850 nm spectral range at once and a set of photomultipliers for collection of single wavelength kinetics with higher sensitivity. The signal was finally processed by a TDS 3032C digital signal analyzer and for transmission change in the absorption after photoexcitation was as follows[10]

$$\Delta DO\ (\tau, \lambda)\ =\ \log\ (I_{probe} / I_{t\ (\tau,\ \lambda)}) \qquad (3.4)$$

Where I_{probe} and I_t are transmitted probe with excitation off and transmitted probe after laser excitation, respectively and τ_1 and τ_2 are time constants.

3.3.9.2 Photoluminescence measurements

Steady-state and time-resolved Photoluminescence (PL) measurements were acquired using a time-correlated single photon counting (TCSPC) setup (FluoTime300, PicoQuant GmbH). The samples were excited using a 405 nm laser pulsed at frequencies between 0.3-10 MHz. The PL was collected using a high resolution monochromator and hybrid photomultiplier detector assembly (PMA Hybrid 40, PicoQuant GmbH).[10,11]

Parameters describing the photoluminescence were obtained by fitting the background-corrected PL with a stretched biexponential decay function of the form

$$y = A_1 \exp^{(-t/\tau 1)} + A_2 \exp^{(-t/\tau 2)} \qquad (3.5)$$

Where A_1 and A_2 are prefactors and τ_1 and τ_2 are time constants. Errors in the fitting parameters were determined by examining the Adjusted R-squares obtained by

independently varying each fitting parameter. For ease of comparison of lifetimes between samples with different quenchers, $\tau 1$ is defined as the time taken after excitation for the PL intensity to drop to 1/e of its peak intensity. The fitting parameters are summarized in Table 4.2. Chapter 4, where all the measurements were performed at room temperature and atmospheric pressure with solid state samples.

For PL measurements films were prepared by dispersing the 25 mg of photocatalyst sample in 1 mL of dimethylformamide (DMF) under well sonication to make slurry. The slurry was than dip-coated onto glass slide and doctor blade technique was employed to ensure the same thickness for each sample and subsequent annealing at 300 °C for 2 hour in air.

3.4 References

[1] X. Wang, K. Maeda, A. Thomas, K. Takanabe, G. Xin, J. M. Carlsson, K. Domen, M. Antonietti, *Nat. Mater.* **2009**, *8*, 76–80.

[2] L. C. A. Oliveira, M. F. Portilho, A. C. Silva, H. A. Taroco, P. P. Souza, *Appl. Catal. B Environ.* **2012**, *117-118*, 29–35.

[3] J. Zhang, J. Sun, K. Maeda, K. Domen, P. Liu, M. Antonietti, X. Fu, X. Wang, *Energy Environ. Sci.* **2011**, *4*, 675.

[4] F. Meng, J. Li, S. K. Cushing, M. Zhi, N. Wu, *J. Am. Chem. Soc.* **2013**, *135*, 10286–10289.

[5] Y. Hou, F. Zuo, A. P. Dagg, J. Liu, P. Feng, *Adv. Mater.* **2014**, *26*, 5043–9.

[6] X. Wang, K. Maeda, X. Chen, K. Takanabe, K. Domen, Y. Hou, X. Fu, M. Antonietti, *J. Am. Chem. Soc.* **2009**, *131*, 1680–1.

[7] J. Zhang, M. Zhang, R.-Q. Sun, X. Wang, *Angew. Chem. Int. Ed.* **2012**, *51*, 10145–9.

[8] Y. Tian, B. Chang, Z. Yang, B. Zhou, F. Xi, X. Dong, *RSC Adv.* **2014**, *4*, 4187–4193.

[9] T. T. Surface, Y. Zhao, C. Eley, J. Hu, J. S. Foord, L. Ye, H. He, **2012**, 1–5.

[10] S. D. Stranks, G. E. Eperon, G. Grancini, C. Menelaou, M. J. P. Alcocer, T. Leijtens, L. M. Herz, A. Petrozza, H. J. Snaith, *Science* **2013**, *342*, 341–345.

[11] C. Ma, C. T.-L. Chan, W.-M. Kwok, C.-M. Che, *Chem. Sci.* **2012**, *3*, 1883.

Chapter 4: Construction of Carbon nitride isotype heterojunctions for improved photocatalytic activity

Overview

This chapter describes the construction of polymeric carbon nitride isotype heterojunctions by controlled thermal condensation of dicyandiamide in a stepwise manner with the aim of improving its intrinsic photocatalytic activity. A series of samples processed at temperatures between 400-600 °C show tremendous changes in physicochemical properties and electronic band structure. As a result, heterojunctions were created by synthesising carbon nitride process at 500 °C over carbon nitride process at 600 °C. The detailed characterisation revealed a favourable type II heterojunction configuration. Photoluminescence (PL) measurements indicated that quenching of static PL intensity wheras time resolve PL showed the effective charge transfer in resulting heterojunctions. As a consequence, photocurrent generation and visible light driven H_2 production activity were enhanced. The improved activity was attributed to the assisted charge transfer of the built-in electric field which arises from the topology-induced band offsets at the intrinsic heterojunction interface of the polymeric materials. These results highlight the rich potential of improving activity by the use of isotype heterojunctions in photocatalysis.

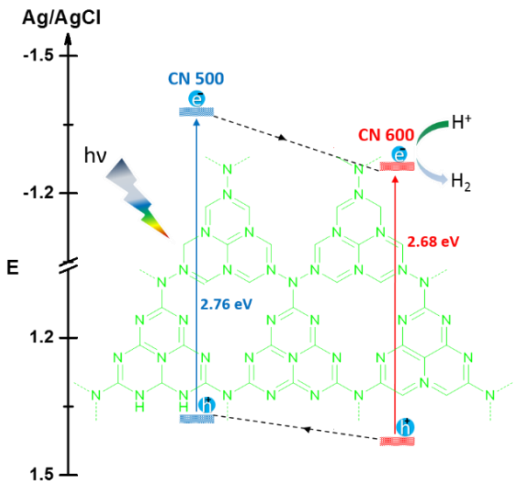

Construction of carbon nitride isotype heterojunctions

4.1 Introduction

Many examples of CN semiconductor heterostructures are reported in the literature (partly outlined in section 1.10.2). However, only a small number of organic heterojunctions comprised specifically of polymeric semiconducting (PS) carbon nitride have been reported.[1–3] In principle, photocatalytic processes involve the photogeneration and separation of excitons which can subsequently participate in redox reactions.[4–7] Hence, the photocatalytic performance is dependent mainly on the intrinsic physicochemical properties of the material, including its surface electronic structure, optical absorption, band gap, band edge positions and the ability for charge separation.[1,6] Carbon nitride, as a metal free PS, exhibits promising photocatalytic activity under visible light due to the presence of delocalized π-electrons on its polymeric backbone, which favour charge separation and transfer while retaining easy processability.[8]

Carbon nitride has a unique layered framework of earth abundant elements, carbon and nitrogen, with a narrow band gap (2.7 eV) and electronic band structure and band edge positions straddling H_2O redox potential.[9] This, coupled with CN's ability to efficiently absorb light, make CN a particularly effective photo-transducer for both the water reduction and oxidation reactions.[10–12] Furthermore, owing to its tolerance and inertness to extremely harsh pH, photo(chemical) and thermal conditions and metal free nature, CN is an attractive photocatalyst, in contrast to the predominant metal oxides, metal sulfides and metal oxy-nitrides and other photo active materials which are unstable and prone to leaching. [4,7,13] Despite CN's distinctive features, its photocatalytic activity and efficiency have been limited mainly due to fast recombination and low mobility of the charge carriers.[14,15]

Recently, various modifications have been devised to deter exciton recombination and promote separation and collection of charges *via* surface passivation, band alignment and

heterojunction strategies. For instance, Au particles were deposited on carbon nitride to accumulate and extract the charge on the metal/polymer interface while doping of heteroatoms (B, S, P etc.) have been used to alter the intrinsic electronic structure.[16] In a number of reports, carbon nitride was coupled with other well aligned/matched band structure semiconductors (C_3N_4-TiO_2, C_3N_4-ZnO, C_3N_4-CdS, C_3N_4-TaON etc.[17–20]) creating an intimate interface between the two components, forming heterojunctions. This approach has shown considerable success in impeding exciton recombination and facilitating space charge accumulation/depletion at the interface, resulting in enhanced photocatalytic performance.

Similarly, the band alignment approach was further advanced by utilizing the slight differences in electronic band structure in different crystal phases of a single substance. For instance, isotype heterojunctions have been fabricated by combining the two phases of same substances such as anatase-rutile TiO_2, α-β phase Ga_2O_3 and α-β phase Bi_2O_3.[21–25] Recently, a sulfur and boron containing polymeric carbon nitride framework CN-CNS and CN-CNB heterojunctions were constructed by coating the surface of unmodified CN with trithiocyanuric acid and tetraphenylborate before a thermal treatment.[1,3] Akin to this, C_3N_4-C_3N_4 isotype heterojunctions were prepared *in-situ* from a molecular composite precursor containing urea and thiourea treated simultaneously under the same thermal conditions.[2] The resulting heterojunctions, in all cases, showed enhanced photocatalytic performance and increased lifetime for the photoinduced charge carriers. Likewise, Vincent *et al.* demonstrated that low molecular weight carbon nitride with a predominantly melem active phase has three times the activity for hydrogen evolution from the water.[26]

4.2 Objectives

Despite the majority of the literature being focused on cumbersome modifications, heterojunction formation with a single precursor has not yet been fully explored. Heterojunctions prepared from the same precursor can provide alternative pathways to address the intrinsic limitations associated with the reliance on extra materials for CN modification.[1] Of particular interest is that the changes in synthetic conditions can yield derivatives with different degrees of polymerization, resulting in changes to the overlap of molecular orbitals within the CN material, in turn facilitating tuning of the electronic band structure (reported band gap of CN ranges from 2.4 to 2.8 eV).[10,11,27] In earlier work, it was found that the conduction band CB and valence band VB values for the CN material synthesized at 500 °C (-0.76 eV and +1.91 eV versus NHE respectively) differ approximately by 0.02 eV from the CN carbon nitride synthesized at 600 °C (-0.78 eV and +1.88 eV versus NHE respectively).[28] In a similar way, David *et al.* demonstrated the enhanced H_2 evolution from water using visible light by exploiting the effects of protonation and tailored polymerization of pristine CN.[29]

Taking these studies into account and the fact that band structure of CN changes with a slight change in pyrolysis temperature, we herein report the construction of isotype heterojunctions using the same precursor (dicyandiamide) with the simple stepwise change in temperature. It is important because the creation of an efficient junction not only depends on the close matching of physical structures of the semiconductors to form intimate interface but also on their electronic properties such as electron affinity and work function. Moreover, it is challenging to identify two closely related semiconductors to form synergetic heterojunctions. Furthermore, the formation of one CN semiconductor over the other utilises the defects and uncondensed NH_2 groups to form an interconnected structure with distinct band edge positions. Due to this simultaneous surface passivation and topology-induced

band offset of the same CN material without introducing two different types of semiconductors, we have found that the resulting isotype heterojunctions show significant improvement in visible light (λ >420 nm) driven H_2 evolution activity and photocurrent generation compared to the pristine CN materials.

4.3 Results and discussion

4.3.1 Synthetic approach

The CN-CN heterojunctions prepared in this study were synthesised by thermal condensation of the same precursor (dicyandiamide, DCDA) in customized semi-closed system at different temperatures in N_2 atmosphere. In this way differences in electron affinity and work function of the coupled semiconductors can be eliminated.

To prepare CN-CN heterojunctions DCDA was heated at 600 °C to produce CN600 semiconductor. This as-prepared CN600 was then coated on CN500 by its dispersed DCDA solution and the dried mixture was then subjected to heat treatment at 500 °C and kept for 3 hours to form the homogenized CN500 layer over CN600. The obtained samples were denoted as CN-CN1, CN-CN2 and CN-CN3 according to variations in the amount of deposited CN500 layers, respectively. Extensive experimental details of synthesis procedures, characterization methods and catalysis testing are given in Chapter 3 section 3.1.2.

4.3.2 Structural characterisation

4.3.2.1 XRD

X-ray diffraction plots of the as-prepared samples are shown in Figure 4.1a. The observed diffraction peaks are in agreement with previous reports on the XRD patterns of the polymer of melem (melon g-C_3N_4) prepared via the thermal condensation route.[9,30,31]

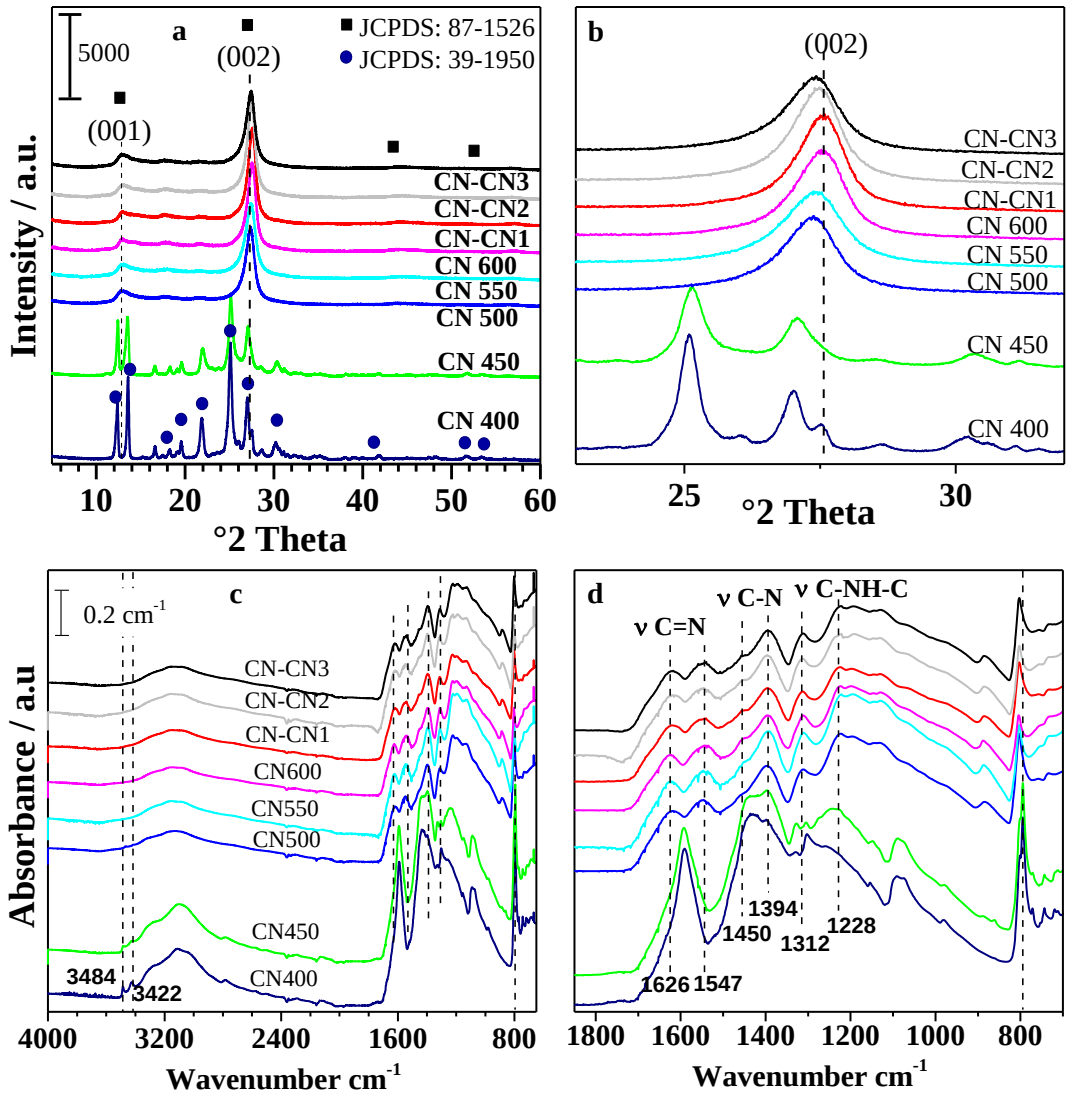

Figure 4.1 (a, b) XRD patterns of carbon nitride materials synthesized via thermal condensation of DCDA at different temperatures. (C) FTIR spectra of CN samples, (d) plot of narrower wavenumber region to emphasised the differences.

The peak around 13.04° can be assigned to the (100) interlayer stacking of conjugated aromatic systems) while the peaks around 27.2° and 44.2° are generally attributed to (002) in-plane structural packing motifs and (200)-reflex of triazine-based graphitic CN materials, respectively.[32] At higher temperature, a gradual decrease in crystallinity with transformation towards amorphous structure is evident. However, Tybroski *et al.* showed that higher process temperatures led to a higher degree of polymerization, and, thus denser packing of stacked polymer sheets. That, in turn, caused the stronger overlap of molecular orbitals of tris-s-triazine units, specifically π orbitals oriented along the (001) direction of the polymer.[32,33] A more careful analysis revealed the higher the process temperature employed, the weaker and broader are the (100) diffraction peak whereas the peak at 27.2° is slightly shifted towards higher diffraction angle. Further, a reduction in FWHM of the 27.2° peak from 1.6° for CN500 to 1.45° for CN600 was also observed, due to increase in number of layers as well as reduced stacking distance. The XRD patterns of CN-CN heterostructures are similar to the XRD patterns of the individual CN600 or CN500 materials, as shown in the Figures 4.1a and b.

4.3.2.2 FTIR

The changes in FTIR spectra of CN materials processed at different temperatures, are shown in Figure 1c-d. In general samples including CN-CN heterojunctions display characteristic IR absorption band for CN materials consistent with previous reports.[26,28] In all samples, the typical bands at 800-812 cm^{-1} of tri-s-triazine/s-triazine ring sextant out of plan bending, linked by -NH- groups at 1200-1400 cm^{-1} and 1200-1630 cm^{-1} of ν (C-NH-C) and ν (C=N, C=C) stretching vibrations were observed.[34,35] However, for CN processed at T < 500 °C a slight peak shifts towards lower wavenumber at 1590 cm^{-1}, 1326 cm^{-1}, and 1253 cm^{-1} were discernible in comparison processed at higher temperature. Interestingly, the key absorption

to identify the ring units in CN500 is located at higher wavenumber than of the samples processed at T < 500 °C and show higher intensity than sample T > 500 °C. This suggests that CN500 possess high tri-s-triazine content whereas the low intensity of the peak for CN600 can be attributed to N defects in tri-s-triazine phase.[28] It is also worth noting that stronger absorption of CN at 1320 and 1250 cm^{-1} may hint at the defective condensation of tri-s-triazine units imparting more C-C and C-N bond character to the CN polymer. These results clearly suggest that the variations in applied temperature during polycondensation of the CN influences the in-plane rearrangement of incomplete sheets, condensation patterns and structural refactoring of polymerising units. The spectrum of all CN-CN heterojunction is largely reminiscent of that of materials processed at a higher temperature having all the characteristics features retained.

4.3.2.3 SEM and TEM

Scanning electron microscopy images (SEM) of CN500, CN600 and CN-CN2 are shown in Figure 4.2. The CN500 sample shows pronounced aggregation however there is a relatively smooth surface with short lamellar structure with no clearly defined boundaries. The higher temperature treated sample CN600 exhibits rather compact and lamellar structure where individual layers are discernible. In CN-CN2 composite two distinct heterostructures are identifiable: smoother yet short CN500 layer and the underneath CN600 lamellar layer. Similarly, the successful formation of CN-CN heterostructure is clearly demonstrated by the TEM (Figure 4.2). The relatively condensed thick lamellar structure is CN600 and smooth paper-fold like layer is CN500, both of which are melded and closely interconnected as a heterostructure. Subsequent optical and electrochemical characterizations using a variety of techniques (UV/Vis PL and Mott-Schottky plots) confirm that CN-CN is definitely present in the form of heterojunctions.

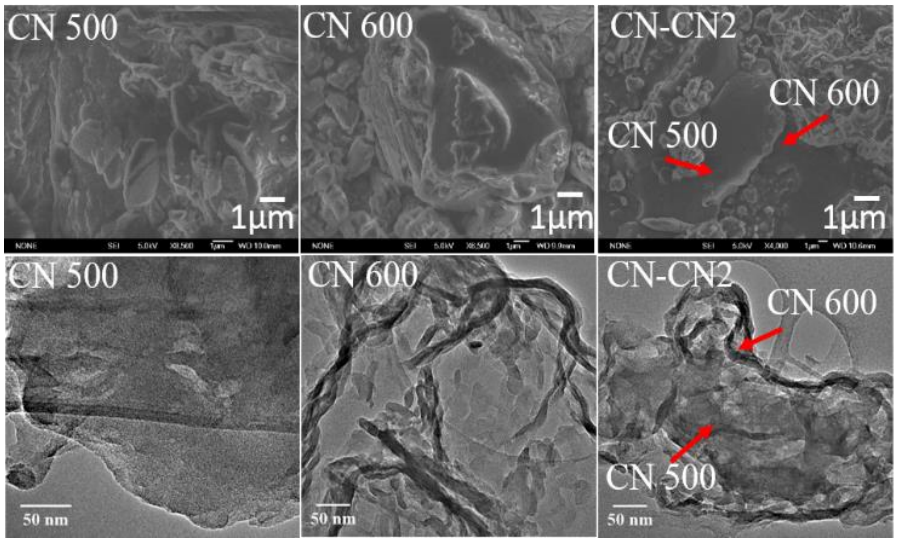

Figure 4.2 SEM images of the carbon nitride materials at the top and TEM images underneath.

4.3.3 Optical analysis

4.3.3.1 UV

The UV-vis spectra and band gap (E_g) values of the CN and CN-CN samples are shown in Figure 4.3. Assuming the parabolic nature and single photon process band gaps were calculated using equation:

$$\alpha h\nu = A(h\nu - E_g)^n \qquad (4.1)$$

where α, ν, and A are the absorption coefficient (Kubelka-Munk function, F(R)[a]), light frequency, and a constant respectively, [36,37] whereas n value depends on direct or indirect nature of transitions. Hence, the $(\alpha h\nu)^{1/2}$ and $(\alpha h\nu)^2$ were plotted *vs.* $h\nu$ and band gap energy was determined by extrapolating the linear port to the $h\nu$ axis intercept.

[a] Assuming that the wavelength dependence of the scattering coefficient can be neglected, the Kubelka-Munk function becomes proportional to the absorption coefficient. A plot of F(R) as a function of the excited light affords therefore the absorption spectrum of the powder.[43]

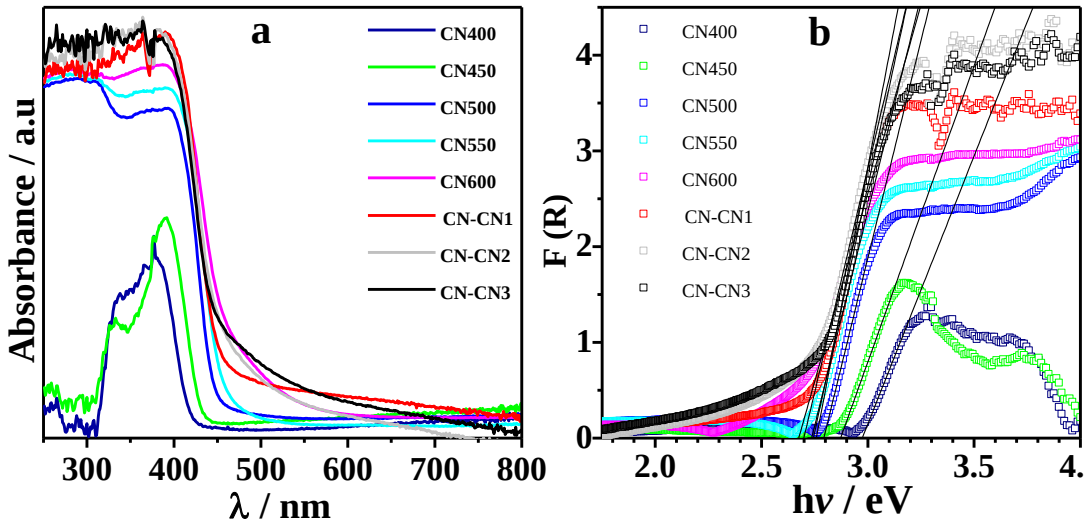

Figure 4.3 (a) UV/Vis absorption spectra of CN materials and the (b) band gap measurements.

The systematic decrease in E_g value with increase in process temperature can be attributed to increasing tri-s-triazine content which results in a strong conjugation between sp^2 N and triazine and stronger n-π* transitions.[28,33,38] This trend suggests that the main optical transitions in the UV-vis spectral range are dominated by the tri-s-triazine core, in CN polymer. In addition, a distinct low energy tail is evident in CN processed at 600 °C and CN-CN heterojunction samples. As mentioned before, this may be due to denser packing of motifs in the CN layers which sets the basis for strong overlap of molecular π-orbitals oriented along the (001) direction of stacked sheets. These results are consistent with the XRD observation of reduced FWHM and shift towards higher diffraction angle of the peak at 27.2°. The spectrum of the CN-CN heterojunction is reminiscent, more or less of the cumulative changes in the absorption spectrum of two materials. The onset absorption at a wavelength near to that of CN500 and long absorption tail similar to that of CN600 absorption spectrum can be seen. It is interesting to note that even a stronger tail in CN-CN heterojunction may be the result of distortions (due to the differences in degree of polymerisation) with increasing layer condensation and enhanced van der Waals interactions

(solvato-chromic effect) between the tri-s-triazine cores of the stacking sheets, suggesting intimate interface formation, however impeding the accurate determination of E_g.

4.3.3.2 Photoluminescence (PL) Studies

4.3.3.2.1 Steady state PL

The PL spectrum mainly arises from the recombination of photo-excited electrons and holes and the intensity is a function of their concentrations, which usually serve as a good candidate for the characterization of the heterostructure, indicating space charge accumulation/depletion, transfer and migration. To probe the behaviour of photogenerated excitons and to understand nature of the structure in CN synthesized at different temperature and CN-CN heterojunctions, steady-state photoluminescence (PL) spectra recorded at room temperature are shown in Figure 4.4a. From the spectra a clear and gradual red shift and FWHM broadening of PL peaks of CN with the increase in sample processing temperature are detected.[39] Also, the observed features near 450 nm correspond to π-π* transitions, whereas the emission around 500 nm is associated to n-π* manifold of the conjugated heptazine units of CN. These results are consistent with previous findings.[38,39] Interestingly, the n-π* band in CN600 shifts to longer wavelength and grows rapidly relative to the π-π* band. This indicates that the transitions involving the N lone pair surpass the latter as the CN sheet condensation or polymerization proceeds.[39]

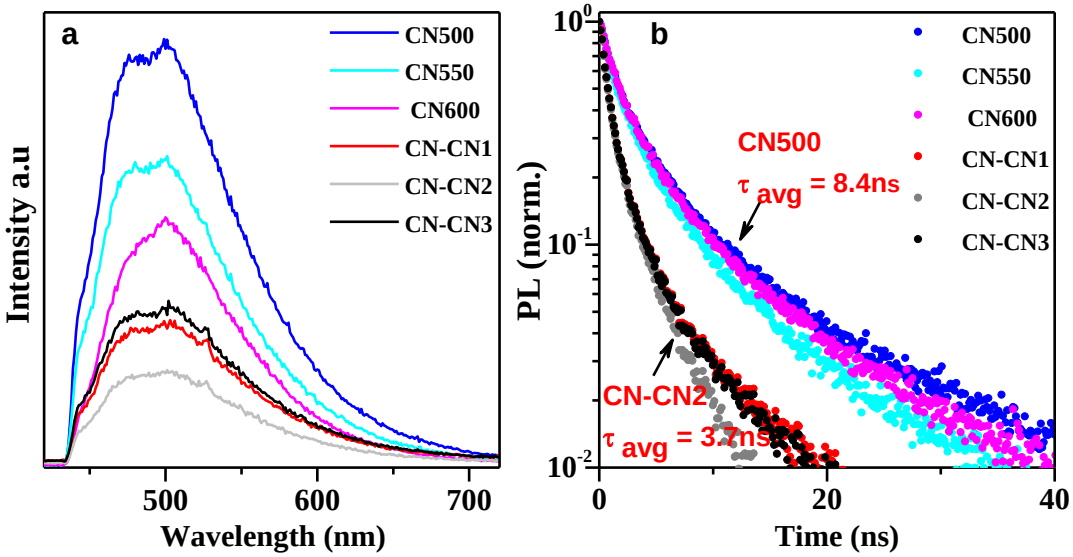

Figure 4.4 (a) Room temperature PL spectra of CN material C_3N_4 film excited by 405 nm laser pulsed at frequencies of 32 MHz. (b) Time-resolved PL measurements were taken at the peak emission wavelength of respective CN materials.

For CN-CN, the attenuation in PL intensity in contrast to CN can be attributed to the localization of charge carriers at the intimate interface and effective separation of charge by the band offsets between two CN materials with a different degree of polymerization and condensation, thus, passivating surface radiative recombination.

4.3.3.2.2 Time resolved PL

In order to appreciate the lifetime of the charge carriers and the time scale for such electron transportation, time-resolved (TR) PL (0-100 ns) from highest emission peak for each sample were measured. Samples were excited using a 405nm laser pulsed at the frequency of 32MHz. All the curves were obtained by fitting the background-corrected PL with a bi-exponential decay function of the form,

$$y = A_1\, exp(-t/t_1) \; + \; A_2\, exp(-t/t_2) \qquad (4.2)$$

Errors in the fitting parameter were determined by examining the Adjusted R^2 and independently varying each parameters to acquire the best fit.[40] The obtained lifetime of different carbon nitride materials are listed in Table 4.1.

Table 4.1 Exciton life-times results of CN materials

Sample	[b] *f 2 %	τ1 ns	*f 2 %	τ2 ns	τ_{avg} ns
CN500	24.9	1.77	75.1	10.79	8.54
CN550	28.3	1.68	71.7	7.35	6.43
CN600	33.1	1.31	66.9	7.75	5.61
CN-CN1	45.8	1.13	54.2	6.44	4.01
CN-CN2	42.4	1.12	57.6	5.60	3.70
CN-CN3	40.6	1.15	59.4	6.39	4.26

PL decay is governed by a fast bimolecular recombination process at the initial stage and slow monomolecular recombination at the long time scale. A part of photogenerated electrons due to the interstitial defects in the band structure of the CN are trapped therefore a relatively short carrier lifetimes τ_1 were obtained (Table 4.1). The rest of electrons reaching the CB are effectively separated/transferred due to the band offsets within the heterostructure, before returning to the VB level consequently long carrier lifetimes τ_2 were obtained. For ease of comparison, the lifetimes are given here in τ_{avg} (weighed average). The PL decay of pristine CN samples processed at 500 °C, 550 °C and 600 °C exhibit a time constant of τ_{avg} = 8.54, 6.43, and 5.61 ns respectively. It is clear that the formation of a CN500 layer over the CN600 in all the CN-CN heterostructures (heterojunctions) accelerated the quenching of charge carriers and PL decay. There is indeed a significantly faster electronic transfer between coupled CN500 and CN600 due to the suitable band off-

[b] *Fraction contribution

set in the resulting isotype heterojunction materials with observed time constants of τ_{avg} = 4.01, 3.70 and 4.26 for CN-CN1, CN-CN2 and CN-CN3, respectively. In particular, the electronic transitions in CN-CN2 are 2.3 and 1.7 times faster than in individual CN500 and CN600 implying that formation of an intimate interface promotes the separation and transfer of photogenerated electron-holes pairs within the coupled heterojunction CN materials. It has been demonstrated that there are some uncondensed NH_2 groups (evident from IR spectra) and other docking sites have remained in the carbon nitride structure due to the fast kinetics of the polymerisation process, and low thermodynamic stability of prebonded C−N core structures such as triazine and heptazine.[1] These structural imperfections enables CN for chemical modification by (the carbon atom in dicyandiamide, the precursor used to synthesised CN, can electrophilically attack the amino group on the parent CN600 to produce the CN-grafted CN hybrid) forming close contact CN-CN junctions at the surface upon thermal sintering.[1]

4.3.4 Electrochemical and Photoelectrochemical measurements

4.3.4.1 Preparation of Photoelectrode

The working electrode was prepared using clean fluoride-tin oxide (FTO) conductor glass, For film formation, 25 mg of photocatalyst sample was mixed with 1 mL of dimethylformamide under well sonication to make slurry. The slurry was then dip coated onto FTO glass substrate employing tape casting / doctor blade technique to ensure the same thickness for each electrode. After air drying, the electrode was annealed at 350 °C for 1 hour in a tubular furnace with a ramp rate of 2 °C/ min in air to improve the adhesion. The details of the preparation of photoelectrode are described in Chapter 3 section 3.2.

4.3.4.2 Photoelectrochemical measurements

Photoelectrochemical measurements were carried out in a standard three-electrode configuration CN film as working electrode, a Pt wire as a counter electrode and Ag/AgCl electrode as the reference electrode. The electrodes were immersed in N_2 purged, 0.2 M Na_2SO_4 solution without the addition of any additive.[41] The distance between irradiation source and the film was kept constant where the light intensity was 1.5 AM and the wavelength of the incident light was controlled by using a 420 nm cut-off filter. For photocurrent measurement, working electrode was irradiated from the back side in order to minimize the influence of thickness of the film. The voltage speed was 0.01 V/s and light was chopped manually. Mott-Schottky experiments were performed in dark on a computer controlled potentiostat three electrode system. The perturbation signal was maintained at 10 mV while applied frequency was scanned between 1 KHz to 3 KHz at a potential range from -0.2 to 0.8 V *vs* $V_{Ag/AgCl}$.

4.3.4.3 Mott-Schottky plot and photocurrent measurements

The flat band potentials of the CN semiconductor materials were determined by electrochemical Mott-Schottky plots. All three CN materials (Figure 4.5) portrayed *n*-type behaviour with positive slopes [41,42] and a steady change in flat band potential values (-1.37 <-1.30 <-1.26 V *vs* $V_{Ag/AgCl}$ pH = 6.6) with the increase in processed temperature was evident. Further, the CB and VB values for CN500 and CN600 (calculated from Figure 4.5, and band gaps values) reflected a difference of 0.03 V and 0.1 V, respectively. This provides the basis for the topology induced band offset required to construct the isotype heterojunctions from the same precursor (presumably through the variations in degree of polymerisation).

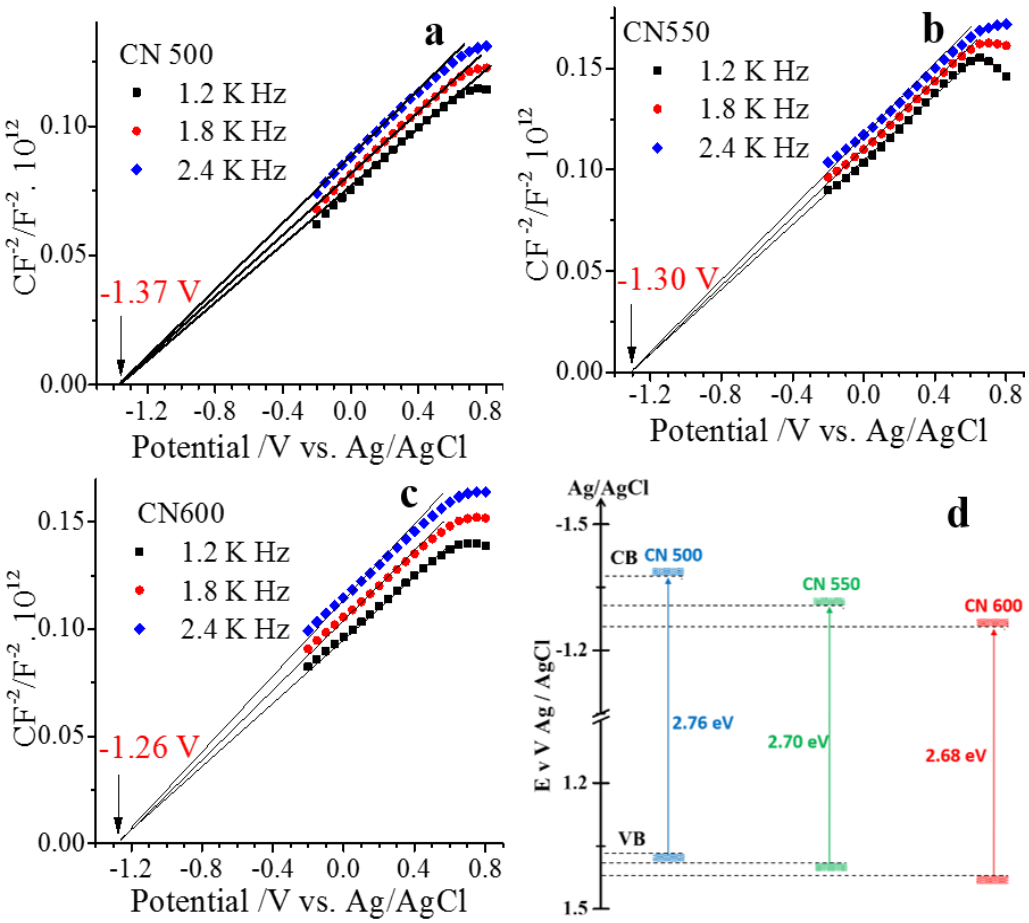

Figure 4.5 Electrochemical Mott-Schottky plot of (a) CN500, (b) CN550 and (c) CN600 samples. (d) Electronic band structure diagram of carbon nitride materials.

To gauge the photoactivity of the CN-CN heterojunctions, the films of heterojunctions as photoelectrodes (see Chapter 3 Figure 3.2) for solar electricity production were tested by recording the photocurrent density as a function of applied voltage under chopped illumination (Figure 4.6). The dark current densities in all the cases were negligible. Due to the formation of intrinsic heterojunction, visible light irradiation the photocurrent density obtained on the CN-CN heterostructure materials was ≈ 2.0 μA cm^{-2}, which significantly exceed CN500 of 1.0 μA cm^{-2}, the highest among the individual materials tested in this work (traditional carbon nitride materials previously showed the similar values). However, only

dark current was observed for CN400 and CN450 photoelectrodes due to their inability to harvest the visible light because of their wide band gaps. For other CN materials, slight changes in photocurrent were observed that follow a trend CN600 ≈ CN550 < 500 < CN-CN. This overall improved efficiency of photocurrent on CN-CN implies the effective charge separation, transfer and a relatively longer lifetime of the charge carriers due to the suitable band off-set and in-built electric field of heterojunctions in carbon nitride heterostructures.[28] This observation is consistent with observed quenching in PL intensity and decay results. However, the photocurrent response for CN550 and CN 600 in contrary to the PL intensity may be attributed to high temperature induced defects and squashed structure and large particle boundaries, as evident from SEM and TEM results, that impede the transfer of photogenerated carriers.[28]

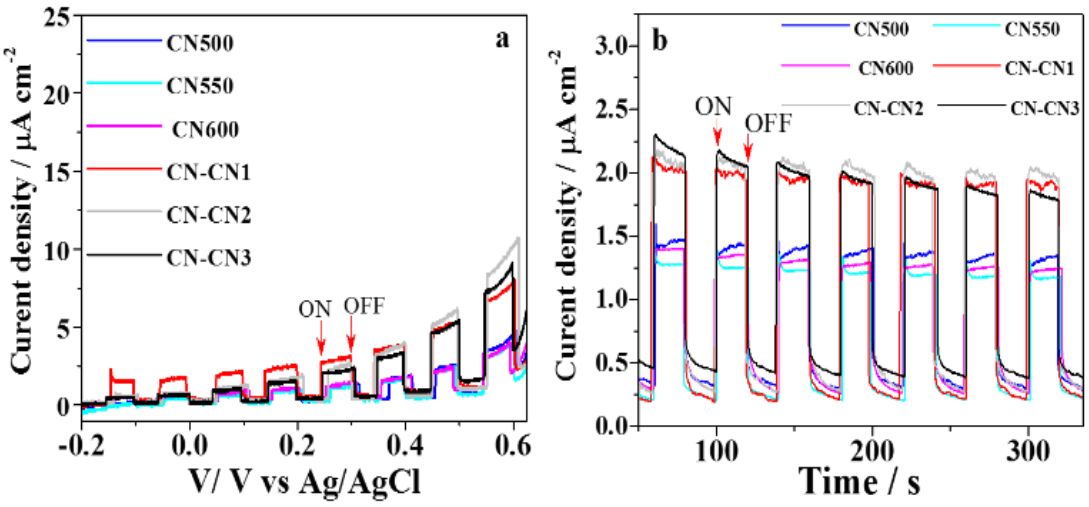

Figure 4.6 Variation of photocurrent density versus applied voltage for CN materials measured in 0.2 M Na_2SO_4 under simulated AM 1.5 x sunlight, (These are typical results for experiments that were performed many times) **(b)** Transient photocurrent density versus time at V = 0.25.

4.3.5 Hydrogen evolution rate (HER) of heterojunctions

Figure 4.7a shows the H_2 evolution rate (HER) of all the CN samples determined in aqueous 10 vol% triethanolamine TEOA using cut off filter, excitation wavelength of $\lambda > 420$ nm and 3% Pt as co-catalyst. The photocatalytic activities of all CN-CN samples in terms of HER were higher than that of the individual samples processed at different temperatures. This is presumably owing to intimate interface between coupled CN layers and band offset that helps to capture more visible light. It can be seen that the H_2 production activity increases slightly in the order of CN500 ≈ CN550 > CN600 whereas CN-CN2 heterojunction demonstrates 2.2 times higher H_2 production rate over CN500 (5.3 µmol/hour) and other CN materials processed at different temperatures. It is important to note that mechanical mixing of CN500 + CN600 that lacks the close interconnection did not match the activity of CN-CN heterojunctions. This result implies that synergic electronic structural modification (heterojunction formation) and interconnection by coupling CN500 and CN600 in CN-CN is necessary to enhance the photocatalytic activity. Further, it is interesting to mention that in two separate recent reports HER on CN was attributed to the higher degree of polymerization,[29] lower protonation (lower hydrogen content) on the surface and presence of active phase low molecular weight oligomer,[26] respectively.

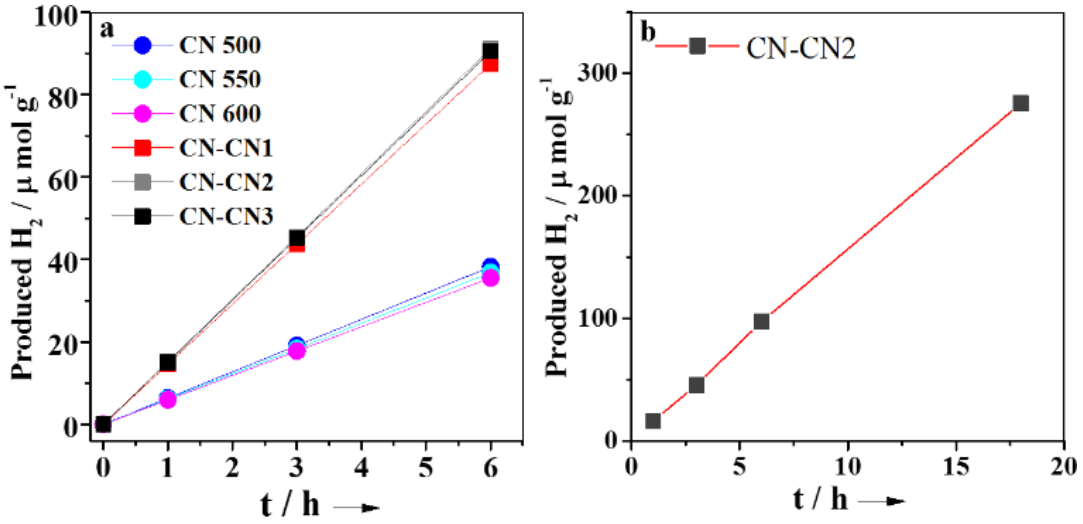

Figure 4.7 Photocatalytic hydrogen evolution on CN samples, (These are typical results for experiments that were performed many times) **(b**) stability test under visible light irradiation (>420 nm).

It is well established that the high temperature treatment results in surface termination sites and defects in CN.[15] However, our results presented show that the hydrogen content or the degree of polymerization (higher process temperature is presumed to give a higher degree of polymerization) in CN material did not correlate to the H_2 production activity. A relatively small H_2 evolution rate of CN600 was in fact obtained with lower hydrogen content (Table 4.2). The higher degree of polymerization suggested that CN500 may have more active tri-s-triazine phase (evident from XRD results) as the hydrogen content of CN500 was higher than that of CN 600. Since the increase in HER is often attributed to variations in surface area, however, BET results (Table 4.2) reveal a negligible difference. This clearly suggests the electronic structure modification rather than surface area is the key dominating factor for enhanced HER for CN-CN.

Table 4.2 Summary of properties of different CN materials

Sample	SSA $m^2 g^{-1}$	C wt%	H wt%	N wt%	Band gap eV	†HER μ mol $h^{-1} g^{-1}$
CN400	3.21	33.62	2.85	61.92	3.0	- -
CN450	4.45	33.85	2.91	61.88	2.90	- -
CN500	4.55	35.03	1.80	59.87	2.80	6.2
CN550	5.39	35.13	1.65	59.84	2.74	6.1
CN600	5.27	35.29	1.57	59.71	2.72	5.9
CN-CN1	5.11	35.33	1.63	59.77	2.68	13.4
CN-CN2	4.66	35.10	1.65	59.68	2.70	15.4
CN-CN3	- -	35.17	1.69	59.60	2.70	14.1
*CN mix						6.2

†The H_2 evolution rate was measured by using visible light ($\lambda > 420$), 3 wt% Pt, and TEOA as a hole-scavenger. *Physical mixture of CN500 + CN600

Further the surface chemical structure of CN-CN2 was analysed by the X-ray photoelectron spectroscopy (XPS) and results are shown in Figure 4.8. XPS showed C 1s and N 1s peaks along with residual O 1s peak. The latter was probably due to surface adsorbed oxygen.[29] C 1s spectra clearly showed the C-C, predominant C-N-C, and traces of C-O bonding at 284.5, 287.56 and 288.38 eV, respectively. The N 1s spectra showed four signals at core levels at 398.2, 400.06, 403.6 and 404 eV, which were attributed to sp^2 C-N-C, sp^3 H-N-[C_3], C-NH_x and terminal nitrate groups with charging effects or π excitations.[29,30] A traces of adsorbed oxygen at 532.038 eV and N-C-O at 530.07 were also observed. No unusual surface feature or deviation from typical carbon nitride structure is evident. These observations confirm that that enhancement of HER on CN-CN is not due to the change in hydrogen content or degree of polymerization but due to the formation of an isotype CN-CN heterojunction between coupled CN materials. The overall enhanced H_2 evolution on CN-CN can be attributed to the prolonged lifetime of the charge carriers, effective charge

separation due to equalised fermi level at the intimate interface that minimises the excitons recombination.

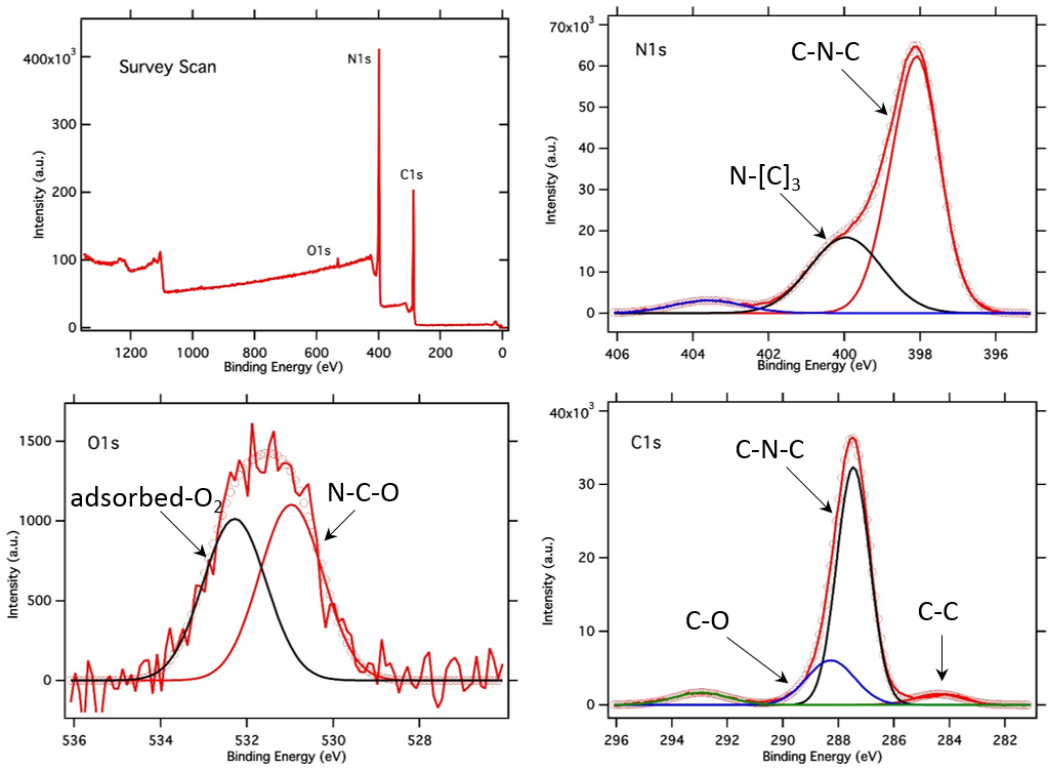

Figure 4.8 XPS survey, N1s, O1s and C1s spectra of CN-CN2 heterojunction, heterostructure synthesised from DCDA.

4.3.6 Stability

The stability of optimized heterojunctions acting as a photocatalyst for HER was also tested over an extended period of time. As seen from Figure 4.7b the CN-CN2 exhibits steady HER performance for 18 hours under the same photocatalytic conditions. The activity remains the same without any noticeable deactivation, showing the material is stable during the testing period. Additionally, the structure of CN-CN before and after reaction tested through the monitor of XRD remained the same, confirming the robustness of the heterojunction materials.

4.4 Conclusion

In this chapter, CN-CN isotype heterojunctions were synthesised by exploiting the difference in CN band structure and surface passivation caused by a simple change in polycondensation temperature. The use of the same starting precursor, without relying on the addition of extra materials, avoided any complication that arises with the different semiconductors of different electron affinity and work functions values. The obtained CN-CN heterojunctions demonstrated to promote the photocatalysed hydrogen evolution reaction from water under visible light irradiation. This is due to the improved charge separation and electron mobility of the built-in electric field which arises from type II heterojunction configuration, of closely related coupled carbon nitride polymers. This approach is simple, green and can be extended to the myriad of existing processes and may have applications to new polymeric systems for improving catalytic activity.

4.11 References

[1] J. Zhang, M. Zhang, R.-Q. Sun, X. Wang, *Angew. Chem. Int. Ed.* **2012**, *51*, 10145–9.

[2] F. Dong, Z. Zhao, T. Xiong, Z. Ni, W. Zhang, Y. Sun, W.-K. Ho, *ACS Appl. Mater. Interfaces* **2013**, *5*, 11392–401.

[3] H. Li, Y. Liu, X. Gao, C. Fu, X. Wang, *ChemSusChem* **2015**, *8*, 1189–96.

[4] A. L. Linsebigler, A. L. Linsebigler, J. T. Yates Jr, G. Lu, G. Lu, J. T. Yates, *Chem. Rev.* **1995**, *95*, 735–758.

[5] M. A. Fox, M. T. Dulay, *Chem. Rev.* **1993**, *93*, 341–357.

[6] X. Chen, S. Shen, L. Guo, S. S. Mao, *Chem. Rev.* **2010**, *110*, 6503–6570.

[7] R. M. Navarro Yerga, M. C. Alvarez Galván, F. del Valle, J. A. Villoria de la Mano, J. L. G. Fierro, *ChemSusChem* **2009**, *2*, 471–85.

[8] A. Facchetti, *Chem. Mater.* **2011**, *23*, 733–758.

[9] X. Wang, K. Maeda, A. Thomas, K. Takanabe, G. Xin, J. M. Carlsson, K. Domen, M. Antonietti, *Nat. Mater.* **2009**, *8*, 76–80.

[10] X. Wang, S. Blechert, M. Antonietti, *ACS Catal.* **2012**, *2*, 1596–1606.

[11] Y. Wang, X. Wang, M. Antonietti, *Angew. Chem. Int. Ed.* **2012**, *51*, 68–89.

[12] A. Thomas, A. Fischer, F. Goettmann, M. Antonietti, J.-O. Müller, R. Schlögl, J. M. Carlsson, *J. Mater. Chem.* **2008**, *18*, 4893.

[13] A. Fujishima, T. N. Rao, D. A. Tryk, *J. Photochem. Photobiol. C Photochem. Rev.* **2000**, *1*, 1–21.

[14] K. Maeda, K. Domen, *J. Phys. Chem. Lett.* **2010**, *1*, 2655–2661.

[15] P. Wu, J. Wang, J. Zhao, L. Guo, F. E. Osterloh, *J. Mater. Chem. A* **2014**, *2*, 20338–20344.

[16] Y. Di, X. Wang, A. Thomas, M. Antonietti, *ChemCatChem* **2010**, *2*, 834–838.

[17] H. Yan, H. Yang, *J. Alloys Compd.* **2011**, *509*, 26–29.

[18] J.-X. Sun, Y.-P. Yuan, L.-G. Qiu, X. Jiang, A.-J. Xie, Y.-H. Shen, J.-F. Zhu, *Dalt. Trans.* **2012**, *41*, 6756.

[19] J. Fu, B. Chang, Y. Tian, F. Xi, X. Dong, *J. Mater. Chem. A* **2013**, *1*, 3083.

[20] S. C. Yan, S. B. Lv, Z. S. Li, Z. G. Zou, *Dalton Trans.* **2010**, *39*, 1488–1491.

[21] T. Kawahara, Y. Konishi, H. Tada, N. Tohge, J. Nishii, S. Ito, *Angew. Chem. Int. Ed.* **2002**, *114*, 2935–2937.

[22] J. Zhang, Q. Xu, Z. Feng, M. Li, C. Li, *Angew. Chem. Int. Ed.* **2008**, *120*, 1790–1793.

[23] D. O. Scanlon, C. W. Dunnill, J. Buckeridge, S. A. Shevlin, A. J. Logsdail, S. M. Woodley, C. R. A. Catlow, M. J. Powell, R. G. Palgrave, I. P. Parkin, et al., *Nat. Mater.* **2013**, *12*, 798–801.

[24] X. Wang, Q. Xu, M. Li, S. Shen, X. Wang, Y. Wang, Z. Feng, J. Shi, H. Han, C. Li, *Angew. Chem. Int. Ed.* **2012**, *51*, 13089–92.

[25] J. Hou, C. Yang, Z. Wang, W. Zhou, S. Jiao, H. Zhu, *Appl. Catal. B Environ.* **2013**, *142-143*, 504–511.

[26] V. W.-H. Lau, M. B. Mesch, V. Duppel, V. Blum, J. Senker, B. V Lotsch, *J. Am. Chem. Soc.* **2015**, *137*, 1064–1072.

[27] S. Cao, J. Low, J. Yu, M. Jaroniec, *Adv. Mater.* **2015**, *27*, 2150–76.

[28] Y. Cao, Z. Zhang, J. Long, J. Liang, H. Lin, H. Lin, X. Wang, *J. Mater. Chem. A* **2014**, *2*, 17797–17807.

[29] D. J. Martin, K. Qiu, S. A. Shevlin, A. D. Handoko, X. Chen, Z. Guo, J. Tang, *Angew. Chem. Int. Ed.* **2014**, *53*, 9240–5.

[30] A. Thomas, A. Fischer, F. Goettmann, M. Antonietti, J.-O. Müller, R. Schlögl, J. M. Carlsson, *J. Mater. Chem.* **2008**, *18*, 4893.

[31] X. Wang, K. Maeda, X. Chen, K. Takanabe, K. Domen, Y. Hou, X. Fu, M. Antonietti, *J. Am. Chem. Soc.* **2009**, *131*, 1680–1.

[32] T. Tyborski, C. Merschjann, S. Orthmann, F. Yang, M.-C. Lux-Steiner, T. Schedel-Niedrig, *J. Phys. Condens. Matter* **2013**, *25*, 395402.

[33] T. Tyborski, C. Merschjann, S. Orthmann, F. Yang, M.-C. Lux-Steiner, T. Schedel-Niedrig, *J. Phys. Condens. Matter* **2012**, *24*, 162201.

[34] K. Schwinghammer, M. B. Mesch, V. Duppel, C. Ziegler, J. Senker, B. V Lotsch, *J.*

Am. Chem. Soc. **2014**, *136*, 1730–3.

[35] Z. Zhou, J. Wang, J. Yu, Y. Shen, Y. Li, A. Liu, S. Liu, Y. Zhang, *J. Am. Chem. Soc.* **2015**, *137*, 2179–82.

[36] Y. Tian, B. Chang, Z. Yang, B. Zhou, F. Xi, X. Dong, *RSC Adv.* **2014**, *4*, 4187–4193.

[37] M. A. Butler, *J. Appl. Phys.* **1977**, *48*, 1914–1920.

[38] A. B. Jorge, D. J. Martin, M. T. S. Dhanoa, A. S. Rahman, N. Makwana, J. Tang, A. Sella, F. Corà, S. Firth, J. A. Darr, et al., *J. Phys. Chem. C* **2013**, *117*, 7178–7185.

[39] Y. Zhang, Q. Pan, G. Chai, M. Liang, G. Dong, Q. Zhang, J. Qiu, *Sci. Rep.* **2013**, *3*, 1943.

[40] S. D. Stranks, G. E. Eperon, G. Grancini, C. Menelaou, M. J. P. Alcocer, T. Leijtens, L. M. Herz, A. Petrozza, H. J. Snaith, *Science* **2013**, *342*, 341–4.

[41] J. Zhang, J. Sun, K. Maeda, K. Domen, P. Liu, M. Antonietti, X. Fu, X. Wang, *Energy Environ. Sci.* **2011**, *4*, 675–678.

[42] Z. Zhang, J. Long, L. Yang, W. Chen, W. Dai, X. Fu, X. Wang, *Chem. Sci.* **2011**, *2*, 1826–1830.

[43] H. Kisch, *Semiconductor Photocatlysis Principles and Applications*, Wiley-VCH Verlag GmbH & Co. KGaA, **2015**.

Chapter 5: Carbon nitride-Nb_2O_5 heterojunctions and their photocatalytic properties

Overview

Graphitic carbon nitride (C_3N_4) modified Nb_2O_5 (C_3N_4-Nb_2O_5) heterojunctions were synthesised *via* a hydrothermal method. The detailed characterisations (XRD, HRTEM, UV-*vis* and PL) showed the uniform distribution of Nb_2O_5 particles, formation of an intimate interface, intensive absorption over a broad visible range and a gradual attenuation of energy-wasteful charge recombination processes in coupled C_3N_4-Nb_2O_5 heterojunction materials. The catalytic testing revealed that the photocatalytic activity for degradation of aqueous methylene blue (MB) was 2.7 to 2.8 times higher than that of individual C_3N_4 and modified Nb_2O_5. Based on free radical scavenger experiments, a photodegradation mechanism of this C_3N_4-Nb_2O_5 heterojunction system was proposed. Moreover, it was found that heterojunction materials also display good stability and reusability.

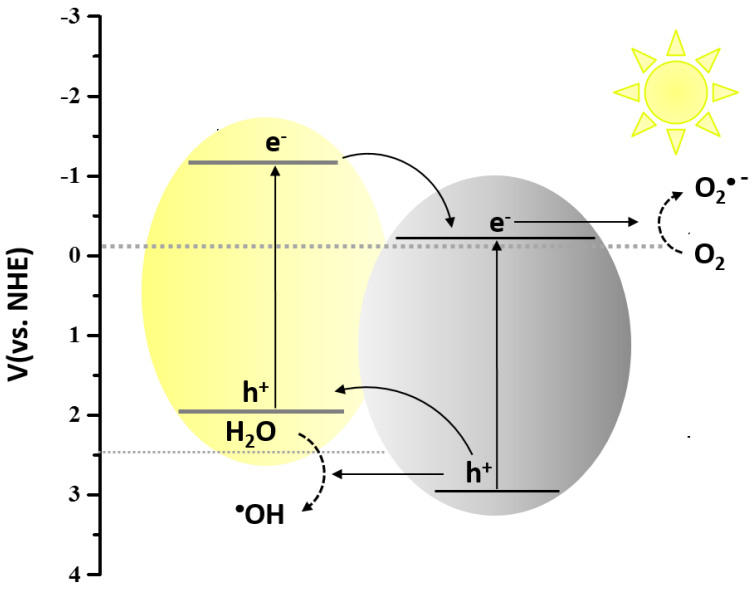

Schematic diagram of C_3N_4-Nb_2O_5 heterojunctions

5.1 Introduction

Environmental pollution as well as the dearth of natural energy resources have drawn much attention to the vital need for ecologically clean materials and chemical technologies.[1] In particular, solar energy driven photocatalysis has emerged as one of the promising technologies for fine chemicals synthesis and water purification.[2–4] The use of semiconducting oxides to harvest sunlight or artificial light (of energy higher than the band gap that induces the photochemical charge generation, charge trapping and subsequent photochemical reaction), has been extensively explored.[1,5] However, most of the metal oxide semiconductors (TiO_2, ZnO etc.) are active in UV region and their quantum yields are generally low due to inherently fast electron hole-pair (exciton) recombination rate at the single semiconducting electronic structure.[1,6]

Currently, several approaches have been explored to deter exciton recombination through the use of heterojunctions. These include phase heterojunctions,[7,8] the combination of two different crystalline phases of a single semiconductor, and semiconductor-semiconductor heterojunctions which is the coupling of two different semiconductors.[9–12] However, the absorption range of the phase heterojunctions cannot be changed due to the intrinsic structural rigidity of individual phases. Conversely, coupling two different well-matched semiconductors, of complimentary phases, may facilitate an efficient charge transfer, improving photocatalytic activity. As a result, the creation of a heterostructure configuration, with an intimate interface and well-aligned band structure, are the fundamental elements in the rational design of new photocatalytic materials.

In addition to the metal oxide semiconductor photocatalysts, polymeric g-C_3N_4 has attracted a great deal of attention owing to its remarkable π-conjugated s-triazine structure and narrow band gap of 2.7 eV.[13] It can capture light in the visible regime without any modification. Unlike many transition metal oxynitrides and sulfides it is a chemically and thermally stable material. Furthermore, its polymeric nature and planar structure can be utilized for anchoring different substrates as well as coupling with other semiconductors to construct efficient heterojunctions.[10] Several kinds of carbon nitride based heterojunctions have been developed, just some of many examples being C_3N_4-TiO_2,[14] C_3N_4-ZnO,[15] C_3N_4-CdS,[16] C_3N_4-TaON,[17] C_3N_4-$SrTiO_3$,[18] C_3N_4-Bi_2WO_6[19], C_3N_4-$BiVO_4$.[20]

As an n-type semiconductor Nb_2O_5 has been widely investigated due to reported high photocatalytic activity and well-documented water-tolerant acidic surface.[21–23] It also exhibits H_2 evolution from water under UV light.[23,24] In previous work, our group has investigated the shape dependent acidity and enhanced photocatalytic properties of the Nb_2O_5 based spheres and rods.[23] As Nb_2O_5 is active only under UV illumination strategies have been developed to modify the electronic structure by metal doping (e.g. Rh, Pb) in order to render it visible light responsive.[25–27] Further, it has been demonstrated that during photooxidation of alcohols, a new donor level is introduced within the forbidden band of Nb_2O_5 through its strong interaction with alcohol molecules, which provides the visible light harvesting ability.[28] Despite having high photocatalytic activity under UV light and a few reports on metal doped visible light active Nb_2O_5, structural modification to the oxide to capture visible light is highly desirable.

5.2 Objectives

Recently the idea of combining semiconductors (eg TiO_2, ZnO) that absorb only in the UV region with carbon nitride to make visible light active catalysts has been demonstrated.

For example, when g-C_3N_4–ZnO composite photocatalysts were fabricated it was found that photocatalytic activity of g-C_3N_4–ZnO for photo-degradation of methyl orange and p-nitrophenol under visible light irradiation was significantly enhanced.[15] Similarly, C_3N_4/TiO_2 nanotube composite heterojunction photocatalysts have been shown to have improved photocatalytic activity under visible light.[29]

Taking these studies into account, in this chapter the use of a hydrothermal method to synthesize Nb_2O_5 spheres and Nb_2O_5-C_3N_4 composite heterojunctions is developed and the photocatalytic activities for the degradation of methylene blue under visible light irradiation are studied. It is demonstrated that the resulting Nb_2O_5-C_3N_4 heterostructures are active under visible light, showing much enhanced photocatalytic activity compared to C_3N_4 or Nb_2O_5, as well as conventional P25 and N-modified TiO_2. Moreover, the photodegradation mechanism of this modified Nb_2O_5-C_3N_4 heterojunction system will be discussed based on our experimental results.

5.3 Results and discussions

5.3.1 Characterisation of C_3N_4-Nb_2O_5 composite heterojunctions

5.3.1.1 XRD

The XRD pattern of as prepared C_3N_4, Nb_2O_5 and C_3N_4-Nb_2O_5 heterojunctions are shown in Figure 5.1.

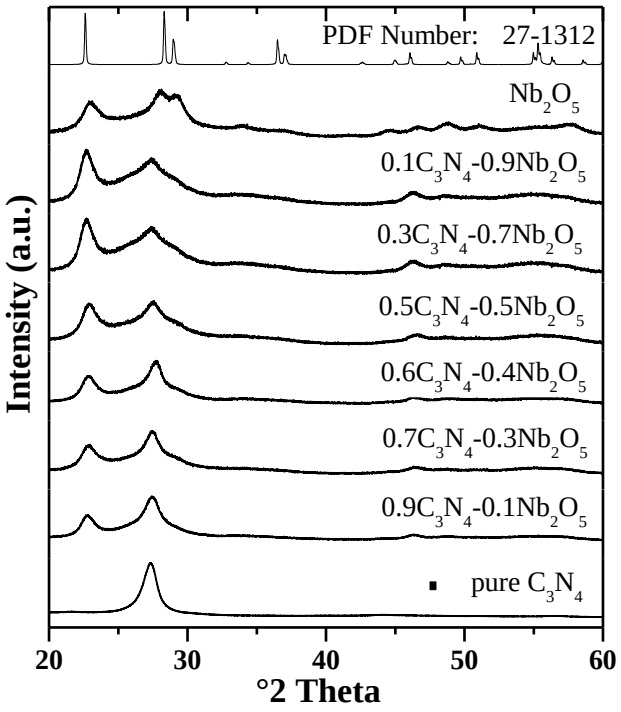

Figure 5.1 XRD patterns of C_3N_4, Nb_2O_5 and C_3N_4-Nb_2O_5 samples.

In pristine C_3N_4 two pronounced peaks at 13.04° (not shown) and 27. 4° can be indexed as the (100) and (002) diffractions planes respectively. The distance *d* = 0.697 nm corresponds to the in-plane structural packing motifs, which is slightly smaller than one tri-s-triazine unit (~ 0.713) and the *d*= 0.329 nm corresponds to the interlayer stacking distance of conjugated aromatic systems, similar to previous reports on graphitic materials.[7,30] Whilst the main diffraction peaks of modified Nb_2O_5 nanospheres follow the XRD patterns of bulk Nb_2O_5 oxide, (PDF no. 00-027-1312) poor crystallinity with low peak intensity is evident, suggesting the relatively short-rang order due to small size and monodispersed nature of the sample. In addition the main peaks ascribed to (-111), (111) and (-311) planes are rather broad and shifted to smaller angles in contrast to the bulk structure prepared by calcination

at 500 °C (ramp 5° min^{-1}, held for 3 h). These peak shifts may be attributed to the lower number of interconnected Nb-O polyhedra with less robust structure.[23,31]

After coupling the two semiconductors as Nb_2O_5-C_3N_4 heterojunction, both the characteristic peaks of C_3N_4 and Nb_2O_5 were present indicating the coupling process has no influence on crystal structure. Besides, the thin C_3N_4 layer and the small size of Nb_2O_5 mean that the intensities of individual C_3N_4 and Nb_2O_5 diffractions gradually change in accordance with the variation in their content in the heterostructure.

5.3.1.2 SEM and TEM

The morphology and microstructure of the modified Nb_2O_5-C_3N_4 heterojunctions were characterized by SEM and TEM. The SEM images show that the morphology of Nb_2O_5 is agglomerated (Figure 5.2a) whereas C_3N_4 exhibits a relatively smooth surface with lamellar structure however lacking clearly defined boundaries (5.2b). In contrast, the morphology of the C_3N_4-Nb_2O_5 composite is significantly different from the individual C_3N_4 and Nb_2O_5 components, showing a pronounced morphology change (Figure 5.2c). Similarly, high resolution TEM images of pristine C_3N_4 samples (Figure 5.2 e-f) show large typical aggregated size with relatively smooth and flat surface. Whereas Figure 5.2d, shows the monodispersed Nb_2O_5 particles of 5-10 nm diameter, obtained by the precipitation hydrothermal method. Moreover, as shown in Figure 3.5e, Nb_2O_5 particles after coupling with carbon nitride are uniformly dispersed but retaining their particle size.

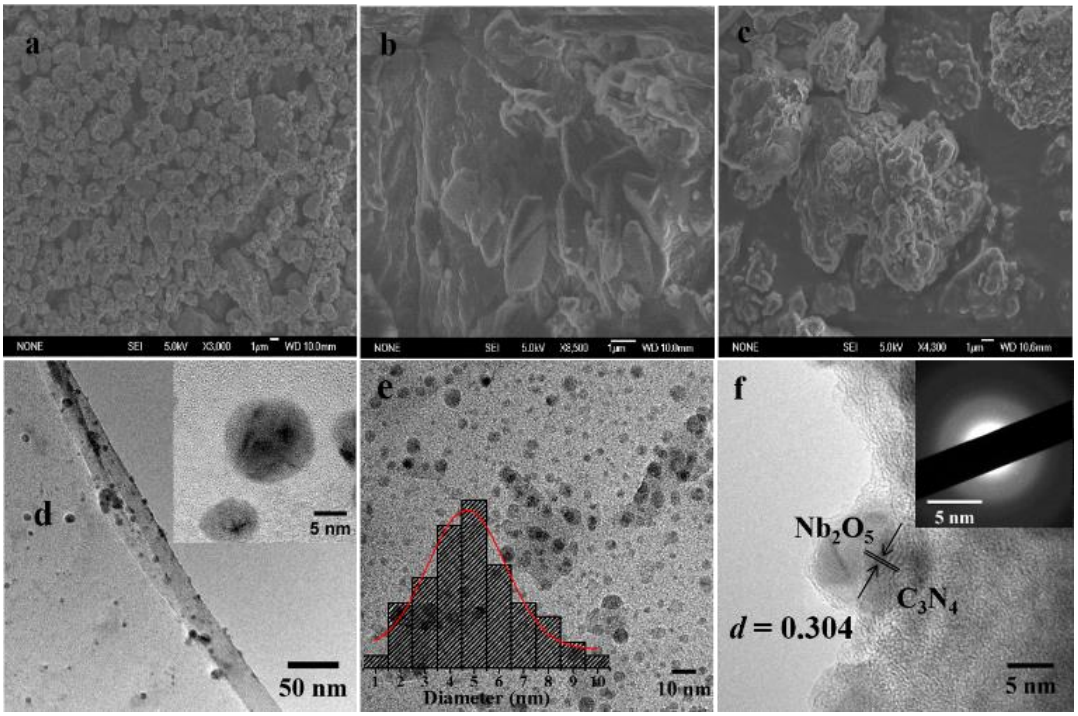

Figure 5.2 SEM images of (a) Nb_2O_5 (b) C_3N_4, (c) C_3N_4-Nb_2O_5. TEM images of (d) Nb_2O_5 particles (e) $0.6C_3N_4$-$0.4Nb_2O_5$ samples with particle distribution and (f) HR-TEM image of $0.6C_3N_4$-$0.4Nb_2O_5$. (Inset SAED pattern).

Furthermore, the TEM image of C_3N_4-Nb_2O_5 (Fig. 1c) confirms that Nb_2O_5 is well dispersed and connected to the carbon nitride forming intimate heterostructure. The HRTEM on $0.6C_3N_4$-$0.4Nb_2O_5$ (Figure 5.2 e-f) is clearly indicative of two distinct phases, the intimate interface between C_3N_4 and Nb_2O_5 can be clearly seen. Because of indistinguishable in-plane diffraction (100) in XRD it is hard to find the lattice fringe of carbon nitride, nevertheless, the observed lattice fringe of d = 0.304 nm can be attributed to (-311) crystallographic plane of monoclinic Nb_2O_5 system which is in agreement with XRD results.

This close connection between the two phases is favourable for the necessary charge transfer between coupled semiconductors, which promotes the separation of photo generated electron-hole pairs, subsequently improving the photocatalytic activity.[19] These results also

confirm that a coupled structure in heterojunctions is heterogeneous unlike the physical mixture with two separate phases of carbon nitride and Nb_2O_5.

5.3.3.2 UV-Vis absorption

Figure 5.3 shows the UV-vis absorption spectra of as synthesized heterojunction. Adjusting the different weight ratio of C_3N_4 and Nb_2O_5 in heterojunctions enables the fine tuning of the optical properties as indicated by the UV-vis absorption. The band gap of C_3N_4 and Nb_2O_5 was estimated using the equation $\alpha h\nu = A(h\nu - E_g)^n$, where α, ν, E_g and A are the absorption coefficient (Kubelka-Munk function), light frequency, band gap, and a constant respectively.[20,32] The value of n is determined by the characteristics transition of the semiconductor. From the plot of $(\alpha h\nu)^{1/2}$ *vs.* hν, the band-gap energy of C_3N_4 and Nb_2O_5 was thus obtained (Figure 5.3b) by extrapolating the linear portion to the hν axis. The calculated value of C_3N_4 is 2.68 eV which is slightly lower than the reported value, whereas the E_g value of Nb_2O_5 is 3.28 eV. This slightly lower E_g value for the Nb_2O_5 may be accounted for by a lower number of interconnected Nb-O polyhedra, which was reflected in poor crystallinity as shown by SAED and XRD analysis. In addition, there might have a contribution from the interaction(s) between defects and absorbed oxygen, which generates the extra donor level within the forbidden band. Previously, a longer absorption tail was observed in Nb_2O_5, indicating a significant absorption range adjacent to inter-band transition due to the presence of defects.[31,33] After combining the two semiconductors, C_3N_4-Nb_2O_5 heterojunction with a band gap energy, E_g, ranges from 2.68 eV to 2.84 eV. Also, an intensive absorption band within the visible range in a large part of solar spectrum is clearly seen.

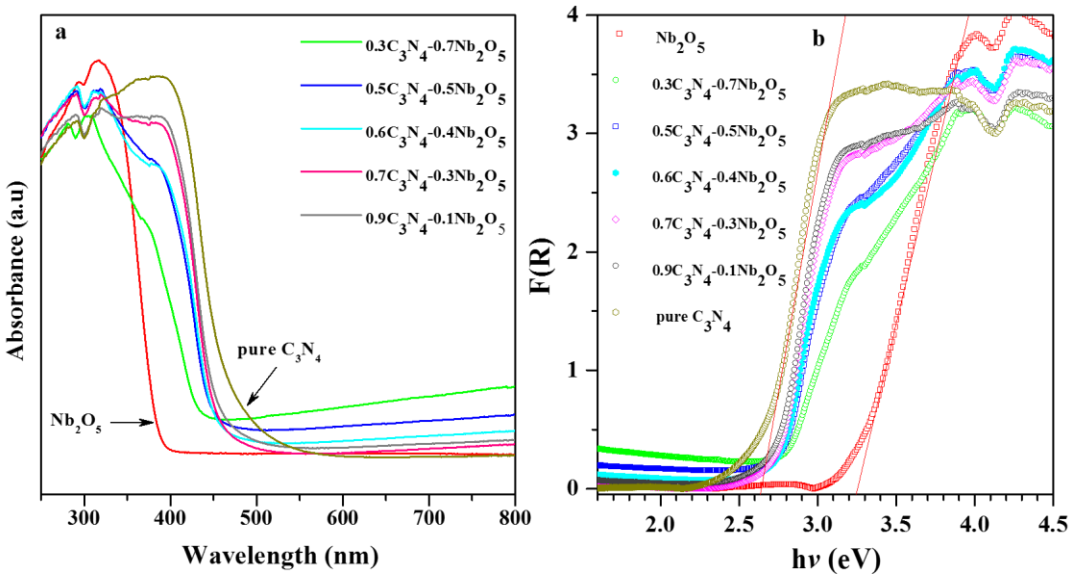

Figure 5.3 (a) UV/Vis absorption spectra of C_3N_4, Nb_2O_5 and C_3N_4-Nb_2O_5 heterojunctions composites and the (b) transformed Kubelka-Munk function F(R) *vs.* light energy plots of C_3N_4, Nb_2O_5 and C_3N_4-Nb_2O_5 heterojunctions.

5.3.3.3 Steady State photoluminescence (PL) spectroscopy

PL measurements were performed to characterise heterostructure by revealing the charge transfer and separation efficiency of photoinduced charge carriers.[34–36] The room temperature emission PL spectra of all C_3N_4-Nb_2O_5 heterojunctions measured under the excitation wavelength of 405 nm, are shown in Figure 5.4. Two clear signals at ca. 470 nm and 490 nm were observed for all C_3N_4-Nb_2O_5 heterojunctions, originating from radiative recombination of free electrons in shallow traps and sub-bands underneath conduction band and free holes at the valence band edge.[34] The intensities of the signals were attenuated in accordance with variation in loading ratio between C_3N_4-Nb_2O_5. As for C_3N_4-Nb_2O_5 heterojunctions with Nb_2O_5 loading level from 10, 30 to 40 wt%, the PL intensities first reduced greatly, but further increasing the Nb_2O_5 loading to 90 wt% led the increase in the intensity again. This suggests that the fluorescence quenching occurs due to the heterojunction formation which, in effect, suppresses the radiative recombination. Therefore

C_3N_4-Nb_2O_5 heterojunctions are expected to show the enhanced activity in photocatalytic reactions.

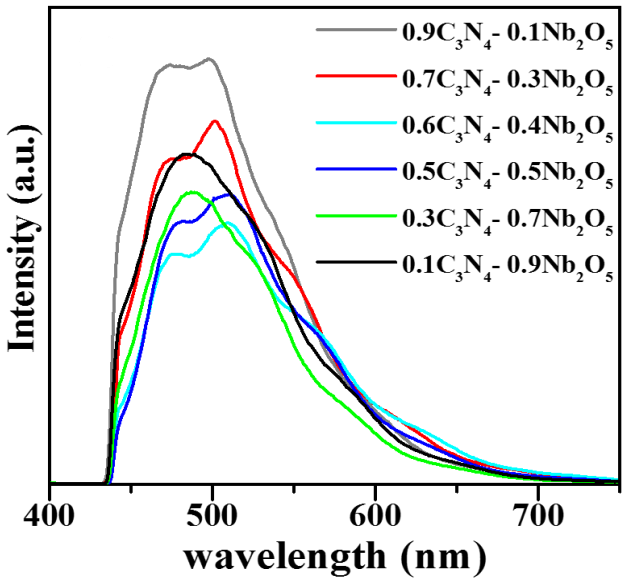

Figure 5.4 Room temperature PL spectra of C_3N_4, Nb_2O_5 and C_3N_4-Nb_2O_5 heterojunctions materials excited by 405 nm laser pulsed at frequencies of 32 MHz.

5.3.2 Photocatalytic activity of C_3N_4-Nb_2O_5 heterojunctions

On the basis of the above results, the visible-light photocatalytic activity of C_3N_4, Nb_2O_5 and C_3N_4-Nb_2O_5 composite semiconductors was evaluated by the degradation of aqueous MB which is used commonly to test the degradation capability of the photocatalyst. In the absence of photocatalyst only a small change (~16 %) in concentration of MB over a period of 90 minutes was observed, indicating self-degradation is negligible. Moreover, both C_3N_4 and Nb_2O_5 show low activities, only 52% and 33 % reduction in MB concentration over the irradiation of time 90 min, respectively. For $0.6C_3N_4$-$0.4Nb_2O_5$, the change in absorption spectra of MB aqueous solution at given time interval after visible light irradiation is displayed in Figure 5.5a. A gradual decrease in the absorption peak at 664 nm with increasing

irradiation time is observed, with the peak nearly disappeared after 90 min. In the meantime, no additional peak appeared in either visible or ultraviolet region, suggesting photocatalytic degradation of the MB (chromophore) structure during the reaction.[20] Figure 5.5b represents the relative degree of MB concentrations (C/C_0) with irradiation time over different catalysts. After combining the C_3N_4 and Nb_2O_5, the significant enhancement in photocatalytic activity of composite heterostructures (C_3N_4-Nb_2O_5) materials was observed in comparison with the individual constituent semiconductors. The photocatalytic activity first increases from $0.9C_3N_4$-$0.1Nb_2O_5$ to $0.5C_3N_4$-$0.5Nb_2O_5$ and then decreases drastically, suggesting the high Nb_2O_5 content surpasses the optimal carbon nitride surface covering for the intimate interface. The highest activity was obtained over $0.6C_3N_4$-$0.4Nb_2O_5$ which showed ~89% degradation of MB within 90 min with visible light irradiation. This significant improvement in activity is presumably due to synergic effect for capture of visible light for the photocatalytic reaction. Apart from the construction of the heterojunction and interface formation, the unique Lewis basic nitrogens of the carbon nitride surface, together with Lewis acid sites in Nb_2O_5 create an efficient interface containing both Lewis acid and base sites thus enhancing surface absorption for the dye and hence photocatalytic decomposition.[37] Such acid and base centres should, in principle, work well with the light generated excitons, and promoting catalytic kinetics for (photo)chemical transformation.[37,38]

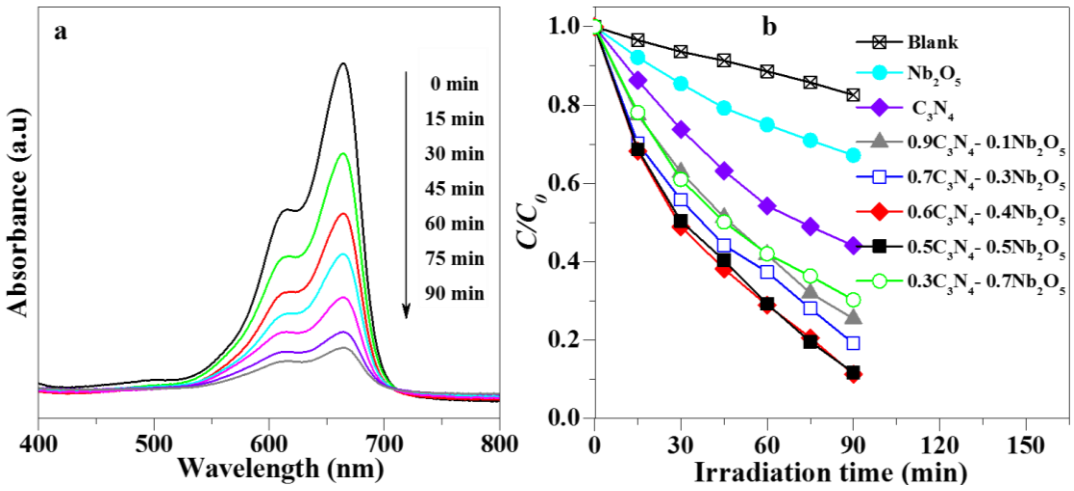

Figure 5.5 Absorption spectra of MB with irradiation time over $0.6C_3N_4$-$0.4Nb_2O_5$ heterojunction; (**b**) degradation rates of MB under visible light with catalyst and in the presence of C_3N_4, Nb_2O_5, and C_3N_4-Nb_2O_5 samples.

The kinetics of the MB photodecomposition on the photocatalyst surface can be described by fitting the experimental data in pseudo first-order model as described by $ln(c_0/c) = kt$, where k is rate constant (min^{-1}) c_0 is the initial concentration of dye and c is the actual concentration of target dye at irradiation time t. All the fitting curves show (Figure 5.6c) linear relationship between $ln(c_0/c)$ and the irradiation time (t) and value of k (determined from the slope of linear relationship of the natural logarithm of the ratio between initial concentration of dye and the concentration after photocatalytic degradation versus the corresponding irradiation time) gives an indication of the activity of the photocatalyst. Apparent rate constant k is much larger for heterojunctions than those of individual C_3N_4 or Nb_2O_5. The $0.6C_3N_4$-$0.4Nb_2O_5$ exhibits the highest MB photodegradation rate constant of 0.0246 min^{-1} which is almost three times faster than the rate constant of carbon nitride. This enhancement implies that the coupling of C_3N_4 and Nb_2O_5 results in prolonging the lifetime for photogenerated electron-hole pairs for efficient photodegradation of MB, as similar to

previous reports.[19,20] To underline the necessity to form good heterojunction, experiments were performed over mechanically mixed $0.6C_3N_4$-$0.4Nb_2O_5$ system as a reference, which showed almost similar photocatalytic activity to C_3N_4. This result demonstrates that coupling C_3N_4 and Nb_2O_5 to form intimate interface in $0.6C_3N_4$-$0.4Nb_2O_5$ heterojunction is crucially important than that of the lose interface in mechanically mixed system (Figure 5.7).

For comparison, rate constant (*k*) value of $0.6C_3N_4$-$0.4Nb_2O_5$ is listed together (Figure 5.6c) with others photocatalysts, including the visible light responsive *N*-modified TiO_2 and visible light inactive TiO_2 (Degussa P25).[20]. As expected, P25 exhibits poor photocatalytic activity because of its inability to be photoexcited under visible light. The rate constant for MB photodegradation over $0.6C_3N_4$-$0.4Nb_2O_5$ is 1.5 times higher than that of *N*-modified TiO_2. This result indicates that coupling C_3N_4 and Nb_2O_5, (visible light and UV light photo-responsive semiconductors) can outperform both the traditional UV light active and visible light responsive photocatalysts for induced photocatalysis.

MB degradation may take place through a self photoinduced dye-sensitized mechanism that does not require any band gap excitation of heterojunction system.[20,39] To exclude this possibility, the study of $0.6C_3N_4$-$0.4Nb_2O_5$ for 2,4 DCP decomposition (a colourless dye) was carried out. It is noted (Figure 5.6d) that 82% of 2,4-DCP molecules were decomposed under the same conditions after 6 h, suggesting that contribution of self-dye sensitized mechanism can be neglected compared to the photocatalytic degradation.

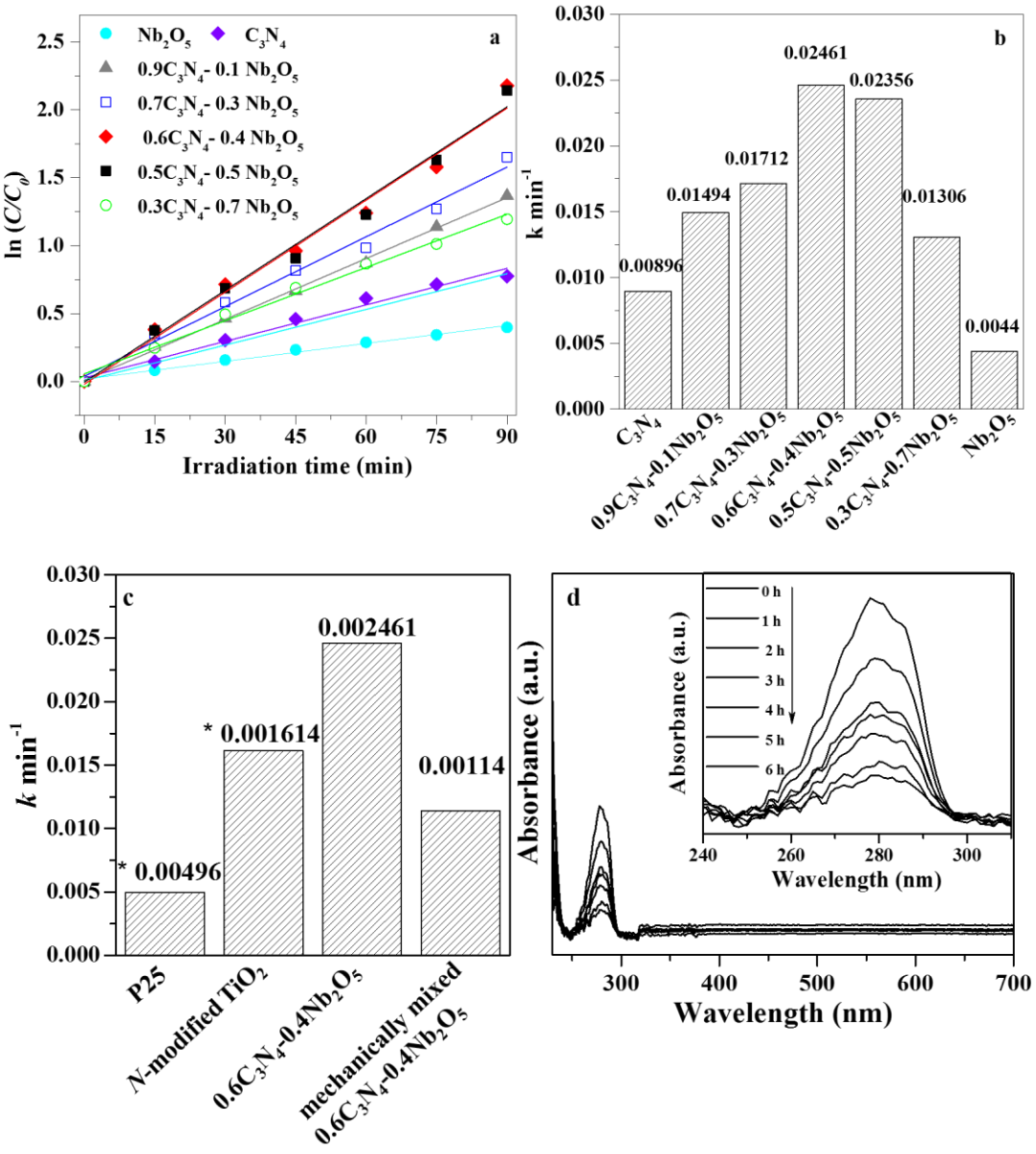

Figure 5.6 First-order kinetic data for photodegradation of MB over C_3N_4, Nb_2O_5, and C_3N_4-Nb_2O_5 samples; (b) value of rate constant *k* of photodegradation of MB over C_3N_4, Nb_2O_5, and C_3N_4-Nb_2O_5 samples. (c) Comparison of rate constant *k* values of photodegradation of MB over mechanically mixed C_3N_4-Nb_2O_5 and P25, *N*-modified TiO_2 from reference.[20] (d) Absorption spectra of 2,4 dichlorophenol (2, 4-DCP) colourless visible light inactive dye with irradiation time over C_3N_4-Nb_2O_5 heterojunction.

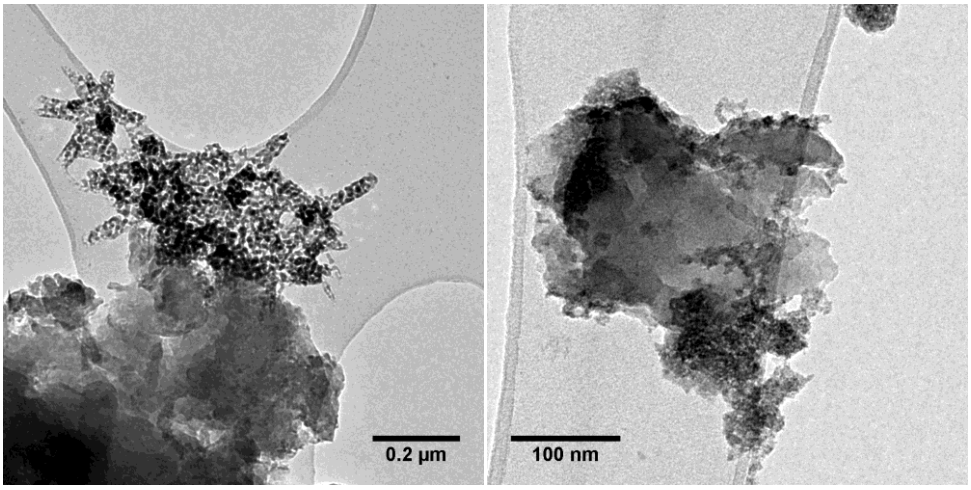

Figure 5.7 TEM images of mechanically mixed $0.6C_3N_4$-$0.4Nb_2O_5$ sample clearly shows coupling is not efficient necessary to create interface in heterojunctions.

5.3.3 Possible photocatalytic mechanism of C_3N_4-Nb_2O_5 heterojunctions

The aforementioned results reveal that the synergetic effects of heterojunction formed between C_3N_4 and Nb_2O_5, and its ability to harvest the light in a broad spectral range, are responsible for improved photocatalytic activities.

It is well known that adsorption of some species on oxide surface may affect both conduction band potential (E_c), valence band potential (E_v) and band gap (E_g).[40] Further, an empirical correlation between the conduction band potential of metal oxide semiconductors having fully electron filled (d^{10}) or empty (d^0) metal ions can be estimated by using following equations:[41]

$$Ec \approx 1.23 - Eg(eV)/2 \qquad (5.1)$$

$$Ev \approx 1.23 + Eg(eV)/2 \qquad (5.2)$$

Thus, the estimated CB and VB values for Nb_2O_5 (calculated from equation 5.1 and 5.2 and band gaps values) -0.39 eV and 2.85 eV, respectively. It is generally accepted that the

conduction band (CB) and valance band (VB) potentials of C_3N_4 (-1.12 eV and 1.58 eV, respectively[4,13,42]) are negative with respect to those of Nb_2O_5 (-0.39 eV and 2.85 eV, respectively) which in principle would create a well-matched type II heterojunction (Figure 5.8). It is interesting to note that the calculated CB standard redox potential of both C_3N_4 and Nb_2O_5, is more negative than the standard redox potential of $O_2/O_2^{\bullet-}$ (-0.28 eV)[20,43] and more positive to that of $OH^-/^{\bullet}OH$ (2.27 eV).[43] This ascertains the fact that upon irradiation, both photooxidation and photoreduction are energetically favourable to take place in the C_3N_4-Nb_2O_5 system. The photo-induced electron transfer from the CB of C_3N_4 to the CB of Nb_2O_5 and the hole transfer from the VB of Nb_2O_5 to the VB of C_3N_4 will occur in a concerted manner, which in effect impedes the exciton recombination, and hence improving the photoactivity.

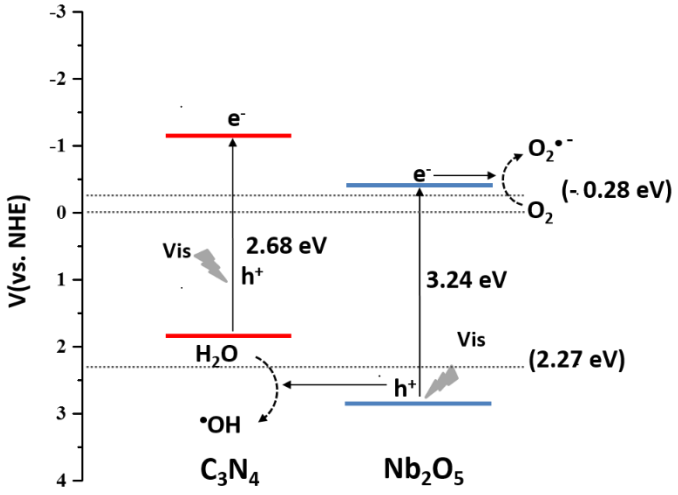

Figure 5.8 Schematic diagram of type (II) C_3N_4-Nb_2O_5 heterojunctions for favoured separation and transfer of photogenerated charges under visible light irradiation.

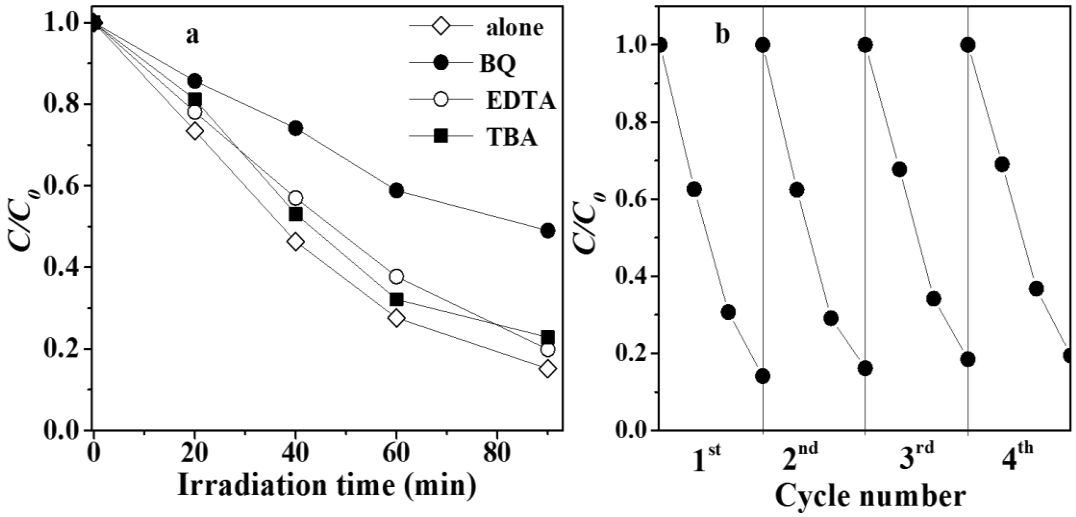

Figure 5.9 Effect of EDTA, TBA or BQ addition degradation of MB over $0.6C_3N_4$-$0.4Nb_2O_5$ heterojunction. (b) Cyclic runs for the photocatalytic degradation of MB over C_3N_4-Nb_2O_5 heterojunction under visible light irradiation.

In order to check the key species involved in MB degradation, trapping experiments were performed (Figure 5.9a). It was examined, on addition of *tert*-butyl alcohol (TBA 2 mM, hydroxyl radical scavenger, with rate constant $k = 6\times10^8$),[44] the rate of MB photocatalytic degradation over C_3N_4-Nb_2O_5 heterojunction was decreased slightly. Further, the addition of disodium ethylenediaminetetraacetate (EDTA, 2mM, hole scavenger) causes a slight change in photodegradation efficiency of C_3N_4-Nb_2O_5. These results imply that $OH^{\bullet}$ or holes are not the main species involved in the photodegradation of MB. It is of interest to note that photogenerated electrons in CB can reduce O_2 adsorbed on semiconductor surface to produce superoxide radical ($O_2^{\bullet-}$) and holes on VB surface can yield $^{\bullet}OH$ from H_2O and thus, theoretically generation of both $O_2^{\bullet-}$ and $^{\bullet}OH$ radicals is possible in C_3N_4-Nb_2O_5 heterojunction system. However, when the benzoquinone (BQ, 0.5 mM, superoxide radical scavenger) was added, the degradation rate of MB was clearly suppressed. Thus, it is

concluded that the photocatalytic degradation of MB is governed mainly by the $O_2^{\bullet-}$ rather than the $^{\bullet}OH$ radicals or photogenerated holes.

5.3.4 Stability

Stability of the composite C_3N_4-Nb_2O_5 catalyst was evaluated by repeated catalytic tests with their powder separated from reaction mixture (filtration) after reaction, and followed by drying (at 80 °C) and re-charging into new batch of substrate intermittently. As seen from the Figure 5.9b, the catalyst shows a good repeatable catalytic performance and only a slight deactivation was observed due to the loss of some superfine powder during the filtration process.

5.4 Conclusions

In summary, a range of C_3N_4-Nb_2O_5 heterojunctions were prepared in an approach based upon the band alignments between C_3N_4 and Nb_2O_5, producing well-matched overlapping band structures and interfaces. It has been demonstrated that this strategy results in heterostructures exhibiting stronger absorption in the visible region and increased rates for the photodegradation of MB. This is clearly due to the suppression of exciton recombination and improved charge extraction and transfer, allowing for efficient redox reactions to take place. The $0.6C_3N_4$-$0.4Nb_2O_5$ heterojunction exhibits the most significantly enhanced activity (3-fold increase in rate constant) relative to the individual C_3N_4 and Nb_2O_5 powder. Further, hole and radical scavenging techniques showed that both the photogenerated $O_2^{\bullet-}$ and $^{\bullet}OH$ are involved in the MB degradation, with the photoreduction reaction pathway preferred over the photooxidation.

5.5 References

[1] P. Pichat, Ed. , *Photocatalysis and Water Purification: From Fundamentals to Recent Applications*, Wiley-VCH, **2013**.

[2] M. Grätzel, *Nature* **2001**, *414*, 338–344.

[3] C. Chen, W. Ma, J. Zhao, *Chem. Soc. Rev.* **2010**, *39*, 4206–19.

[4] Y. Wang, X. Wang, M. Antonietti, *Angew. Chem. Int. Ed.* **2012**, *51*, 68–89.

[5] V. Roon, D. Leeuw, S. W. Breakdown, Z. Zou, J. Ye, K. Sayama, H. Arakawa, *Nature* **2002**, *414*, 625–627.

[6] M. R. Hoffmann, S. T. Martin, W. Choi, D. W. Bahnemann, *Chem. Rev.* **1995**, *95*, 69–96.

[7] J. Zhang, M. Zhang, R.-Q. Sun, X. Wang, *Angew. Chem. Int. Ed.* **2012**, *51*, 10145–9.

[8] F. Dong, Z. Zhao, T. Xiong, Z. Ni, W. Zhang, Y. Sun, W. Ho, **2013**, *5*, 11392–11401.

[9] J. Zhang, M. Zhang, R.-Q. Sun, X. Wang, *Angew. Chem. Int. Ed.* **2012**, *124*, 10292–10296.

[10] Z. Zhao, Y. Sun, F. Dong, *Nanoscale* **2015**, *7*, 15–37.

[11] J. Zhang, Q. Xu, Z. Feng, M. Li, C. Li, *Angew. Chem. Int. Ed.* **2008**, *47*, 1766–1769.

[12] D. O. Scanlon, C. W. Dunnill, J. Buckeridge, S. A. Shevlin, A. J. Logsdail, S. M. Woodley, C. R. A. Catlow, M. J. Powell, R. G. Palgrave, I. P. Parkin, et al., *Nat. Mater.* **2013**, *12*, 798–801.

[13] X. Wang, K. Maeda, A. Thomas, K. Takanabe, G. Xin, J. M. Carlsson, K. Domen, M. Antonietti, *Nat. Mater.* **2009**, *8*, 76–80.

[14] X. Zhou, B. Jin, L. Li, F. Peng, H. Wang, H. Yu, Y. Fang, *J. Mater. Chem.* **2012**, *22*, 17900.

[15] J.-X. Sun, Y.-P. Yuan, L.-G. Qiu, X. Jiang, A.-J. Xie, Y.-H. Shen, J.-F. Zhu, *Dalt. Trans.* **2012**, *41*, 6756.

[16] J. Fu, B. Chang, Y. Tian, F. Xi, X. Dong, *J. Mater. Chem. A* **2013**, *1*, 3083.

[17] S. C. Yan, S. B. Lv, Z. S. Li, Z. G. Zou, *Dalton Trans.* **2010**, *39*, 1488–1491.

[18] X. Xu, G. Liu, C. Randorn, J. T. S. Irvine, *Int. J. Hydrogen Energy* **2011**, *36*, 13501–13507.

[19] Y. Tian, B. Chang, J. Lu, J. Fu, F. Xi, X. Dong, *ACS Appl. Mater. Interfaces* **2013**.

[20] Y. Tian, B. Chang, Z. Yang, B. Zhou, F. Xi, X. Dong, *RSC Adv.* **2014**, *4*, 4187–4193.

[21] K. Nakajima, Y. Baba, R. Noma, M. Kitano, J. Kondo, S. Hayashi, M. Hara, *J. Am. Chem.*

Soc. **2011**, *133*, 4224.

[22] H. Liu, N. Gao, M. Liao, X. Fang, **2015**, 1–9.

[23] Y. Zhao, C. Eley, J. Hu, J. S. Foord, L. Ye, H. He, S. C. E. Tsang, *Angew. Chem. Int. Ed.* **2012**, *51*, 3846–9.

[24] K. Nakagawa, T. Jia, W. Zheng, S. M. Fairclough, M. Katoh, S. Sugiyama, S. Chi, E. Tsang, *Chem. Commun.* **2014**, *50*, 13702–13705.

[25] Y. Okamoto, S. Ida, J. Hyodo, H. Hagiwara, T. Ishihara, *J. Am. Chem. Soc.* **2011**, *133*, 18034–18037.

[26] Y. Hu, L. Guo, *ChemCatChem* **2015**, *7*, 1–5.

[27] K. Maeda, M. Eguchi, T. Oshima, *Angew. Chem. Int. Ed.* **2014**, *53*, 13164–8.

[28] S. Furukawa, T. Shishido, K. Teramura, T. Tanaka, *ChemPhysChem* **2014**, *15*, 2665–2667.

[29] Z. Zheng, X. Zhou, *Chinese J. Chem.* **2012**, *30*, 1683–1686.

[30] Y. Wang, X. Wang, M. Antonietti, *Angew. Chem. Int. Ed.* **2012**, *51*, 68–89.

[31] R. Brayner, F. Bozon-Verduraz, *Phys. Chem. Chem. Phys.* **2003**, *5*, 1457–1466.

[32] M. A. Butler, *J. Appl. Phys.* **1977**, *48*, 1914–1920.

[33] T. T. Surface, Y. Zhao, C. Eley, J. Hu, J. S. Foord, L. Ye, H. He, **2012**, 1–5.

[34] J. Yan, G. Wu, N. Guan, L. Li, *Appl. Catal. B Environ.* **2014**, *152-153*, 280–288.

[35] B. Liu, X. Zhao, Q. Zhao, X. He, J. Feng, *J. Electron Spectros. Relat. Phenomena* **2005**, *148*, 158–163.

[36] H. Li, Y. Liu, X. Gao, C. Fu, X. Wang, *ChemSusChem* **2015**, *8*, 1189–96.

[37] Z. Lin, X. Wang, *Angew. Chem. Int. Ed.* **2013**, *52*, 1735–8.

[38] L. Greb, P. Oña-Burgos, B. Schirmer, S. Grimme, D. W. Stephan, J. Paradies, *Angew. Chem. Int. Ed.* **2012**, *51*, 10164–10168.

[39] J. He, G. Benkö, F. Korodi, T. Polívka, R. Lomoth, B. Åkermark, L. Sun, A. Hagfeldt, V. Sundström, *J. Am. Chem. Soc.* **2002**, *124*, 4922–4932.

[40] G. Liu, P. Niu, C. Sun, S. C. Smith, Z. Chen, G. Qing, M. Lu, H. Cheng, *J. Am. Chem. Soc.* **2010**, *132*, 11642–11648.

[41] Y. Matsumoto, *J. Solid State Chem.* **1996**, *126*, 227–234.

[42] X. Wang, S. Blechert, M. Antonietti, *ACS Catal.* **2012**, *2*, 1596–1606.

[43] L. Wu, J. C. Yu, X. Fu, *J. Mol. Catal. A Chem.* **2006**, *244*, 25–32.

[44] G. V Buxton, C. L. Greenstock, W. P. Helman, A. B. Ross, *J. Phys. Chem. Ref. Data* **1988**, *17*, 513–886.

Chapter 6: Carbon nitride catalysed photoacetalization of aldehydes/ketones

Overview

Semiconductive g-C_3N_4 material is shown *for the first time* to catalyse photoacetalization of aldehydes/ketones with alcohols efficiently to acetals at high yields using visible light under ambient conditions (25°C/1 atm. O_2). Mechanistic studies suggest that transient charge (excitons) separation of this solid material upon light excitation is effective to catalyse the reaction in absence of Lewis or Brønsted acids or additional solvent systems. The experiments using ^{18}O labelled benzaldehyde showed that the oxygen leaves as water, whereas negative ρ (rho of Hammett) value suggests the build-up of positive charge in transition state. This unprecedented photoacetalization ability of carbon nitride is of a wide scope, which may be used as a green practical alternative in organic synthesis.

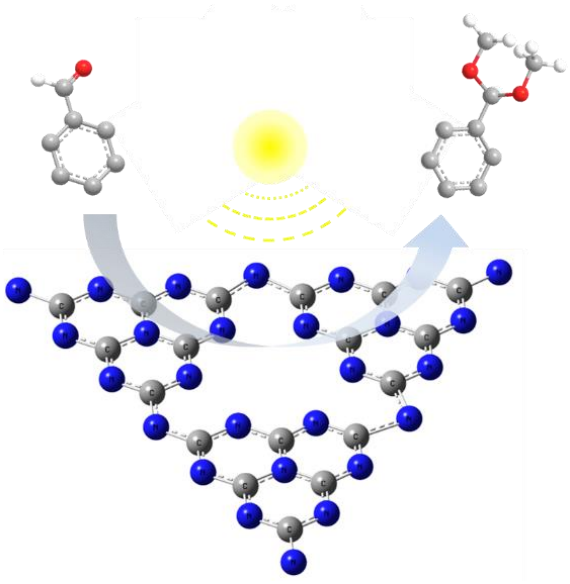

Photoacetalization of aldehyde/ketones using carbon nitride and visible light.

6.1 Background

The use of sunlight to catalyse chemical reactions has long been desired owing to its renewable, clean and economical nature. Although, most of the organic molecules absorb in UV/UV*vis* region, only a few are responsive to visible light, (region (400−800 nm) that accounts for 43% of incoming solar spectrum. This limitation, hampers the visible light induced molecular transformations, ostensibly calling search for a method that can efficiently be employed to utilize the visible light for organic synthesis.

One possible way to do targeted chemical reactions is by photosensitizing and activating *via* a charge-transfer process, exploiting a visible light harvesting homogenous catalyst (inorganic ions and organometallic complexes) or heterogeneous (solid state semiconductor) catalysts. For homogeneous catalysis Ru-$(bipy)_3^{2+}$ and its derivatives are widely known for light driven photochemical oxidation, reductions and alkylation reactions. Despite the difficulty of separation from products, these photo active systems are usually highly selective due to presence of finely tuned active sites. On the other hand most of the easy to separate heterogeneous, photoactive metal oxide semiconductors that have high oxidation potential of O 2p level vs. NHE, can easily generate strong nonselective hydroxyl radical ($^{\bullet}OH$) during photoreaction and usually have poor selectivity. Hence, for specific photo-induced organic transformation a photocatalytic pathway that compasses the essential high selectivity with easy separation of catalyst from products is needed.

6.2 Introduction

Acetalization is one of the key reactions to protect and introduce other functionalities in carbonyl compounds during multistep organic synthesis.[1] Although many reported

methods have been employed for this conversion, most of them are using acid catalysts which also often involve the use of toxic and corrosive reagents.[2–5] Acidic environment is unsuitable when acid moiety groups of the substrates (e.g., carrying silyl groups or unsaturation)[1] are involved. Acetals are also highly unstable for reversible reactions to hemiacetals and starting substrates in acidic conditions but are stable in basic or neutral pH.[6,7] The typical mechanism involves the formation of hemiacetal by adding an alcohol to the C=O π bond; then losing the OH group by breaking what was the C=O σ bond to form an electrophilic oxonium ion and adding the second alcohol to form acetal.[1,6] During acetalization reaction, by-product, water is produced that requires additional physical and chemical means for its removal in order to avoid equilibrium shifting back to reactants (scheme 6.1).[1,7]

Scheme 6.1 Acid catalysed acetal formation reproduced from reference [1].

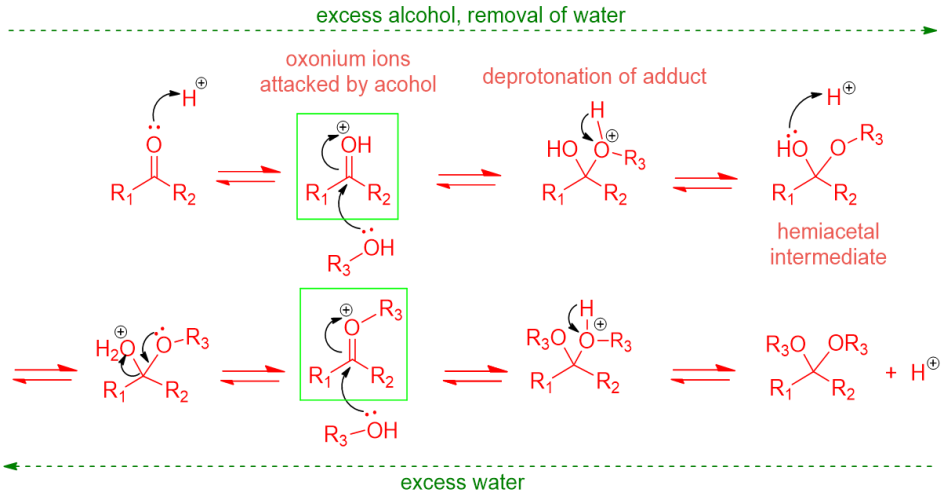

Acetalization reactions are traditionally catalysed by Lewis or Brønsted acids in aqueous medium. However, only few exceptions are acetalizations in the presence of homogeneous catalysts with examples in organic solvents such as $LiBF_4$,[4] thiourea,[8] ionic liquids,[9] N-Bromosuccinimide,[10,11] and *N*,*N*′-bis[3,5-bis(trifluoromethyl)phenyl] [12]. Apart from

separation problems incurred with these systems some of them are toxic, costly and they suffer from a lack of generality. Solid catalytic systems are deemed to be relatively less deleterious to the environment.[13–20] It would thus be highly desirable to develop a general *acid-free*, non-transition metal containing solid catalyst so that a wide range of substrates can also be acetalized in an environmental friendly manner. Since such a method does not exist, we therefore set out to develop this route in this work.

One exciting approach is to employ light to polarize a semiconducting material to generate excitons under transient conditions (positive hole and electron). The excitons can then activate organic molecules for their conversion to products (most of the organic molecules do not absorb visible light) before they are self-recombined. Recently semiconducting carbon nitrides consisting of earth abundant elements of carbon and nitrogen have attracted a lot of attention due to their ability to capture light efficiently without any use of transition metal. In reported works, using thermal polycondensation of common organic monomers to synthesize graphitic carbon nitrides (g-C_3N_4) with tunable band positions has been achieved.[21–24] The graphitic planes are derived from tri-s-triazine units inter-connected by planar amino groups with a band gap of about 2.7 eV (Figure 6.1). Their HOMO and LUMO band positions are placed in such a way that the band gap energy is capable of activating molecular O_2 by photoelectrons to generate mild and selective $O_2^{\bullet-}$ radicals for organic transformations using visible light but the production of nonselective $^{\bullet}OH$ radicals are thermodynamically prohibited.[25,26] Using the transient $O_2^{\bullet-}$ radicals, recent reports on selective oxidations of alcohols to aldehydes, C-H[27], O-H[25,26] and N-H[28] oxidations over these materials have been claimed but the kinetics are yet to be improved. Such studies prompted us to employ this system for the acetalization reactions of carbonyl compounds.

6.3 Objectives

The examples discussed above show that the carbon nitride can utilise visible light for targeted green photochemical transformations in a controlled manner. Specifically, building on earlier work of alcohol oxidation in halogenated solvents, here in this chapter, focus is on acetal formation an undocumented reaction using carbon nitride without any acid additive. This reaction in particular is of importance due to its ability to efficiently produce acetals using visible light without recourse to the use of high temperature. The chapter also details the mechanistic considerations and reaction pathways for the observed photoacetalization reactions.

6.4 Experimental details

Extensive experimental details of synthesis procedures, characterization methods and catalytic testing are given in chapter 3, a brief summary of the synthesis and testing is given here. C_3N_4 was synthesized by heating dicyandiamide (DCDA) in customized semi closed system to 550 °C in N_2 atmosphere, as similar to the method described in previous reports.[25,29] The catalytic tests were carried out in an outer irradiation-type photoreactor. Approximately 0.025 g of the photocatalysts were dispersed in 5 mL of methanol and 1mM of substrate was added. The system was irradiated with visible light while maintaining the oxygen pressure of one bar and the reaction products were identified and quantified by GC-MS.

6.5 Results and discussion

6.5.1 Characterization

A detailed discussion about structure of carbon nitride is given in chapter 4. Here, only representative features are listed to ascertain the material structure is carbon nitride. XRD pattern showed three distinct diffraction peaks which are located around 2θ = 13.1˚, 27.2˚, 44.2˚, respectively. The 13.04˚(100) peak due to interlayer stacking distance of conjugated aromatic systems, 27.2˚(002) of in-plane structural packing motifs and 44.2˚(200) is of triazine-based graphitic CN materials, respectively as similar to previous reports. In FTIR spectrum, typical bands at around 800-812 cm^{-1} breathing mode of tri-s-triazine/s-triazine ring sextant out of plan bending, linked by -NH- groups at 1200-1400 cm^{-1} and 1200-1630 cm^{-1} of ν (C-NH-C) and ν (C=N, C=C) stretching vibrations in fingerprint region are present. The solid state ^{13}C MAS NMR signal at approximately 155 and 164 ppm related to the formation of poly(tri-s-triazine) motifs of melem further confirm the structure is essentially carbon nitride. The side bands with asterisk indicate the spinning side bands in ^{13}C spectra. The UV-vis spectra also show typical optical absorption of carbon nitride around 460 nm and inset the band gap $E_g = 2.7$ calculated using equation $\alpha h\nu = A(h\nu - E_g)^n$, where α, ν, and A are the absorption coefficient (Kubelka-Munk function), light frequency, and a constant, respectively.

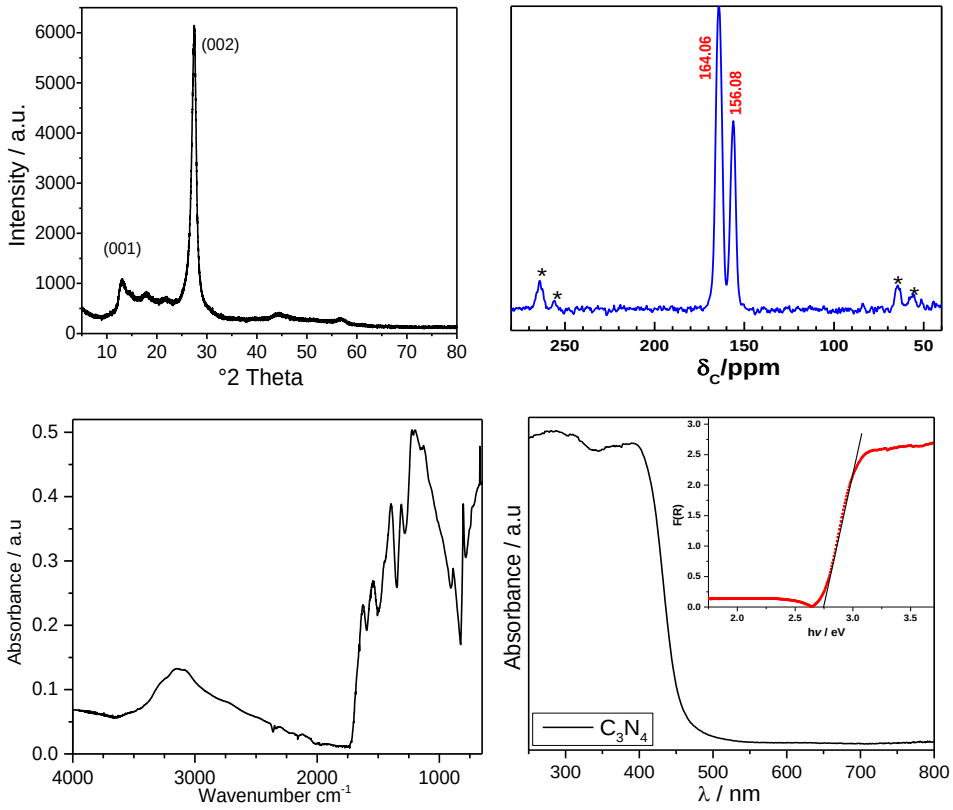

Figure 6.1. XRD patterns (top left), solid-state ^{13}C MAS NMR (* spinning side bands in ^{13}C spectra, top right), FTIR profile (bottom left) and UV-vis absorption spectra (bottom right) with the inset showing a band gap of 2.7eV of graphitic carbon nitride powder.

X-ray photoelectron spectroscopy (XPS) showed the typical C 1s and N 1s peaks along with residual O 1s peak. They were probably due to the surface adsorbed oxygen obtained from the thermal treatment in the air, as similar to previous studies.[30] C 1s spectra clearly showed the C-C, predominant C-N-C, and traces of C-O bonding at 284.5, 287.8 and 289.1 eV, respectively. Whereas the N 1s spectra showed four signals at core levels, namely: 398.3, 400.1, 401.2 and 404 eV attributing to sp^2 C-N-C, (atomic % of bond 69.3) sp^3 H-N-[C_3] (14.8), C-NH_x (12.2) and terminal nitrate groups, charging effects or π excitations.[30,31] A traces of adsorbed oxygen at 532.9 eV and N-C-O at 530.8 were also

observed however predominant structure remained was mainly comprised of polymeric carbon nitrogen framework.

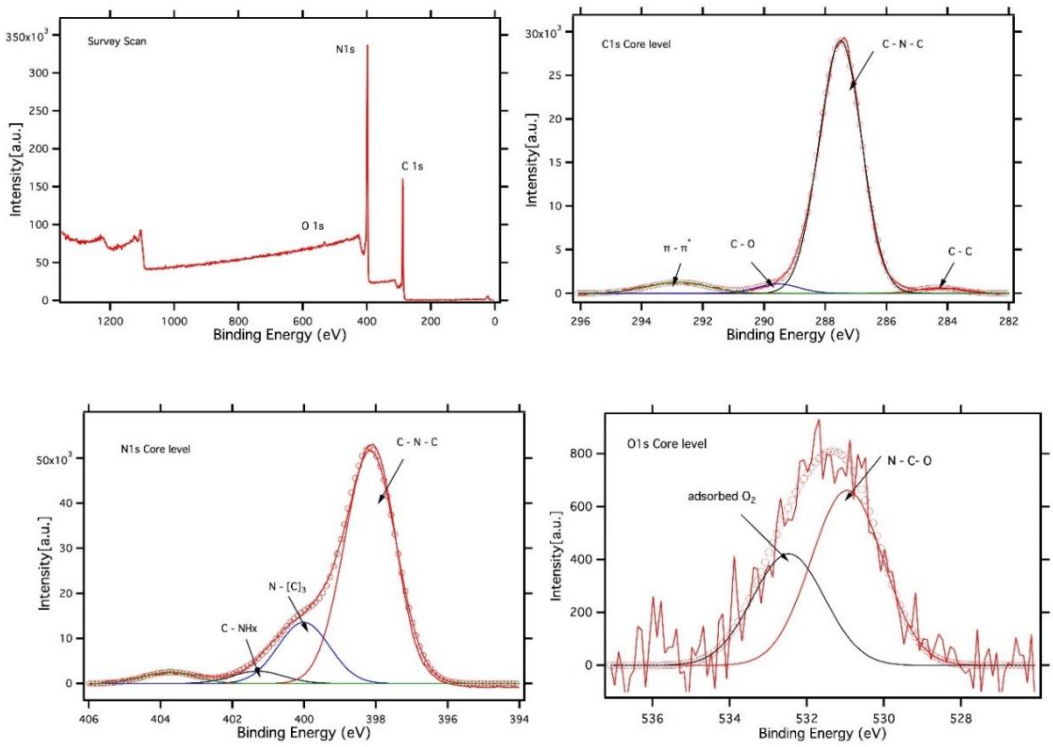

Figure 6.2 XPS spectra of carbon nitride (a) survey spectra (b) C 1s (c) N 1s (d) O 1s synthesized from thermal polycondensation of dicyandiamide (DCDA).

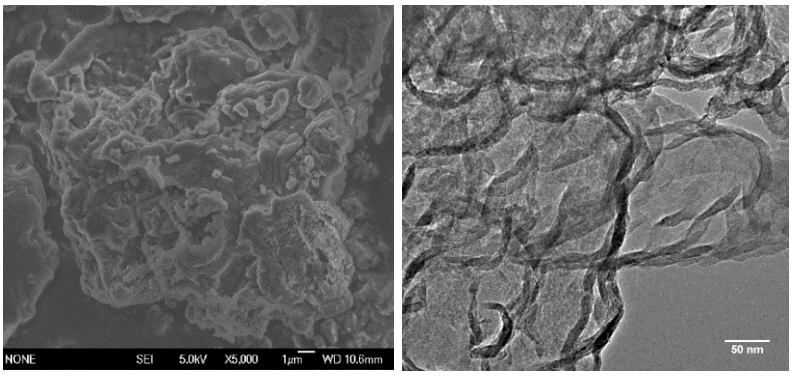

Figure 6.3 SEM and HRTEM image of Carbon nitride processed at 550 °C.

TEM and SEM images of pristine C_3N_4 samples showed typical aggregated large size morphology and relatively smooth and flat surface structure.

6.5.2 Reaction Progress and conditions

A series of photocatalytic reaction were performed with the aim of acetalization of aldehyde/ketones over carbon nitride in molecular oxygen and visible light under ambient conditions. It is found that the conversion of benzaldehyde **2** with excess methanol to corresponding acetal is > 97 % and with selectivity > 98 % in absence of any acid additive. As far as we are aware, this is the first example of heterogeneous photoacetalization of aldehyde/ketones in alcohol over g-C_3N_4, at room temperature and oxygen pressure of 1 bar in environmental friendly manner (Scheme 6.2). Notice that formation of acetals in aqueous acid medium at ambient conditions is thermodynamically limited because of their relatively low equilibrium constants (K~0.01-0.05 mol^{-1}) and with a loss in entropy when two or three molecules of starting materials (aldehyde or ketone plus alcohol) condense to hemiacetal/acetal products. Also by product water is produce, thus, separation of products is necessary.[1] The presently observed high yields from a single pot reaction are attributed to the preferential strong adsorption of polar organic substrates and oxygen and water molecules on the surface, which enables photoacetalization reactions to take place favourably by pre-concentrated substrates over this carbon nitride surface under transient charge (excitons) separation upon light excitation.

First, the time course for acetalization reaction of benzaldehyde **2** with methanol was monitored and results are shown in the Figure 6.4. Under visible light irradiation, reaction proceeded at a steady rate and reached completion at about 6 h, giving the final high conversion and selectivity for the acetal formation. The acetal remained to be the main

product with traces of formaldehyde, ester and acid (<1%) were also detected. To ascertain g-C_3N_4 is required to catalyse the reaction, control experiment without g-C_3N_4 addition was conducted. No acetal was found from benzaldehyde under irradiation of light and oxygen pressure of 1 bar. Under same conditions in the dark with g-C_3N_4, negligible product was also detected over prolonged period (48 h).

Scheme 6.2. Photoacetalization of benzaldehyde to benzaldehyde dimethyl acetal

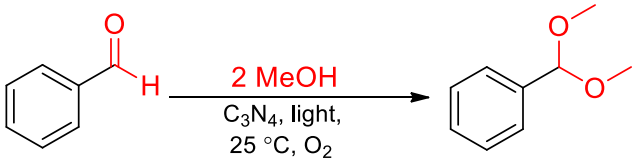

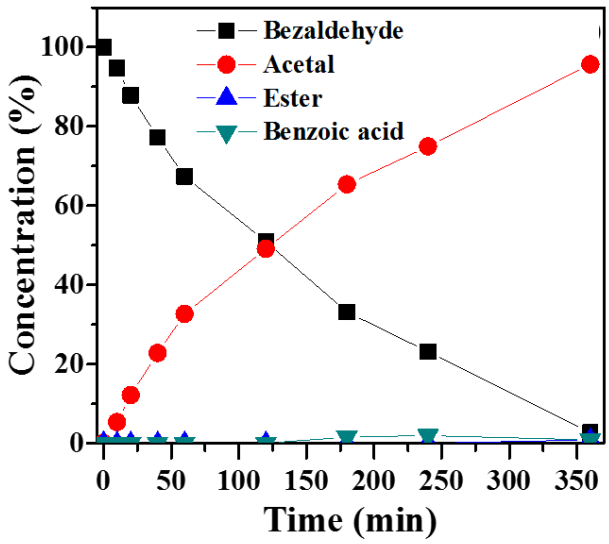

Figure 6.4 Acetalization kinetics of benzaldehyde catalysed by carbon nitride. Conditions: substrate (1mM); C_3N_4 (25mg); alcohol (5 mL); 1bar (O_2); visible light.

6.5.3 Role of Oxygen

To gauge the role of O_2, the reaction was carried out in argon atmosphere instead of using molecular oxygen (Table 6.1). Complex condensation products but with poor selectivity to

acetal (10 %) at relatively low conversion (35 %) were observed. These tests confirm that reaction clearly requires heterogeneous nitride surface whereby O_2, light and substrates are essential ingredients for the cooperative catalysis. Further, the addition of more reactive oxidation agent H_2O_2 (0.5 mL of 30wt %) instead of O_2 to the system, poor conversion and selectivity was noted. Previously it was shown that O_2 interacts with light generated excitons to compensate for the charge within the catalyst.[25] Thus, it is possible, if not entirely plausible that oxygen plays a role, presumably of interacting with the light generated excitons to assist the controlled photoacetalization reaction. This also could explain the observed poor conversion and selectivity in presence of H_2O_2 suggesting not the oxidizing ability is main factor, as the high perhydrol concentration in the medium deters the chemoselectivity of acetalization reaction. These tests confirms that reaction is clearly due to heterogeneous organo-photocatalysis where O_2, light and carbon nitride play a cooperative role. It was found that the catalytic application is also wide ranging and the g-C_3N_4 system appears to work well with a variation of aromatic, alicyclic aldehydes and ketones under ambient conditions using visible light.

Table 6.1 Control experiments under different conditions specified below

Entry	Substrate	Time / h	Conversion %	Selectivity / %
				Acetal
*Ar	Benzaldehyde	48	35.15	10.18
+H_2O_2	Benzaldehyde	6	71.2	42.30
‡BQ	Benzaldehyde	6	98.30	99.41

* Reaction purged during 5 min with argon; + Reaction with addition of 0.5 mL of H_2O_2; ‡ Reaction carried out in the presence of 100mg benzoquinone (BQ);

6.5.4 Reaction and Substrate scope

The system readily promoted the acetalization of benzaldehyde **2** and a range of aromatic aldehydes/ketones with relatively low catalyst loadings (Table 6.2)

Table 6.2 Carbon nitride catalysed photoacetalization of different aldehyde/ketones with ethanol[a]

No	Substrate	Product	Time / h	Conversion / %	Selectivity / %
1	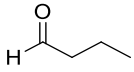	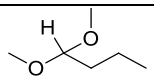	20	93.35	91.90
2	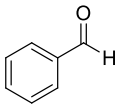	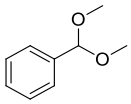	6	97.33	98.30
3	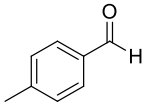	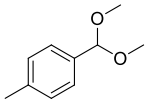	3	87.44	97.44
4	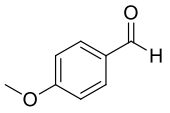	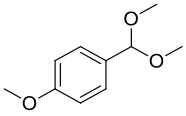	4	83.65	98.20
5	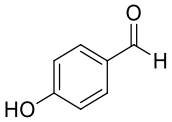	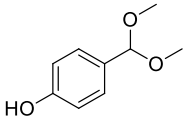	6	0	0
6	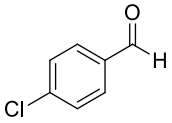	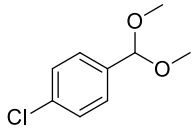	6 10	69.76 96.72	98.85 97.48
7	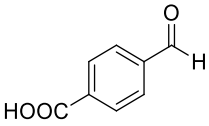	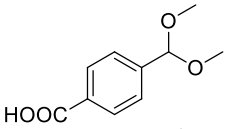	6	53.91	94.94
8	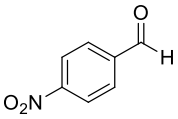	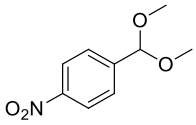	6 24	6.50 25.35	85.00 66.25
9	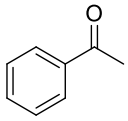	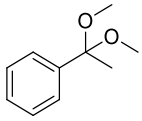	24	21.22	70.94
10	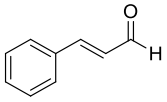	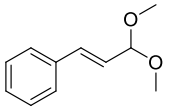	3	84.48	86.53
11	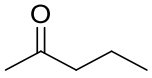	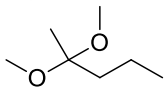	6	42.72	93.43
12	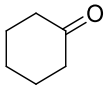	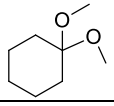	6	84.68	90.85

[a] Conditions: substrate (1mM); C_3N_4 (25mg); methanol (5 mL); 1bar (O_2); visible light. Conversion and selectivity were determined by GC.

A moderate increase in reactivity for electron donating (-CH_3 and -OCH_3) groups **3-4** at para position of substituted benzaldehyde was observed whereas electron withdrawing (-Cl and -NO_2) analogues **6-8** underwent acetalization considerably at a slower rate, however all still displayed high selectivity. As expected, steric hindered acetophenone **9** although gives high electron density at the carbonyl carbon which exhibited sluggish acetalization response, but the failure of 4-Hydroxybenzaldehyde **5** to yield any product, notwithstanding the electron donating nature of the OH group, is surprising and not understood. It could be due to strong inter H-bonding formed between the molecules which prohibit the photoacetalization on the surface. In case of α, β unsaturated cinnamaldehyde **10**, corresponding acetal was obtained with good yield and selectivity, while the double bond remained intact. This clearly demonstrates the synthetic usefulness to sensitive unsaturation moiety groups of this photocatalytic system. The reactions of butyraldehyde **1**, 2-pentanone **11,** and cyclohexanone **12** without conjugated stabilization to the carbonyl group were also successful without requiring the general use of high temperatures. Thus, the versatility of the catalytic system to efficiently drive the photoacetalization in the absence of acid catalysts is evident.

The extension of substrate scope for the catalytic system beyond the reaction with methanol was realized by performing reactions with ethanol and rather difficult but more desirable ethylene glycol (biomass derivative)[5,32] (Table 6.3). The reaction of benzaldehyde **13** with ethylene glycol, whose nucleophilicity is reduced due to mutual inductive withdrawal with the proximal oxygen atoms, to produce more stable cyclic acetal still proceeded with high conversion and selectivity. Similarly the reaction of butyraldehyde **14** with ethylene glycol also furnished five-member cyclic 1, 3-dioxolane product with 78 % selectivity and 70 % conversion. Under same conditions

the reaction with ethanol **15** afforded corresponding acetals with good selectivity nonetheless low yield suggest the kinetics of the reaction is slower than the reaction with methanol. The low selectivity of **16** is probably due observed polymerization products. A challenging reaction[33] with alcohol larger than C_3 **17** (butanol) was also successful showing moderate conversion and selectivity for the corresponding acetal product. These results extend the range and flexibility of the catalytic system to catalyse substrates for targeted acetals using light excitation.

Table 6.3 Carbon nitride catalysed photoacetalization of aldehyde/ketones with different alcohols

No	Substrate	Alcohol	Product	Time / h	Conversion / %	Selectivity / %
13	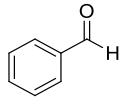		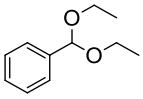	6	38.94	91.12
14	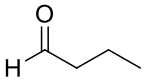		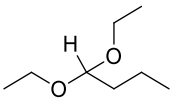	6	32.45	11.37
15	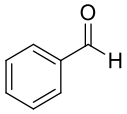	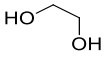	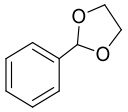	6	90.85	87.13
16	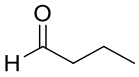	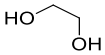	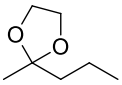	6	70.88	78.42
17	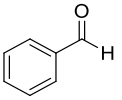	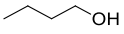	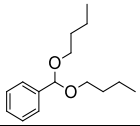	12	43.49	55.73

[a] Conditions: substrate (1mM); C_3N_4 (25mg); alcohol (5 mL); 1bar (O_2); visible light. Conversion and selectivity were determined by GC.

6.5.5 Electronic effects

The tests of carbonyl compound other than aldehyde/ketones, where conjugation is possible between carbonyl and proximal oxygen such as in case of methyl benzoate and benzoic acid reaction did not yield acetal. This clearly indicates the sensitivity of the

reaction to the electronic effects. The slow reaction and low yield in case of acetophenone that have high density at carbonyl carbon is rather mixed and probably due to both steric and electronic effects. Moreover, the failure of 4-Hydroxybenzaldehyde to produce any products as discussed above, despite electron donating nature of the OH group is suspected to be the competing nature of two functionalities, as hydroxyl group may undergo although very slow oxidation reaction, in conditions favouring the both acetalization and oxidation reaction. This is significant because it possibly offers a way to specifically do the acetalization on one of two carbonyl groups in a molecule important for synthetic chemistry.

6.5.6 Effect of Electron donating and electron withdrawing groups

To elucidate the origins of the observed catalysis, kinetics data were collected at different reaction times using benzaldehyde derivatives with some selected *para*-substituted electron donating and electron withdrawing groups of substituted benzaldehyde with methanol (Figure 6.5). The reaction follow first order kinetics and relative rates of the reaction are listed in Table 6.4.

Table 6.4 Photocatalytic rate constants (*k*-values) for H, CH_3, Cl, and NO_2 substituted benzaldehyde

	k-value [min^{-1}]	Adj. *R*-Square
p-(H)C_6H_4CHO	$-0.00587 \pm 1.12\times10^{-4}$	0.99715
p-(CH_3)C_6H_4CHO	$-0.00758 \pm 5.31\times10^{-4}$	0.97588
p-(Cl)C_6H_4CHO	$-0.00337 \pm 2.9\times10^{-4}$	0.97717
p-(NO_2)C_6H_4CHO	$-1.388\times10^{-4} \pm 1.1\times10^{-5}$	0.97798

It is revealed that the rates of electron donating substituents are significantly faster than those of electron withdrawing groups in comparison to benzaldehyde. Following the

kinetics at progressive increasing conversions, the derived reaction rates follow a trend of CH_3->H->Cl->NO_2- (Table 6.4). This distinctive change in reactivity of reacting substrates suggests the possible involvement of electron deficient charged intermediate during the photochemical transformation.

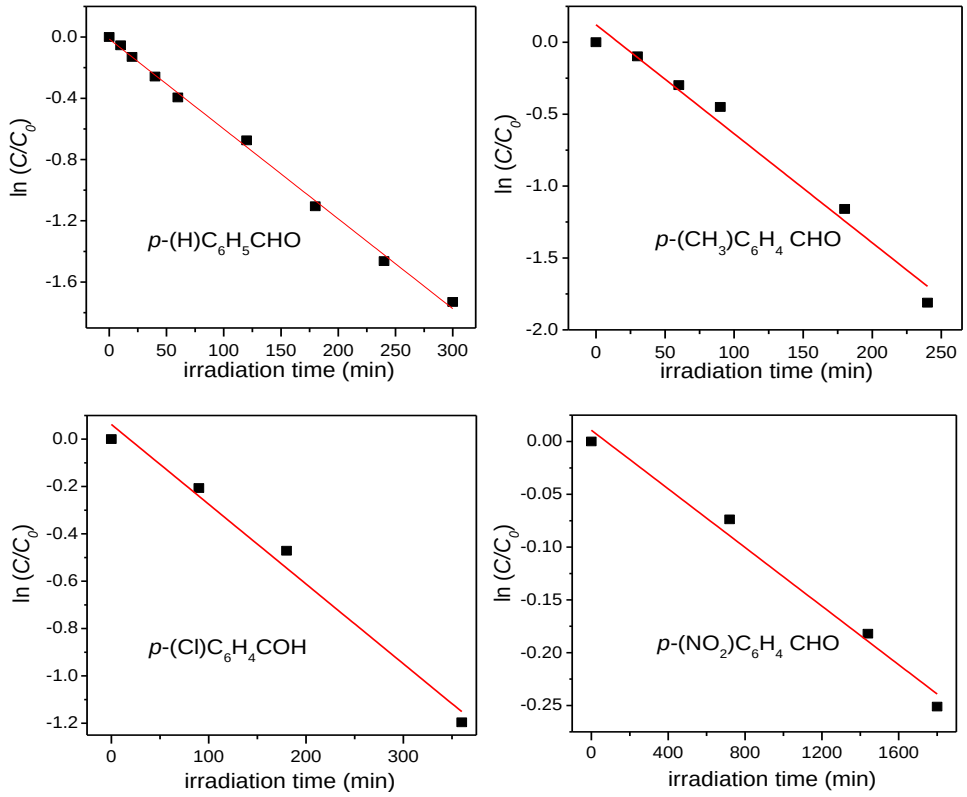

Figure 6.5 Plots of ln(C/C_0) vs time for benzaldehyde with (a) H, (b) CH_3 (c) Cl (d) NO_2 groups.

6.5.7 Hammett Studies

To understand the nature of charge on transition state or intermediate involve in acetalization reaction and sensitivity of reaction to electronic effects Hammett studies were performed. The relative rate obtained from kinetic data of the *para* substituted benzaldehyde were plotted against the σ (Hammett substitution constant). Figure 6.6 show

a good correlation between the log (k_X/k_H) and the σ values and the gradient of this best fit line gave the moderate negative ρ (Hammett reaction constant) value of -1.9. This is slightly smaller than the acid catalysed value ρ value[a] confirming the positive charge accumulation or the fewer electrons in the transition state. This also suggest that the cation formed is not delocalized round the ring, however, remained near the ring in a way that the flow of electrons out of the ring is undeterred.[1] These results are in agreement with the observed faster rates for electron-donating substituents that help stabilization of the transition state.

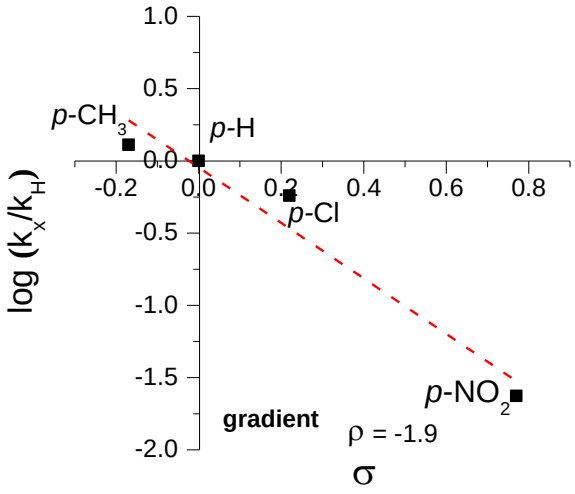

Figure 6.6 Hammett plot for the rate constants for acetalization of benzaldehyde with electron donating and electron withdrawing functionalities at para position.

6.5.8 Regeneration and reusability of the catalyst

Stability of the g-C_3N_4 powder catalyst was evaluated by repeated catalytic tests with powder separation from reaction mixture (centrifugation), drying (overnight at 80 °C) and re-charging into new batch of substrates intermittently. As seen from Figure 6.7 the

[a] The Hammett reaction constant (ρ) value for acid catalysed reaction is between -2 to -4.

catalyst exhibits repeatable catalytic performance when re-employed with new substrate mixture for five consecutive cycles. Only a small appreciable loss of activity was noticed after the first cycle due to the loss of the most superfine particles during centrifugation whereas negligible loss of activity was then recorded in subsequent cycles. In addition, no difference in activity was found regardless of whether the spent catalyst was with or without heat treatment at 200 °C. This suggests that the working catalyst had not suffered from any major surface fouling. The result clearly suggests that g-C_3N_4 can be re-used without any vigorous catalyst regeneration after the photoacetalization.

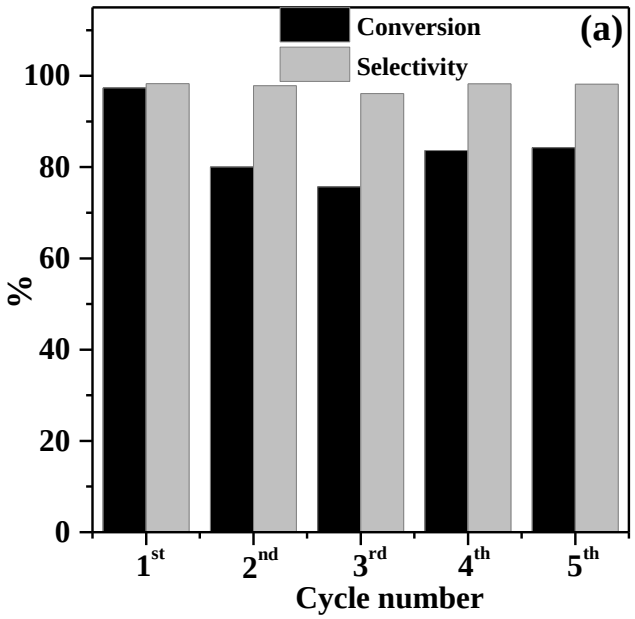

Figure 6.7 A stability test for photoacetalization of g-C_3N_4 of 5 cycles. Conditions: substrate (1mM); alcohol (5 mL); 1bar (O_2); visible light.

6.5.9 Mechanistic considerations

We considered the mechanism for this new but efficient light-induced heterogeneous catalysis reaction and the particular high yield of acetal under ambient conditions. Static (Chapter 4) and time-resolved photo-luminescence (PL) spectroscopy were thus employed

on a g-C_3N_4 film. In static PL, the observed peak around 500 nm is associated to n-π* manifold of conjugated heptazine units suggesting a charge transfer from nitrogen (positive hole) to conjugated carbon (negative electron) under the photo-excitation.[34] This matches with previous theoretical HOMO and LUMO calculations.[29]

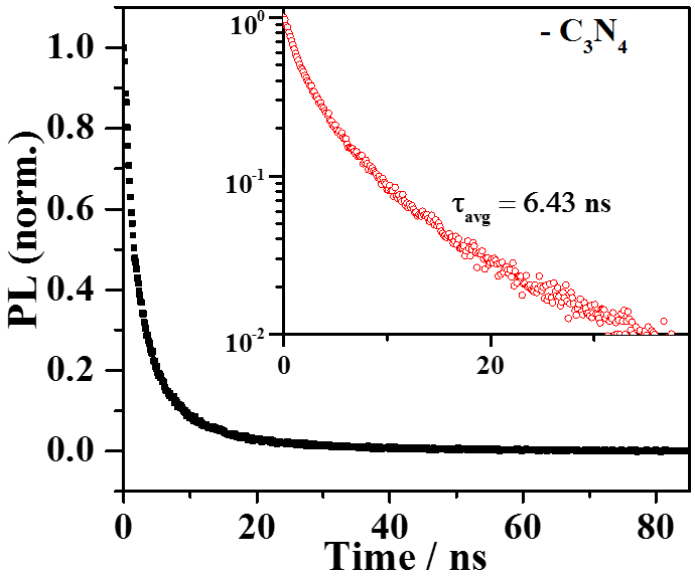

Figure 6.8 Time-resolved photoluminescence of g-C_3N_4 excited by 405 nm laser pulsed at frequencies of 32 MHz.

The time-resolved photoluminescence decay curve of carbon nitride (Figure 6.8) showed a rather long exciton (average) lifetime of 6.43ns, which is within the typical timescale to initiate chemical reactions (10^{-10}-10^{-5} s).[35] Clearly the semiconducting carbon nitride upon our visible light excitation (λ >420nm) can generate long-lived excitons (charge separation) where the excited photogenerated electron takes residence in conduction band (CB) and positive hole on valence band (VB) to catalyse the photoacetalization.[25,34,36],[37] It has been reported that CB of this material at -1.3 V possesses a large thermodynamic driving force with a long live photoelectron to reduce molecular O_2 to form $O_2^{\bullet-}$ (E° O_2/

$O_2^{\bullet-}$= -0.16 V) but the potential of the photogenerated hole in the VB at 1.4 V is inadequate to oxidize –OH to hydroxyl radicals $^{\bullet}OH$ (E° -OH/$^{\bullet}OH$ = 2.4V).[29,38] Despite the possible existence of $O_2^{\bullet-}$ we did not see any typical unselective radical reactions giving a wide range of different products. Instead, ultra-high selectivity was observed and the negative Hammett reaction constant value clearly reflects an ionic mechanism. In addition, we neither observed a significant conversion of alcohol substrate to corresponding aldehyde in **2** at ambient temperature in contrast to those previous studies due to the $O_2^{\bullet-}$ catalytic role generated by g-C_3N_4 under light irradiation at elevated temperature (in our case, trace of formaldehyde was only observed). On addition of more reactive H_2O_2 (radicals promoter) to the catalytic system **2**, poor conversion and selectivity were noted. Importantly, by blending benzoquinone, a superoxide radical scavenger, into the reaction **2**, we did not detect much of its effect to alter the intrinsic high conversion and selectivity of the reaction **2** (Table 6.1). We therefore argue that $O_2^{\bullet-}$ is likely retained on the carbon nitride surface as electron trap unless elevated temperature is used to release it into solution phase. Thus, we conclude that $O_2^{\bullet-}$ does not play a significant role in the charge-sensitive photoacetalization reaction. The surprisingly high yield for photoacetalization at ambient temperature also suggests a clear 'pre-concentration effect' for the polar substrates on confined surface sites presumably due to the characteristic transient charge separation of this material. We believe that the polar organic substrates, O_2 and water could strongly bind on this material surface during the light illumination. Despite the fact that the activation is momentarily conducted under the light irradiation before the recombination of exciton, the local strong field intensity and high charge density (positive nitrogen in close proximity to negative carbon in carbon nitride surface) will facilitate the remarkable catalytic performance for the forward reaction especially in the absence of solvent, additive or diluent. Notice that our GC-MS clearly indicated

preferential binding of polar substrates than the less polar product on catalyst when the reaction was continuously monitored hence reversible reaction with no acidic protons in solution phase was not facilitated. H_2 ^{18}O was still the product from the reaction of ^{18}O labelled benzaldehyde and dried methanol, however, it did not seem to evolve quantitatively from the material. Thus, the g-C_3N_4 reflected by morphological and surface characterization (Figures 6.1-6.3) could have also trapped the by-product water dragging the equilibrium further.

Scheme 6.3 Proposed pathway for photoacetalization

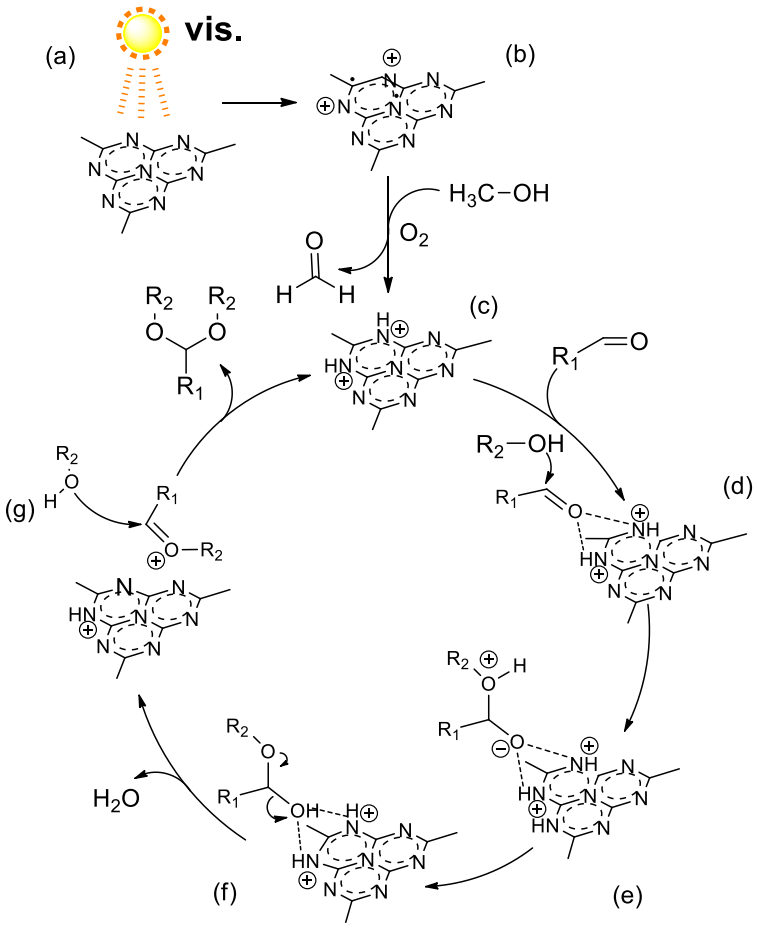

Although more detailed studies are needed to elucidate the mechanism, a simplified pathway for photoacetalization is summarized in Scheme 6.3. From this Scheme, visible

light impinging on g-C_3N_4 can generate surface charge separation of $^{\oplus}N$ and $O_2^{\bullet-}$ which may help to deprotonate alcohol to form adsorbed protons on the surface initially. Such transient surface charge species will also induce fast acetalization from polar aldehyde and alcohol by ionic mechanism on the material surface. This may involve the formation of oxonium ion (**g**) as reflected by the negative value of the Hammett study ($\rho = -1.9$) to form acetal. We anticipate that it is stabilized by carbon nitride surface presumably through cation-π interactions.[39] Such transition state specie is known to exist in the rate determining step in solution phase in the presence of acid catalysts. However, in our case, there is no need to add aqueous acid catalysts as the surface protons can be quickly regenerated from the reaction cycle on confined surface with high affinity for the polar terminal oxygen group of substrates under transient conditions.

Scheme 6.4 Proposed transition states and pathways from hemiacetal to acetal formation.

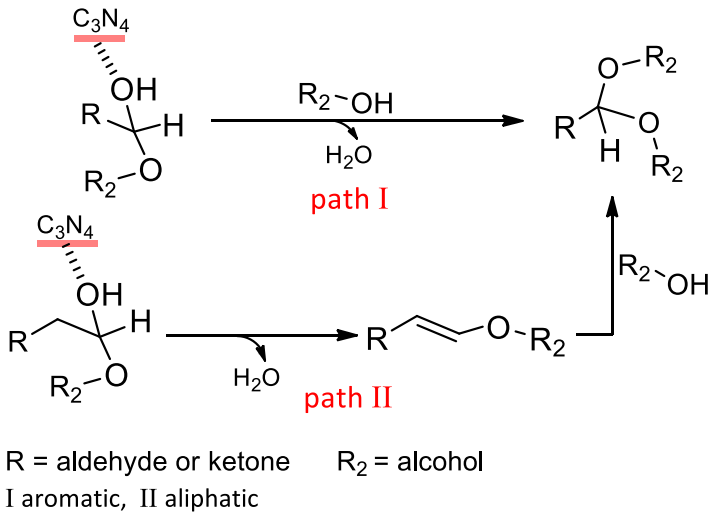

It is interesting to note that, for substrates with β-hydrogens, the photoacetalization reaction may also have a vinyl ether intermediate (Scheme 6.4), which upon the addition of

alcohol to C=C bond will produce acetal.[33,40] Indeed, we observed trace of vinyl ether species for **11, 12** to corresponding acetals.[33]

6.6 Conclusion

In conclusion, we have demonstrated efficient photoacetalization of aldehydes and ketones with alcohols using g-C_3N_4 as photocatalyst, which gives impressive selectivity and conversion in high rate and yield at ambient conditions. The reaction takes place at room temperature in oxygen atmosphere involving substrates and acid-free solid catalyst without adding solvent and hence is clearly a new green synthesis method. The broad reaction scope and remarkable versatility of this catalytic system could enable us to tackle a wide spectrum of aldehyde/ ketones /alcohols of interests for specific acetals production with favoured equilibrium.

References

[1] J. Clayden, N. Greeves, W. Stuart, *Organic Chemistry*, Oxford University Press, **2012**.

[2] M. A. Butler, *J. Appl. Phys.* **1977**, *48*, 1914–1920.

[3] B. T. Gregg, K. C. Golden, J. F. Quinn, *J. Org. Chem.* **2007**, *72*, 5890–5893.

[4] N. Hamada, K. Kazahaya, H. Shimizu, T. Sato, *Synlett* **2004**, 1074–1076.

[5] S. Rudrawar, R. C. Besra, A. K. Chakraborti, *Synthesis (Stuttg).* **2006**, 2767–2771.

[6] M. B. Smith, J. March, *March's Advanced Organic Chemistry*, John Wiley & Sons, Inc., Hoboken, New Jersey, **2007**.

[7] A. Clerici, N. Pastori, O. Porta, *Tetrahedron* **1998**, *54*, 15679–15690.

[8] M. Kotke, P. R. Schreiner, *Tetrahedron* **2006**, *62*, 434–439.

[9] D. Li, F. Shi, J. Peng, S. Guo, Y. Deng, *J. Org. Chem.* **2004**, *69*, 3582–3585.

[10] B. Karimi, H. Seradj, G.-R. Ebrahimian, *Synlett* **1999**, *1999*, 1456–1458.

[11] B. Karimi, H. Hazarkhani, J. Maleki, *Synthesis (Stuttg).* **2005**, *2005*, 279–285.

[12] R. Gopinath, S. J. Haque, B. K. Patel, *J. Org. Chem.* **2002**, *67*, 5842–5845.

[13] F. Zhang, J. Shi, Y. Jin, Y. Fu, Y. Zhong, W. Zhu, *Chem. Eng. J.* **2015**, *259*, 183–190.

[14] A. S. Poyraz, C.-H. Kuo, E. Kim, Y. Meng, M. S. Seraji, S. L. Suib, *Chem. Mater.* **2014**, *26*, 2803–2813.

[15] N. Narkhede, A. Patel, *RSC Adv.* **2014**, *4*, 19294.

[16] J.-L. Luche, A. L. Gemal, *J. Chem. Soc. Chem. Commun.* **1978**, 976.

[17] S. K. De, R. a. Gibbs, *Tetrahedron Lett.* **2004**, *45*, 8141–8144.

[18] H. Firouzabadi, N. Iranpoor, B. Karimi, *Synth. Commun.* **1999**, *29*, 2255–2263.

[19] J. Y. Qi, J. X. Ji, C. H. Yueng, H. L. Kwong, A. S. C. Chan, *Tetrahedron Lett.* **2004**, *45*, 7719–7721.

[20] R. Sugimura, K. Qiao, D. Tomida, C. Yokoyama, *Catal. Commun.* **2007**, *8*, 770–772.

[21] Y. Wang, X. Wang, M. Antonietti, *Angew. Chem. Int. Ed.* **2012**, *51*, 68–89.

[22] M. B. Ansari, B.-H. Min, Y.-H. Mo, S.-E. Park, *Green Chem.* **2011**, *13*, 1416.

[23] Y. Wang, J. Zhang, X. Wang, M. Antonietti, H. Li, *Angew. Chem. Int. Ed.* **2010**, *49*, 3356–3359.

[24] L. Möhlmann, M. Baar, J. Rieß, M. Antonietti, X. Wang, S. Blechert, *Adv. Synth. Catal.*

2012, *354*, 1909–1913.

[25] F. Su, S. C. Mathew, G. Lipner, X. Fu, M. Antonietti, S. Blechert, X. Wang, *J. Am. Chem. Soc.* **2010**, *132*, 16299–16301.

[26] B. Long, Z. Ding, X. Wang, *ChemSusChem* **2013**, *6*, 2074–2078.

[27] Z. Ding, X. Chen, M. Antonietti, X. Wang, *ChemSusChem* **2011**, *4*, 274–281.

[28] F. Su, S. C. Mathew, L. Möhlmann, M. Antonietti, X. Wang, S. Blechert, *Angew. Chem. Int. Ed.* **2011**, *50*, 657–660.

[29] X. Wang, K. Maeda, A. Thomas, K. Takanabe, G. Xin, J. M. Carlsson, K. Domen, M. Antonietti, *Nat. Mater.* **2009**, *8*, 76–80.

[30] D. J. Martin, K. Qiu, S. A. Shevlin, A. D. Handoko, X. Chen, Z. Guo, J. Tang, *Angew. Chem. Int. Ed.* **2014**, *53*, 9240–5.

[31] A. Thomas, A. Fischer, F. Goettmann, M. Antonietti, J.-O. Müller, R. Schlögl, J. M. Carlsson, *J. Mater. Chem.* **2008**, *18*, 4893.

[32] B. Karimi, G. R. Ebrahimian, H. Seradj, *Org. Lett.* **1999**, *1*, 1737–1739.

[33] C. Gunanathan, L. J. W. Shimon, D. Milstein, *J. Am. Chem. Soc.* **2009**, *131*, 3146–3147.

[34] Y. Shiraishi, S. Kanazawa, Y. Sugano, D. Tsukamoto, H. Sakamoto, S. Ichikawa, T. Hirai, *ACS Catal.* **2014**, *4*, 774–780.

[35] A. L. Linsebigler, A. L. Linsebigler, J. T. Yates Jr, G. Lu, G. Lu, J. T. Yates, *Chem. Rev.* **1995**, *95*, 735–758.

[36] X. Wang, S. Blechert, M. Antonietti, *ACS Catal.* **2012**, *2*, 1596–1606.

[37] M. R. Hoffmann, S. T. Martin, W. Choi, D. W. Bahnemann, *Chem. Rev.* **1995**, *95*, 69–96.

[38] Y. Cao, Z. Zhang, J. Long, J. Liang, H. Lin, H. Lin, X. Wang, *J. Mater. Chem. A* **2014**, *2*, 17797–17807.

[39] D. A. Dougherty, *Acc. Chem. Res.* **2013**, *46*, 885–893.

[40] E. Kossoy, Y. Diskin-Posner, G. Leitus, D. Milstein, *Adv. Synth. Catal.* **2012**, *354*, 497–504.

Chapter 7: Concurrent tandem photo-oxidation /acetalization of alcohols over carbon nitride

Overview

Direct catalytic transformation of alcohols to acetal is challenging. This chapter presents the first example of visible light that induces concurrent tandem catalytic (CTC) conversion of alcohol to acetal employing metal free carbon nitride as photo transducer under mild conditions. The distinctive electronic structure and nitrogen rich surface of C_3N_4 allow it to act in tandem to catalyse the alcohol oxidation and subsequent acetalization of the products obtained with primary alcohols introduced at the outset. The process is essentially green using visible light, oxygen and heterogeneous system. The broad substrate scope with good selectivity for aromatic, cyclic and secondary alcohols offer a practical way to produce variety of acetals for green synthetic chemistry applications.

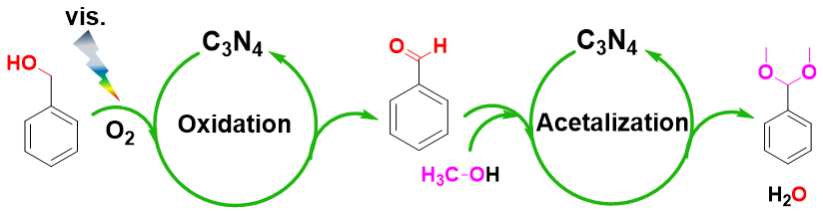

Concurrent tandem oxidation/ acetalization of alcohols over carbon nitride

7.1 Introduction

Acetals usually produced by condensation of aldehyde and alcohols are important intermediates in synthetic chemistry for the introduction of other functional groups.[1,2] Generally available methods for acetal formation have overwhelming focus on acid catalysed reaction using aldehyde and ketone as a reactant.[3–9] To circumvent the need of aldehyde and ketone derivatives, particularly, atom economic, selective conversion of alcohols to acetal is desired but challenging. To the best of our knowledge in all of the existing reports precious metal (Pd, Ru and Re) based complexes were employed in homogeneous media to catalyse the direct transformation of alcohols to acetals in stringent conditions.[10–12] Partly, high cost, the cumbersome synthetic nature of complex catalytic systems and the inherent problem of separation of catalyst from products, restrict their large scale use. Moreover, to avoid the acetal hydrolysis back to its starting components, water produced during the reaction must be removed by a process such as a molecular sieves or a Dean-Stark trap.[2] It would be desirable to develop a sustainable and cost effective metal free catalytic method towards acetal formation from alcohols.

It is likely that acetal production from alcohol undergoes via aldehyde that usually is an oxidation product, followed by alcohol and aldehyde reaction to acetal in sequential manner, both the reactions are well known. In particular, oxidation of alcohols to aldehydes is important reaction and traditional methods employ strong oxidizing agents (Mn^{7+}, Cr^{6+}, and V^{5+}) and halogenated solvents that generate corrosive and toxic metal waste. In relatively less harmful protocols, heterogeneous catalytic system using expensive noble metals Au, Ag, Pd, Ru, and mild oxidant (O_2 and H_2O_2) for alcohol oxidations have

emerged. Further, TiO_2 and Fe^{+3} or Rh^{+3} ion modified TiO_2 have widely employed recently for alcohol oxidation reactions under visible light conditions. Shishido *et.al* demonstrated rather intriguing photooxidation with high selectivity over Nb_2O_5, proposing excitations from donor O 2p level of Nb only localized at alcoholic oxygen binding to conduction band of Nb_2O_5 in contrast to the classical band gap excitation mechanism.[13] Recently, chemoselective alcohol oxidation on metal free, mesoroporous carbon nitride using visible light and high oxygen pressure (8 bar) in acetonitrile and in water has been achieved. Separately, acetalization of the oxidation products of alcohols i.e. aldehydes/ketones traditionally requires catalytic activation by Lewis and Brønsted acids.[2,6,14–16] To address the acid problem of acid sensitive substrates and environmental concerns attempts have been made to synthesize acetals in acid free conditions in homogenous media.[3,17,18] As an advancement, recent literature focus is on production of acetals from carbonyl compounds, exploiting easy to separate alternative heterogeneous solid acid catalytic systems in conjunction with protic/Lewis acids on solid supports which are deemed relatively less deleterious to environment.[5,7,9,19–24] However, an alternative, sustainable and environmentally benign metal free catalytic pathway towards acetal formation is needed.

To address the problems of waste and effective energy utilization, one possible approach is concurrent tandem catalysis (CTC) which combines two or more catalytic cycles that are mechanistically distinct, into one synthetic operation.[25,26] In CTC, all the reagents are added at the beginning and same conditions are maintained during the course of all transformations. This way not only improves the catalyst utilization, work up and process efficiency but also avoids waste generation, separation and purification step of intermediate products of the cycles.[27] Regardless of the fact that the majority of catalysts involved in CTC are homogeneous, it still constitutes a significant challenge to find the conditions

compatible with coupled chemical transformations without the interference or to avoid the side reactions.

Another way is the use of sunlight to run targeted chemical reactions owing to its clean and renewable nature.[28,29] Recently, π-conjugated layered framework comprising earth abundant elements carbon and nitrogen, carbon nitride, has stirred an interest for its ability to harvest visible light for fine chemical synthesis.[30–32] Carbon nitride having chemical and thermal stability at high temperature (< 600 °C in air) and in extreme pH conditions together with its capability to utilize visible light makes it a rational choice to be employed in photochemical transformations. It is of particular interest that, most of the photo induced oxidation reactions using metal oxide semiconductors generate photoactive radicals and usually have poor product selectivity. Carbon nitride, unlike metal oxides, have low valance band potential that prohibits the generation of such strong nonselective ˙OH radical. Whereas, its conduction band potential is sufficient enough to activate the O_2.

In the past several reports have emerged about reductive activation of O_2 for photo oxidation of alcohols and other fine chemical synthesis over carbon nitride and in Chapter 6 we demonstrated the photoacetalization of aldehydes to acetal with high selectivity using O_2 as green oxidant.[33–36] In context of CTC, previously, acetals were produced from alcohols in tandem, using MnO_2, trialkyl orthoformates and catalytic quantities of indium triflate in homogeneous acidic media.[37] Similarly, hydroformylation/acetalization has been reported using $RhCl_3$ in combination with $P(OPh)_3$ as auxiliary ligands under homogeneous non acidic conditions.[38] As mentioned earlier, a small body of work about direct conversion of alcohols to acetal exists but to date no metal free heterogeneous photocatalytic systems have been employed to produce acetal from alcohols.

7.2 Objectives

Intrigued by the unusual catalytic ability of carbon nitride to catalyse photooxidation of alcohol to aldehyde and alcohol and aldehyde reaction to acetal, this chapter focuses on coupling the two reactions in one pot to comply with the principle of green synthesis. Further, emphasis is on development of a heterogeneous system having broad substrate scope with good selectivity for aromatics, and aliphatic alcohols as an alternative pathway to produce a variety of acetals for green, synthetic chemistry applications.

7.3 Experimental details

Synthetic details of carbon nitride are given in chapter 6 experimental detail section, as similar to the previous reports.[30,33]

7.4 Characterization

The physical and chemical structures of carbon nitride were determined using various analytical techniques. As shown by solid-state ^{13}C NMR, FTIR and UV spectra, XRD pattern, SEM and TEM images in Chapter 4 and 6 the chemical structure, optical and surface properties, packing motifs, textural structure representative of typical molecular carbon nitride, similar to literature reports, were revealed.

7.5 Results and discussion

As advancement to our previous work, here we combine two approaches, CTC and the use of visible light, employing a single photocatalyst for oxidation/acetalization in one

synthetic operation under mild conditions. This is the *first report* on auto-tandem heterogeneous photocatalytic conversion of alcohols to corresponding acetals, where light as a clean and renewable reagent and two distinct catalytic processes in one-pot substantially avoids the waste generation and tedious work up. All the reagents, O_2 and carbon nitride were added at the outset. The unique band structure of carbon nitride together with its nitrogen rich surface, have large thermodynamic force to activate oxygen which deters total oxidation and assists controlled subsequent chemical transformations.[39] For acetal formation carbon nitride upon irradiation, first catalyses the photooxidation of alcohols to intermediate aldehydes and ketones which undergo subsequent reaction with a primary alcohol to yield acetals (scheme 7.1). Detailed description of photochemical reaction together with synthesis of carbon nitride are given in experimental chapter (Chapter 4).

Scheme 7.1. One pot catalytic conversion of Alcohols to acetals

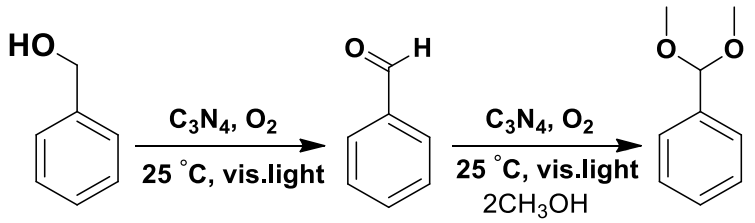

A series of experiments were performed in O_2 pressure of 1 bar at room temperature under visible light irradiation. As expected, conversion of alcohols to acetal occurred in stepwise manner. Figure 7.1 clearly shows the time-dependent change in the amount of product during photoreaction and indeed reaction proceeds in two distinct cycles. Particularly, the reaction of benzyl alcohol in methanol under visible light irradiation exhibits high selectivity > 91 % and 27 % conversion for acetal formation, in green mild conditions.

Initially, in cycle one, light excited carbon nitride activates O_2 and oxidation of alcohols occurs. Mostly aldehyde molecules are observed in the first 3 hours with traces of the acetal. This suggests that first step is limiting as the kinetics of alcohol oxidation are usually slow and the acetalization step does not proceed until a critical concentration of aldehyde is reached. Besides, acknowledging the fact that second cycle is challenging due to unfavourable decrease in entropy during acetalization reaction,[2] with the passage of time selectivity for the acetal gradually improved to a near constant after 24 hours. In addition, the ascent of conversion also indicates if reaction is kept for longer time, higher conversion can be achieved.

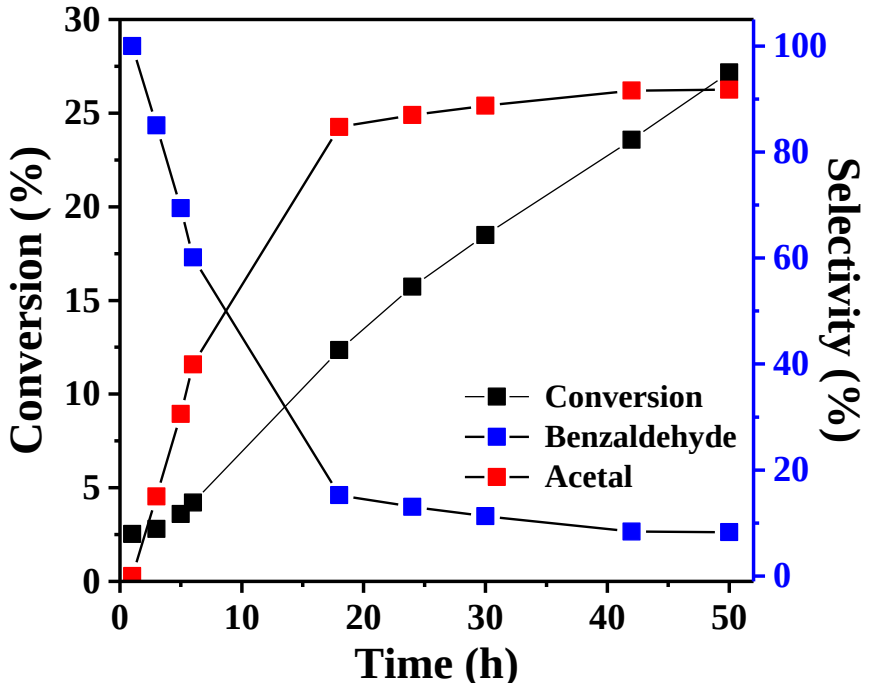

Figure 7.1 Acetalization kinetics of benzyl alcohol with methanol catalysed by carbon nitride. Conditions: substrate (1mM); C_3N_4 (25mg); methanol (5 mL); 1bar (O_2); visible light ($\lambda > 420$). Conversion and selectivity were determined by GC.

7.5.1 Role of oxygen, hydrogen peroxide

To explore the conditions for reaction keeping the green and mild pathway as priority only the O_2 and H_2O_2 as mild oxidant were considered. First in a control experiment, as reference, at 25 °C and oxygen pressure of 1 bar in the dark, reaction did not happen. The system also failed to yield any product in the absence of photocatalyst, carbon nitride. To check the dependence of activity on oxygen presence, the system was purged several times with argon followed by reaction in argon atmosphere. Random condensation product mixture was observed confirming the requirement for O_2 for the controlled oxidation and acetalization reaction.

Table 7.1 Reaction conditions for carbon nitride catalysed photoacetalization of alcohols.[a]

Catalyst	Time (h)	Conversion. %	selectivity %			
			acetal	aldehyde / ketone	ester	others
C_3N_4- Dark	48	0	0		-	
*C_3N_4 -H_2O_2	24	8.7	28.3	60.3	11.4	
C_3N_4 -H_2O_2	48	14.7	28.0	25.9	26.9	
C_3N_4 -O_2	24	15.5	74.1	08.8		
C_3N_4 -O_2	48	27.3	91.2	91.2		
C_3N_4 -Ar	48	0	0	0	0	

All reactions were carried out at 25 °C. *H_2O_2 was used instead of O_2

[a] Conditions: substrate (1mM); C_3N_4 (25mg); methanol (5 mL); 1bar (O_2); visible light. Conversion and selectivity were determined by GC.

When H_2O_2 was tried instead of O_2, poor selectivity was seen. This suggest that only the species on the surface are sufficiently mild and high perhydrol concentration in the medium

does not favour selectivity. However we did not tried reaction in air.[a] Previously, it has been demonstrated that nitrogen rich surface of carbon nitride can reductively adsorb O_2 which presumably remains on the surface via acid base interaction and act as an interface bound exciton to compensate the charge during photochemical oxidation of alcohols. These tests suggest a cooperative system of O_2, light and photocatalyst, all, are necessary for the acetalization process.

7.5.2 Substrate scope of reaction

Given the relationship and cooperative role of carbon nitride, molecular oxygen and light for photochemical transformation of alcohols to acetals, we subsequently investigated the substrate scope for this photocatalytic system and the results are listed in Table 7.2. As a model compound, benzyl alcohol, often employed to evaluate the oxidation activity of alcohols, was selected for the acetalization reaction with methanol and ethanol. It is noteworthy that both the reactants are alcohols and acetal formation is controlled by kinetics of the chosen reactants in such a way that short chain primary alcohols are relatively resilient to oxidation and therefore preferentially react in the second step. In both cases, corresponding acetals were obtained with remarkable selectivity > 90 % with good conversion. Further, taking benzyl alcohol as reference, effect of substitution was also studied. Experiments revealed that electron donating group (-CH_3) enhanced both selectivity and conversion **(entry 2)** whereas, reaction was slow and less selective when withdrawing substituents (-Cl and -NO_2) were attached **(entry 3 and 4).** These results apparently indicate the involvement of electron deficient intermediates during

[a] The chemical reaction that proceeds under mild green conditions is desirable that reaction. It is envisaged that photoacetalization reaction can proceed in the air.

photochemical transformation. Interestingly, for α-methylbenzyl alcohol **(entry 5),** the predominant product was corresponding aldehyde instead of acetal. This may be attributed to relative stability, increased charge density on carbonyl function and steric hindrance that obstruct acetalization step.[6] The acetalization reaction of benzophenone in our earlier work also failed to produce any product on similar grounds. It is of merit to note that unlike the already reported systems which can only work with particular type of substrate,[10] our systems show good selectivity with secondary, cyclic and aromatic alcohols suggesting their substrate flexibility and wider broad scope to carry out different reactions.

Table 7.2 Carbon nitride catalysed photoacetalization of alcohols to acetal[a]

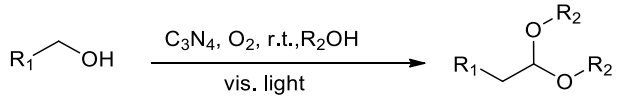

entry	R_1⟨OH	T / h	Conv. %	selectivity %		
				acetal	Aldehyde/Ketone	Others
1	$C_6H_5CH_2OH$	48	27.17	91.72	8.27	-
2	*p*-$(CH_3)C_6H_4CH_2OH$	48	38.36	92.09	7.90	-
3	*p*-$(Cl)C_6H_4CH_2OH$	48	15.39	69.31	19.43	11.25
4	*p*-$(NO_2)C_6H_4CH_2OH$	48	20.60	54.56	38.76	6.66
5	$C_6H_5CH(CH_3)OH$	50	19.77	5.47	89.32	5.20
6	$CH_3CH(OH)CH_3$	72	4.54	100	-	-
7	$C_6H_{11}OH$	48	3.82	100	-	-
*8	$C_6H_5CH_2OH$	48	23.95	63.21	22.64	14.14
†9	$C_6H_5CH_2OH$	48	14.69	28.05	45.36	26.59

*Reaction was carried out with ethanol i.e.,$R_2 = C_2H_5OH$; † H_2O_2 was used instead of O_2

[a] Conditions: substrate (1mM); C_3N_4 (25mg); methanol (5 mL); 1bar (O_2); visible light. Conversion and selectivity were determined by GC-MS.

7.5.3 Comparison with direct acetalization results

To highlight the significance of our one pot method, comparison was made to the best results reported for direct conversion of aromatic alcohols to acetals under neutral conditions (Table 7.3). It is worth mentioning that bis(acetonitrile)bis(triphenyl-phosphine)ruthenium(II) Sulfate [Ru $(PPh_3)_2(NCCH_3)_2$ (SO_4)] complex showed conversion of benzyl alcohol to acetal with 59 % selectivity at 110 °C.[11] In addition to this, same group reported the similar direct conversion of primary alcohols to acetal at high temperature using acridine-based Ru pincer complex with good selectivity but the system failed to catalyse the benzyl alcohol.[10] Another limitation associated with these systems is that only acetal of the reacting molecule can be obtained and the reaction becomes difficult with secondary and aromatic alcohols.

Table 7.3. Comparison of results for alcohols to acetal with Ru complexes and carbon nitride

Catalyst	Alcohol	T (°C)	Time (h)	Conv. %	selectivity %			
					acetal	aldehyde / ketone	ester	
C_3N_4	benzyl alcohol	25 / 1	48	27.2	91.7	8.3	-	this work
RuHCl(CO)(A-^{i}Pr-PNP)	benzyl alcohol	168	72	100	-	-	99	Ref. [10][b]
$Ru(PPh_3)_2Cl(NCCH_3)_2(SO_4)$	benzyl alcohol	110	48	80	59	4	0	Ref. [11][b]

In contrast our result is the first report of photochemical transformation from alcohol to acetal using heterogeneous catalytic system having higher selectivity in comparison to any literature method. In addition it offers a practical way to choose different alcohols to make

[b]These homogeneous catalyst (Ru complexes) showed high conversion and selectivity for primary alcohols

variety of acetals. For instance, the reaction of benzyl alcohol with ethanol, **(**Table 7.1, **entry 8)** produced corresponding benzaldehyde diethyl acetal with selectivity (> 92) Figure 7.2. Likewise, in the reaction of aliphatic alcohols; 2-propanol **(entry 6)** and cyclic cyclohexanol **(entry 7)**, corresponding acetal were formed with high selectivity though low conversion mainly due to slower kinetics of the oxidation step. We in fact also observed the acetal formation when primary alcohol alone were used over prolonged period of time nevertheless reaction is faster with aromatic alcohols.

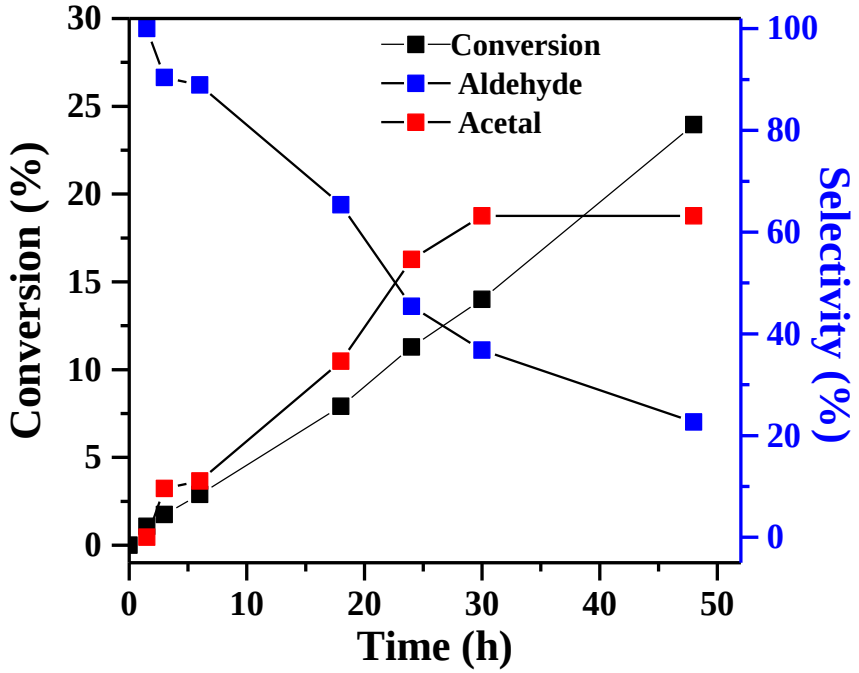

Figure 7.2 Acetalization kinetics of benzyl alcohol with ethanol catalysed by carbon nitride. Conditions: substrate (1mM); C_3N_4 (25mg); methanol (5 mL); 1bar (O_2); visible light (λ> 420). Conversion and selectivity were determined by GC.

7.5.4 Benzoquinone tests

In order to differentiate that two separate cycles having distinct mechanism are operative in tandem, benzoquinone (BQ), a superoxide radical scavenger, was added during the photoacetalization reaction. For photoacetalization of benzaldehyde on addition of BQ, reaction showed unaltered selectivity and conversion **(entry 12)**. This result confirmed that $O_2^{\bullet-}$ does not participate in the acetalization step. In contrast, the addition of BQ to the reaction of benzyl alcohol oxidation (**entry 12**) lead to the significant decrease in activity (or cessation of the reaction). This result clearly indicates (similar to previous reposts)[34,40] that $O_2^{\bullet-}$ radical is involved in alcohols oxidation, however, both oxidation and acetalization reactions have different mechanistic pathway (Table 7.4).

Table 7.4. Effect of benzoquinone on conversion and selectivity of benzyl alcohol to acetal

Entry	Alcohol/aldehyde	time / h	conversion %	selectivity %	
				acetal	Aldehyde/Ketone
10‡	Benzyl alcohol	48	5.90	68.27	31.73
11+	Benzaldehyde	6	97.33	98.30	-
12‡	Benzaldehyde	6	98.30	99.41	-

‡ Reaction carried out in presence of benzoquinone (BQ); + Reaction without BQ
Conditions: substrate (1mM); C_3N_4 (25mg); methanol (5 mL); 1bar (O_2); visible light. Conversion and selectivity were determined by GC-MS.

7.5.6 Catalyst Recyclability

Due to its heterogeneous metal free nature carbon nitride was easily collected by simple filtration without contaminating the reaction/product media. Further, to test the surface structure and stability of photocatalyst, the collected carbon nitride was washed with ethanol and dried overnight at 80 °C and then reanalysed by FTIR, XRD, and SEM.

Analysis results seemingly showed no apparent change in physical and chemical structure of the carbon nitride, confirming the chemical and structural stability of the catalyst. However, no testing was done to evaluate the reusability of the catalyst, but it is evident from isopropanol reaction that catalyst is active continuously for at least 72 h reaction testing (Table 7.2, **entry 6**).

7.6 Proposed reaction pathway

Although further studies are needed to decipher the mechanistic details and species involved in the reaction, it has been demonstrated that nitrogen rich surface of carbon nitride can reductively adsorb O_2 which presumably remains on the surface via acid base interaction. This may act as an interface bound exciton to compensate the charge during photochemical oxidation of alcohols. On photoexcitation electron and hole localized states on conduction band (CB) and valance band (VB) of carbon nitride are generated respectively (**a)**.[39,41] The hole at VB removes α and β hydrogen of interacting alcohol molecule to aldehyde whereas electron at CB is reductively captured by electrophilic surface bound oxygen to generate $O_2^{\bullet-}$ radical (**b**).[33,34] Consequently, the protons formed during oxidation of the alcohol became localized at the electron rich nitrogen of the carbon nitride via Lewis acid-base interaction (**c**).[41,42] As soon as aldehyde/ketones are produced photocatalytic acetalization begins with activation of carbonyl group with protons in vicinity which remained bound to nitrogen of carbon nitride (**d**).[43] This follows the nucleophilic addition of the primary alcohol, (R_2-OH) present at the outset (**e**), which induces the formation of the incipient zwitterion and substantial increase in charge is preferentially stabilized by concomitant surface bound protons (**f**).[44] The oxonium ion formed is stabilized by electron rich carbon nitride surface,[44,45] presumably through

cation-π interactions[46] (**f-g**). As the oxonium ion is electrophilic that rapidly reacts with the second alcohol molecule to produce acetal and water. Contrary to the usual single electron reduction of O_2 to $^{\bullet}OOH$ it is presumed that superoxo radical is further reduced rapidly to endoperoxide species which on protonation produces H_2O_2 and to complete the photocatalytic cycle.[41,47] The high selectivity of reaction rules out any possible involvement of strong nonselective hydroxyl radical $^{\bullet}OH$, which is also supported by the fact that the low valance band potential of carbon nitride prevents thermodynamically the generation of $^{\bullet}OH$ via direct reaction between hole and hydroxyl group.[33,34] In addition, substrates that have β-hydrogens with possible formation of stable enol intermediate, acetalization may also proceeds via enol route.[10] However, to trace the origin and exact nature of observed catalysis (not clear at this stage), it requires a more intensive study.

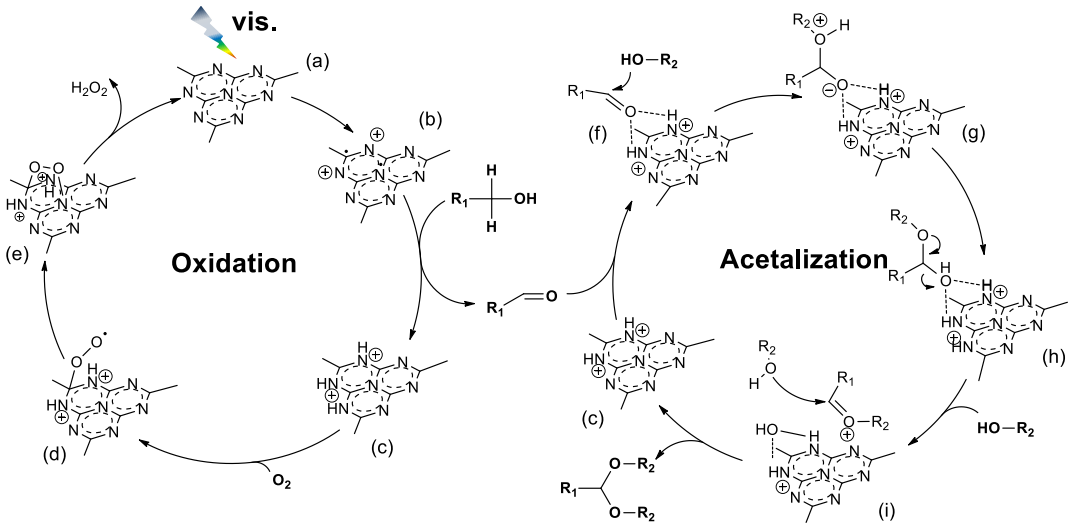

Figure 7.3 Proposed concurrent tandem catalytic pathway for photo-oxidation/acetalization catalysed by carbon nitride.

7.7 Conclusion

In conclusion, we have successfully demonstrated the auto-tandem photo oxidation/acetalization reaction using metal free carbon nitride as single catalyst. The promising scope of this new catalytic system for both aliphatic and aromatic alcohols has been realized at room temperature and oxygen pressure of 1 bar. We believe that this report describing the use of carbon nitride as heterogeneous photocatalyst for CTC, will stir a new interest to employ other heterogeneous catalysts for fine chemical synthesis in related manner.

7.8 References

[1] M. B. Smith, J. March, *March's Advanced Organic Chemistry*, John Wiley & Sons, Inc., Hoboken, New Jersey, **2007**.

[2] J. Clayden, N. Greeves, W. Stuart, *Organic Chemistry*, Oxford University Press, **2012**.

[3] N. Hamada, K. Kazahaya, H. Shimizu, T. Sato, *Synlett* **2004**, 1074–1076.

[4] N. M. Leonard, M. C. Oswald, D. A. Freiberg, B. A. Nattier, R. C. Smith, R. S. Mohan, *J. Org. Chem.* **2002**, *67*, 5202–5207.

[5] S. K. De, R. a. Gibbs, *Tetrahedron Lett.* **2004**, *45*, 8141–8144.

[6] R. Gopinath, S. J. Haque, B. K. Patel, *J. Org. Chem.* **2002**, *67*, 5842–5845.

[7] J.-L. Luche, A. L. Gemal, *J. Chem. Soc. Chem. Commun.* **1978**, 976.

[8] B. Procuranti, S. J. Connon, *Org. Lett.* **2008**, *10*, 4935–4938.

[9] J. Y. Qi, J. X. Ji, C. H. Yueng, H. L. Kwong, A. S. C. Chan, *Tetrahedron Lett.* **2004**, *45*, 7719–7721.

[10] C. Gunanathan, L. J. W. Shimon, D. Milstein, *J. Am. Chem. Soc.* **2009**, *131*, 3146–3147.

[11] E. Kossoy, Y. Diskin-Posner, G. Leitus, D. Milstein, *Adv. Synth. Catal.* **2012**, *354*, 497–504.

[12] A. C. Bueno, J. A. Gonçalves, E. V. Gusevskaya, *Appl. Catal. A Gen.* **2007**, *329*, 1–6.

[13] T. Shishido, T. Miyatake, K. Teramura, Y. Hitomi, H. Yamashita, T. Tanaka, *J. Phys. Chem. C* **2009**, *113*, 18713–18718.

[14] M. A. Butler, *J. Appl. Phys.* **1977**, *48*, 1914–1920.

[15] B. T. Gregg, K. C. Golden, J. F. Quinn, *J. Org. Chem.* **2007**, *72*, 5890–5893.

[16] S. Rudrawar, R. C. Besra, A. K. Chakraborti, *Synthesis (Stuttg).* **2006**, 2767–2771.

[17] B. Karimi, H. Hazarkhani, J. Maleki, *Synthesis (Stuttg).* **2005**, *2005*, 279–285.

[18] M. Kotke, P. R. Schreiner, *Tetrahedron* **2006**, *62*, 434–439.

[19] F. Zhang, J. Shi, Y. Jin, Y. Fu, Y. Zhong, W. Zhu, *Chem. Eng. J.* **2015**, *259*, 183–190.

[20] A. S. Poyraz, C.-H. Kuo, E. Kim, Y. Meng, M. S. Seraji, S. L. Suib, *Chem. Mater.* **2014**, *26*, 2803–2813.

[21] N. Narkhede, A. Patel, *RSC Adv.* **2014**, *4*, 19294.

[22] H. Firouzabadi, N. Iranpoor, B. Karimi, *Synth. Commun.* **1999**, *29*, 2255–2263.

[23] R. Sugimura, K. Qiao, D. Tomida, C. Yokoyama, *Catal. Commun.* **2007**, *8*, 770–772.

[24] K. I. Shimizu, E. Hayashi, T. Hatamachi, T. Kodama, Y. Kitayama, *Tetrahedron Lett.* **2004**, *45*, 5135–5138.

[25] J. C. Wasilke, S. J. Obrey, R. T. Baker, G. C. Bazan, *Chem. Rev.* **2005**, *105*, 1001–1020.

[26] D. E. Fogg, E. N. Dos Santos, *Coord. Chem. Rev.* **2004**, *248*, 2365–2379.

[27] A. Ajamian, J. L. Gleason, *Angew. Chem. Int. Ed.* **2004**, *43*, 3754–3760.

[28] D. A. Nicewicz, T. M. Nguyen, *ACS Catal.* **2014**, *4*, 355–360.

[29] C. K. Prier, D. A. Rankic, D. W. C. Macmillan, *Chem. Rev.* **2013**, *113*, 5322–5363.

[30] X. Wang, K. Maeda, A. Thomas, K. Takanabe, G. Xin, J. M. Carlsson, K. Domen, M. Antonietti, *Nat. Mater.* **2009**, *8*, 76–80.

[31] Y. Wang, X. Wang, M. Antonietti, *Angew. Chem. Int. Ed.* **2012**, *51*, 68–89.

[32] X. Wang, S. Blechert, M. Antonietti, *ACS Catal.* **2012**, *2*, 1596–1606.

[33] F. Su, S. C. Mathew, G. Lipner, X. Fu, M. Antonietti, S. Blechert, X. Wang, *J. Am. Chem. Soc.* **2010**, *132*, 16299–16301.

[34] B. Long, Z. Ding, X. Wang, *ChemSusChem* **2013**, *6*, 2074–2078.

[35] Y. Wang, H. Li, J. Yao, X. Wang, M. Antonietti, *Chem. Sci.* **2011**, *2*, 446.

[36] F. Su, S. C. Mathew, L. Möhlmann, M. Antonietti, X. Wang, S. Blechert, *Angew. Chem. Int. Ed.* **2011**, *50*, 657–660.

[37] B. M. Smith, A. E. Graham, *Tetrahedron Lett.* **2007**, *48*, 4891–4894.

[38] M. C. de Freitas, C. G. Vieira, E. N. DosSantos, E. V. Gusevskaya, *ChemCatChem* **2013**, *5*, 1884–1890.

[39] M. N. Huda, J. a. Turner, *J. Appl. Phys.* **2010**, *107*, 2–7.

[40] F. Su, M. Antonietti, X. Wang, *Catal. Sci. Technol.* **2012**, *2*, 1005.

[41] Y. Shiraishi, S. Kanazawa, Y. Sugano, D. Tsukamoto, H. Sakamoto, S. Ichikawa, T. Hirai, *ACS Catal.* **2014**, *4*, 774–780.

[42] Y. Shiraishi, S. Kanazawa, D. Tsukamoto, A. Shiro, Y. Sugano, T. Hirai, *ACS Catal.* **2013**, *3*, 2222–2227.

[43] M. Kotke, P. R. Schreiner, *Tetrahedron* **2006**, *62*, 434–439.

[44] M. A. Khan, I. F. Teixeira, M. J. L. Molly, Y. Kioto, S. C. E. Tsang, *Chem Commun.* **2016**, *52*, 2772–2775.

[45] F. Su, S. C. Mathew, G. Lipner, X. Fu, M. Antonietti, X. Wang, *Situ* **n.d.**, 1–5.

[46] D. A. Dougherty, *Acc. Chem. Res.* **2013**, *46*, 885–893.

[47] M. Zhang, Q. Wang, C. Chen, L. Zang, W. Ma, J. Zhao, *Angew. Chem. Int. Ed.* **2009**, *48*, 6081–6084.

Chapter 8: Conclusions and Future Perspective

8.1 Conclusions

Of the systematic modifications for the improvement of the photocatalytic activity of the carbon nitride based materials (doping, metal/semiconductor junctions, semiconductor/semiconductor heterojunctions), this thesis has demonstrated that the construction of metal-free isotype and type II metal oxide/carbon nitride semiconductor heterojunctions are both effective in designing the highly active carbon nitride based photocatalysts.

Polymeric carbon nitride heterostructures were constructed by controlled thermal condensation of dicyandiamide. The resulting heterojunctions exhibited a two fold increase in photocatalytic activity for hydrogen evolution from water. In particular, the charge transfer in CN-CN2 significantly faster than that of individual CN500 and CN600 materials, respectively. This implies that the generation of intrinsic CN500/CN600 interface promotes the separation and transfer of photogenerated electron-holes pairs. It also suggests that the improved electron mobility is likely to be due to the built-in electric field which arises from the topology induced band offsets of coupled heterostructure carbon nitride polymers. This approach can be extended to the myriad of the existing systems to improve their catalytic activity in a similar way.

In this thesis, the band edge positions of typical carbon nitride and niobium oxide materials were aligned to construct corresponding type II heterojunctions. Thus, C_3N_4-Nb_2O_5 heterojunctions were successfully synthesised *via* a hydrothermal method. The resulting heterojunctions in these composite materials showed the formation of an intimate interface. As a result, a significant suppression of unproductive charge exciton recombination processes was achieved. Catalytic testing showed the optimum photocatalytic activity was

2.7 to 2.8 times higher than that of individual C_3N_4 and Nb_2O_5, respectively. In addition, employing free radical and hole scavengers, the key intermediate species involved in the mechanism were identified: the superoxide radical was concluded to be the main active species. This investigation is expected to be useful for the further development of new heterojunction photocatalysts for water purification and environmental remediation.

Chemical utilisation of solar energy in organic synthesis on heterogeneous SCs is based on the activation and interactions of organic molecules at the surface. We have demonstrated in this thesis a new photocatalytic system for efficient photoacetalization of aldehydes and ketones with alcohols over the g-C_3N_4, which gives impressive selectivity and conversion at ambient conditions. The reaction takes place at room temperature in an oxygen-containing atmosphere, without requiring addition of acid or solvent, and is therefore considered to be a new green synthesis method. We have also successfully demonstrated the visible light induced concurrent tandem photocatalytic (CTC) conversion of alcohol to acetal over the carbon nitride materials under mild conditions.

8.2 Future Perspective

Carbon nitride is a fascinating material with both the HOMO and LUMO positions in a range which makes it a mild electron transfer agent with a large chemical potential. The carbon nitride structure is extremely sensitive to synthesis conditions, the fine control of these conditions and the goal of synthesising defect free material, consisting only of carbon and nitrogen, is yet be realised. The isotype carbon nitride heterojunctions shown in this work, and the recently reported isotype heterojunctions formed by coating sulfur at the carbon nitride surface, both display *n*-type semiconductor behaviour. It is predicted that applying a similar approach to systematically increase the boron sites, either by doping or

coating of the carbon nitride surface, could impart partial *p*-type character. In this way, constructing *p-n* junctions for improved photocatalytic charge transfer should be possible.

While great attention has been paid to water splitting and exhaustive aerobic degradation of pollutants, only a small amount of research has been carried out in the context of organic synthesis, despite the realisation of carbon nitride's ability as a visible light transducer to catalyse a variety of reactions. This work has demonstrated this point, through the development of efficient photoacetalization of aldehydes/ ketones with alcohols and auto-tandem oxidation/acetalization using g-C_3N_4 as photocatalyst.

It is acknowledged that metal free SCs that allow systematic tuning of surface reactivity and band structure are advantageous for controlled photo organic synthesis. The surface reactivity of the carbon nitride can be tuned by facile elemental doping into the surface structure. Specifically, doping of B,[1] S,[2] and P[3] (and other similar modifications) can induce the formation of sites of varied electron density, imparting the necessary Lewis acid or basic character. Further, the possibility of electronic structure modification in carbon nitride by facile elemental and molecular doping, to shift the conduction and valence band positions can render an additional control in design of a particular photoreaction.

It is believed that continued research in the field will open up these new facets of heterogeneous photochemical organic synthesis, a fundamental step towards the utilisation of solar energy in the production of fuels and food.

[1] Z. Lin, X. Wang, *Angew. Chem. Int. Ed.* **2013**, *52*, 1735–8.
[2] J. Zhang, M. Zhang, R.-Q. Sun, X. Wang, *Angew. Chem. Int. Ed.* **2012**, *51*, 10145–9
[3] Y. Zhang, T. Mori, J. Ye, M. Antonietti, *J. Am. Chem. Soc.* **2010**, *132*, 6294–6295.